In presenting this dissertation as a partial fulfillment of the requirements for an advanced degree from Emory University, I agree that the Library of the University shall make it available for inspection and circulation in accordance with its regulations, governing materials of this type. I agree that the permission to copy from, or to publish, this dissertation may be granted by the professor under whose direction it was written, or, in his absence, by the dean of the Graduate School when such copying or publication is solely for scholarly purposes and does not involve potential financial gain. It is understood that any copying from, or publication of, this dissertation which involves potential financial gain will not be allowed without written permission.

_____

Steven N. Dublin

The Rational Design of Environmentally-Responsive Elements in Synthetic Helical Fibers

By

Steven N. Dublin

Department of Chemistry

_____
Dr. Vincent P. Conticello
Advisor

_____
Dr. Stefan Lutz
Committee Member

_____
Dr. Dale Edmondson
Committee Member

Accepted:

_____
Dean of the Graduate School

_____
Date

The Rational Design of Environmentally-Responsive Elements

in Synthetic Helical Fibers

By

Steven N. Dublin

B.S., Evergreen State College, 1999

Advisor: Vincent P. Conticello, Ph.D.

An Abstract of
a dissertation submitted to the Faculty of the Graduate
School of Emory University in partial fulfillment
of the requirements for the degree of
Doctor of Philosophy

Department of Chemistry
Emory University

2007

Protein fibrils are among the principal synthetic targets for biomimetic materials design, primarily due to their frequent occurrence as major structural and functional components of native biological systems. The intricate morphological features and impressive array of functionalities exhibited by these native protein fibrils in biological systems has positioned these structures as vital models in the design of synthetic fibril systems which may be ultimately be utilized as functional components of nanoscale devices.

In this volume, a series of synthetic peptides are described which reversibly self-assemble into well-defined fibrous materials in a manner similar to native protein fibrils. Furthermore, we have designed environmentally-responsive mechanisms into the peptide primary sequences, which couple the folding of the supramolecular structure to the ability to sense incremental changes in the local environmental conditions. We show that the assembly of the synthetic peptides into long aspect-ratio fibers occurs as a consequence of environmental conditions such as changes in pH, temperature, metal ion and small molecules concentration.

Solid phase peptide synthesis is utilized to synthesize a series of 41 residue peptides whose sequence is inspired by the GCN4 leucine zipper. Structural studies of native coiled-coil systems show the a- and d-positions are determinants of peptide oligomerization, while the e- and g-positions strongly influence inter-strand orientation. Consequently, the *a*- and *d*-positions in our parental peptide **S6K** are occupied by a majority of isoleucine residues to bias the system toward the generation of a three-stranded coiled-coil assembly. Furthermore, the capacity to form helical fibers was engineered into the peptide sequence through the arrangement of charged residues in the

e- and *g*-positions such that cooperative electrostatic interactions between adjacent peptides occurs only in a staggered alignment which favors fiber formation.

Environmentally-responsive conformational switching mechanisms were introduced into the system by manipulating the identity of the amino acids occupying the core *a*- and *d*-positions which define the inter-strand interface. First, a pH and metal-ion sensitive switch was created through the mutation of isoleucine in the *d*-position of alternate heptads to the ionizable histidine residue. Protonation of the histidine side chain provides an electrostatic repulsion within the hydrophobic core of the coiled-coil causing the destruction of the fiber assembly. This mechanism links peptide self-assembly to the pK_a of the imidazole side chain.

Next, a canonical coiled-coil primary sequence is shown self-assemble into either a β-sheet or α-helical fiber based on a combination of pH and temperature. This is achieved by mutating the *d*-positions of alternate heptads from isoleucine to threonine, the later of which possesses high β-sheet propensity. The helical secondary structure of the assembly is presumably destabilized at neutral pH through an interaction between the threonine side chain hydroxyl group and the charged form of the *e*- and *g*-position glutamic acids, resulting in the formation of a β ribbon-like fiber. Under acidic buffering conditions below pH 4.5, α-helical secondary structure is regained in the sample, accompanied by the observation of helical fiber formation by TEM.

Finally, efforts toward an allosteric switch are described in which a destabilizing cavity is engineered into a helical fiber. The addition of a small hydrophobic molecule such as benzene or cyclohexane is shown to trigger the disassembly of the fibrous aggregate into a smaller helical fragments. Presumably, this occurs due stabilization of

the non fiber-forming structure as a consequence of ligand binding in the hydrophobic cavity.

The Rational Design of Environmentally-Responsive Elements in Synthetic Helical Fibers

By

Steven N. Dublin

B.S., Evergreen State College, 1999

Advisor: Vincent P. Conticello, Ph.D.

A dissertation submitted to the Faculty of the Graduate

School of Emory University in partial fulfillment

of the requirements for the degree of

Doctor of Philosophy

Department of Chemistry

Emory University

2007

enduring faith in the triumph of the underdog, he taught me the most important lesson I learned in graduate school … to always believe in yourself, even if the whole world says you're wrong.

Finally, I would like to acknowledge my family and friends. It is one of greatest regrets that my mother Marianne is not here with me today to share this achievement. She provided me with the sense of humor and humility necessary to make it through graduate school. Additionally, my brother Scott and my father Nate have been nothing short of models in strength and courage in the face of adversity. And of course, no words could capture my appreciation for my wife and partner Marike, who inspires me everyday to be the best person I can be.

TABLE OF CONTENTS

Chapter V: Efforts toward engineering an allosteric switch into

an α-helical fiber   152

LIST OF FIGURES

LIST OF TABLES

ABBREVIATIONS

aa	Amino acid
AUC	Analytical Ultracentrifugation
CD	Circular dichroism
DMF	Dimethyl Formamide
EDT	1,2-Ethanedithiol
Fmoc-	(9H-fluoren-9-ylmethoxy)carbonyl
FTIR	Fourier transform infrared spectroscopy
GCN4	"General Control Nondepressible", leucine zipper transcriptional activator
GuHCl	Guanidine hydrochloride
HBTU	1H-Benzotriazolium, 1-[bis(dimethylamino)methylene]-, hexafluorophosphate(1-), 3-oxide ; 1-[Bis(dimethylamino) methylene]-1H-benzotriazoliumhexafluorophosphate(1-) 3-oxide
HOBT	1-Hydroxy-1,2,3-benzotriazole
hr	Hour
HRSEM	High resolution scanning electron microscopy
kDa	Kilo Daltons
mg	Milligram
mL	Milliliter
mM	Millimolar
min	Minute
MRE	Mean residue ellipticity
nm	Nano meter
NMM	4-Methyl-morpholine ; N-Methylmorpholine
rpm	Rotations per minute
S1	Self-assembling peptide 1 (Homodimeric self-assembling system)
S6K	Self-assembling peptide 6 (Homotrimeric self-assembling system), employing Lysine as the only positively charged amino-acid residue
SAXS	Small Angle X-ray Scattering
SEM	Scanning Electron microscopy
SPSS	Solid State Peptide Synthesis
TEM	Transmission electron microscopy
TZ1H	S6K analog with the substitution I5H, I19H, I33H
TZ1T	S6K analog with the substitution I5T, I19T, I33T
μg	Micro gram
μl	Micro liter
μm	Micro meter
μM	Micro molar
x g	Rcf or relative centrifugal force

Chapter I: Introduction

1.1 Motivation for developing biomimetic nanoscale materials

The development of functional, nanoscale devices, envisioned for applications in nanoscience and medicine, has made great advances over the past decades. Notable successes have been achieved in the areas of novel drug delivery systems, artificial biomaterial scaffolding for tissue or cell engineering, and nanoscale fluidic devices for use as biosensors or computational devices.[2,3,4] Using a wide variety of materials, from synthetic polymers to engineered proteins, an array of functional nanostructures have been constructed in the laboratory (**Figure 1.1**). As these creations have gradually moved from the bench to the clinic, the demand for increasingly complex miniaturized components has subsequently followed.
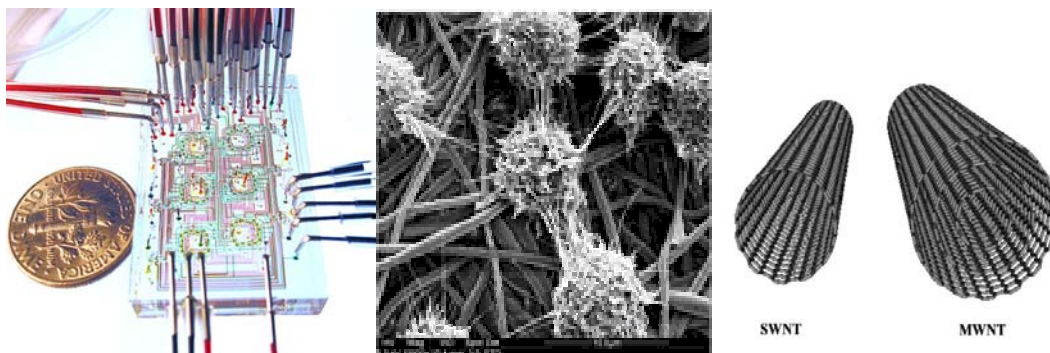
Figure 1.1. From left to right: A polymeric microfluidic chip on which bacteria can be cultured (Prof. Steven Quake, Stanford University), hematopoietic stem cell (HSC) expanded on electrospun nanofibers (Prof. Hai-Quan Mao, Johns Hopkins University) and single and multi-walled nanotubes (SWNT / MWNT) delivery systems for therapeutic molecules.

However, a formidable challenge still exists in the rational design and structural characterization of complex assemblies within the required nanoscale regime. Fortunately, inspiration can be gained from biological systems, in which life-sustaining functions are routinely performed by nanoscale architectures, which are dynamically assembled from small self-organizing components without the aid of external, physical manipulations.[5] This construction strategy is termed "bottom-up assembly" and it is achieved through features programmed into the primary sequences of the participating polypeptide and polynucleotide components. Using this construction approach, biological systems are able to achieve near-perfect architectural control over the assembly of complex, multi-component macrostructures.

Consequently, design strategies for generating synthetic nanoscale materials commonly borrow from nature's structural motifs in hopes of emulating the key self-recognition elements encoded within these native sequences. Using the basic building blocks of native protein fibers, biomimetic design strategies have been developed for the self-assembly of peptide subunits into well-defined aggregates with predictable biophysical features, functions and morphologies.

In this introductory chapter, several points of interest regarding the *de novo* design of biomimetic nanomaterials will be discussed. Specifically, an outline of the physical forces utilized by native biological constructs will be presented, with an elaboration on how key design elements within their primary sequences convey this information. Next, a brief review of existing strategies for assembling nanoscale peptide fibers will be presented, with a special focus of coiled-coil fiber assemblies. Finally, an

overview of the origin and applications of the specific synthetic peptide fiber strategy utilized in this thesis will be offered.

1.2   Self-assembly in native protein fibers

It has been written that "self-assembly is one of the few practical strategies for making ensembles of nanostructures".[5] In this context, the process of self-assembly can be described broadly as the spontaneous and deliberate organization of distinct components in a disordered system. Two major themes dominate this process: (1) the components must be able to recognize their counterpart with great specificity in a complex environment and (2) associations between the components must be locally reversible for the final structure to achieve thermodynamic equilibrium.[6] These qualities ultimately arise from the primary sequence of the individual components and effectively govern the interactions between the participating actors.

The spontaneous construction of thermodynamically-stable aggregates through self-organization of smaller components is termed "bottom-up" self-assembly and its basic tenets are commonly utilized in modern materials design strategies. Bottom-up self-assembly is a process perfected in biological systems, where functional supramolecular complexes are dynamically assembled and disassembled in aqueous environments without the aid of exogenous energy sources.

Native protein fibers provide a prime example of well-defined supramolecular structures which are generated through a bottom-up self-assembly strategy and as a consequence, these structures are among the foremost synthetic targets in the area of

biomimetic materials design. In their roles as omnipresent structural and functional nanoscale elements of biological systems, they are known to display many diverse functionalities, ranging from facilitation of motion (flagellar locomotion, muscle contraction) to acting as critical structural components of cells (exoskelatal and extracellular matrices).[7,8,9] Therefore, it is not surprising that native protein fibers often serve as models for the generation of synthetic fibers designed for use as functional elements in nanoscale devices. Classical examples of native fibers such as collagen, tropomycin, intermediate filaments, tubulin and F-actin, provide valuable insight the bottom-up assembly of these natural systems, since they represent the most simplistic model of supramolecular assembly (**Figure 1.2**).
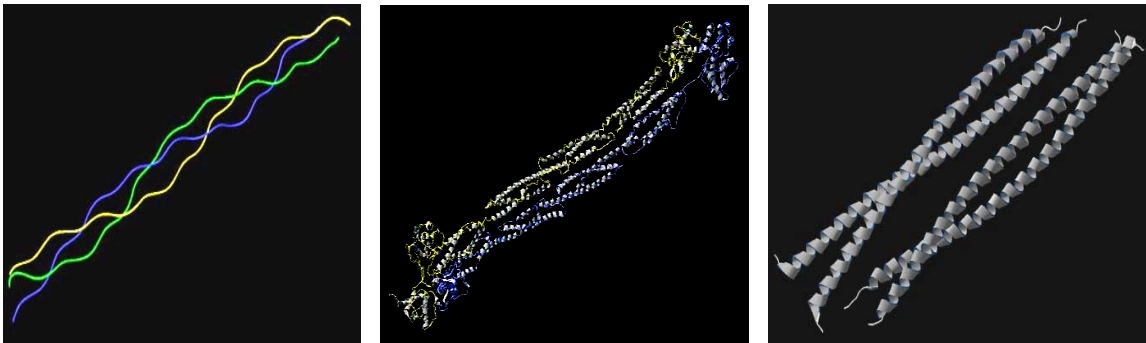
Figure 1.2. Representative examples of naturally occurring protein fibrils from the RCSB Protein Data Bank; collagen (1CGD), actin (1SJJ) and tropomysin (1IC2).

In an ideal self-assembly strategy, a well-defined functional aggregate could be generated through the controlled oligomerization of protein subunits or protomers, where the pool of protomers are composed of identical amino acid sequences and originate from a single structural motif (**Figure 1.3**). These two properties provide several desirable
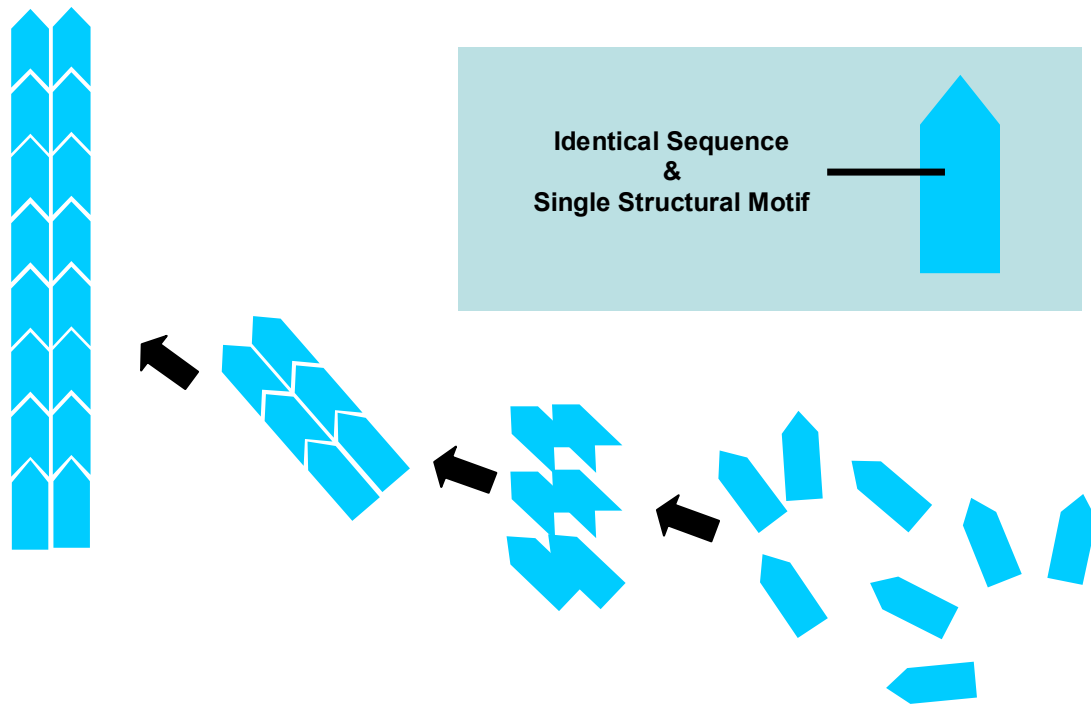
Figure 1.3. **The functional properties of the fibril are manifested as a consequence of the self-assembly of the protomers into supramolecular structures. In the simplest paradigm, a protein-based fibril is composed of identical protomers corresponding to a single structural motif.**

qualities for a *de novo* synthetic strategy. First, a single primary sequence facilitates a simplified design and synthesis process. Moreover, preparation of a single-component solution is uncomplicated since the assembly proceeds through the interaction of two identical helices, whereas in multi-component systems, determination of proper component stoichiometry and mixing is required to achieve the desired self-assembly. Lastly, the additional condition that the protomers originate from a single structural motif serves to simplify the characterization of the resulting fiber such that readily available

techniques can be utilized, such as circular dichroism (CD) spectrometry and fourier transform infrared (FTIR) spectroscopy.

1.2.1 Minimalist structural motifs

Nearly all self-assembling aggregates in biological systems are composed of endogenously-produced biopolymers, broadly grouped into three major categories of nucleic acids, proteins and carbohydrates. It has been argued that the greatest structural diversity is achieved in protein-based suprastructures, where a dizzying array of 3D structures can be produced on a simple amide backbone using merely the 20 natural amino acids organized into a small number of common structural motifs.

Two major structural motifs commonly found in native protein fibers are the β-strand and α-helix. Both motifs are composed of relatively small amino acid sequences, which utilize intentional spacing of simple amphiphilic building block to achieve their final secondary structure. Folding of these domains is driven through the pairing of hydrophobic and hydrophilic faces, which are generated through primary sequence design. These motifs offer not only simplicity of design but additionally, ease of construction, since the number of residues defining the primary sequences range between 5 to 50 amino acids, which is well within the reach of modern solid phase peptide synthesizers.

1.2.2 β-strand inspired peptide assemblies

The β-strand structural motif is the basic structural subunit of amyloid-like materials, the later of which has enjoyed significant attention in the scientific literature over the past decade.[10-12] A simplistic model of self-assembly in amylogenic fibers begins with short oligopeptides assuming a traditional β-strand fold, either intentionally or as result of a misfolding event. Next, controlled hydrogen bonding between individual β-strand monomers results in the formation of a β-sheet structure. Often, alternating hydrophobic residues in a short amino acid sequence with an (i, i+2) arrangement can be sufficient to induce β-sheet formation. Higher-order aggregates are subsequently constructed by the packing of alternating residues which project their side chain moieties on opposite sides of the β-sheet, facilitating facial discrimination of the protomers Finally, the individual β-sheets pair to form protofilaments, which in turn pack together to ultimately generate mature fibers.

A number of elegant synthetic schemes for the generation of β-sheet fibers have been reported in the literature, ranging from a minimalist approach utilizing short amino acid sequences displaying alternating cationic, anionic, and hydrophobic residues, such as Arg-Ala-Asp (RAD) or Glu-Ala-Lys (EAK), to a more sophisticated class of peptides based on the β-turn motif which self-assembles via engineered lateral and facial interactions.[12, 13,14] However, many β-strand systems display a strong tendency to gel, which is frequently attributed to the tendency of shorter persistence length β-sheet fibers to entangle to form dense macroscale networks. Consequently, materials which display gelation tendencies are better suited as synthetic matrices and hydrogelators.[15]

1.2.3   The α-helical structural subunit

Examples of biomimetic design strategies which utilize the α-helical structural motif are significantly fewer in number then those based on β-strand subunits. The architecture of fibers composed of α-helical subunits differs significantly from β-sheet fibers, including unique periodicities of the aggregate suprastructure and orientation of protomers with respect to the fibril axis, suggesting synthetic peptide fibers composed of α-helical subunits offer a complimentary approach to the established work on β-sheet assemblies.

The α-helix is one of the most studied biological components and furthermore, is widely recognized as a key component of native protein structures. Consequently, this ubiquitous secondary structure has been extensively studied and its key structural features have been thoroughly characterized. A typical helix is formed by winding a polypeptide backbone into a right-handed helix. This arrangement is stabilized by an internal network of hydrogen-bonding patterns between carbonyl oxygen of residue i to the amide hydrogen of (i + 4) residue, since a single turn on the helix is defined by approximately 3.6 residues.

However, isolated α-helical strands are rarely observed in nature, which suggests contributions to stability in addition to intramolecular forces must be required to establish a long-lived, well-defined helical structure in solution. In naturally occurring proteins, α-helices are commonly found packed together to achieve greater stability through interstrand hydrophobic side chain packing and van der Waals forces. This phenomenon

is most evident in native coiled-coil assemblies, exemplified by the conserved leucine zipper motif.

1.3 Coiled-coil assemblies

Canonical coiled-coil assemblies are composed of two or more right-handed α-helices, which subsequently bundle with a slight left-handed helical twist to form a superhelix. The coiled-coil motif is ubiquitously found in several classes of proteins, including muscle, α-keratin, bacterial surface proteins, intermediate filaments, laminins, dynein, tumor supressors, and oncogene products. Each helical strand in the coiled-coil is composed of 30 to 40 amino acids arranged in periodic repeats of seven residues termed heptads. For convenience, a single heptad unit is commonly denoted as $(a\text{-}b\text{-}c\text{-}d\text{-}e\text{-}f\text{-}g)_n$ and can be graphically represented in a helical wheel diagram (**Figure 1.4**).

Native α-helical forming sequences can produce a uniform face on the resulting helix through the positioning of amino acids of similar properties every 3 or 4 residues. In this manner, coiled-coil primary sequences often position hydrophobic sidechain residues in an (i, $i+4$) spacing to generate a hydrophobic face on the helix. This arrangement is commonly represented as *H-P-P-H-P-P-P*, where *H* is any residue containing a hydrophobic sidechain (primarily Ala, Leu, Ile, or Val) and *P* represents any of the recognized polar amino acids. It is the burial of the resulting hydrophobic face which is the key driving force for the formation of the unique coiled-coil topography. Consequently, understanding of hydrophobic and polar residue patterns and their
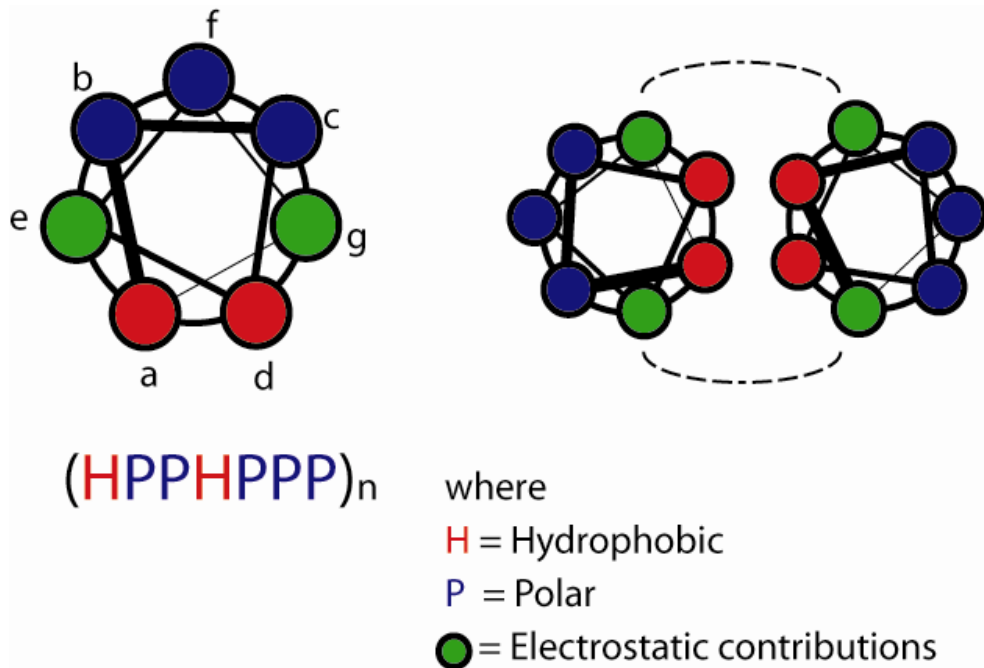
Figure 1.4. **(Left) Generic helical-wheel diagram illustrating a cross-sectional view down the axis of the coil. (Right) Association of two amphiphilic peptides into a dimeric coiled-coil. Burial of hydrophobic faces of amphiphilic helices (composed of red residues) and cooperative inter-strand electrostatics hold the non-covalent assembly together.**

orchestrated interactions between protein side chains and bulk solvent, can link the primary sequence of a peptide to higher order secondary / tertiary structure to a first approximation.

1.3.1 *a*- and *d*-positions influence coiled-coil oligomerization state

In addition to comprising the hydrophobic face of the helical strand, the *a*- and *d*-position residues in the canonical coiled-coil heptad can strongly influence the

oligomeric state of the coiled-coil assembly. Pioneering studies on engineered mutants of the coiled-coil transcription regulator protein GCN4 by Alber and coworkers, established a foundation on which a plethora of *de novo* coiled-coil designs have been built.[1] This held that the three-dimensional structure of the coiled-coil assembly was independent of the geometry of the hydrophobic amino acid side chains in the canonical *H-P-P-H-P-P-P* pattern. Instead, Alber showed that a 31-residue coiled-coil primary sequence comprised of the standard heptad repeat $(a$-b-c-d-e-f-$g)_n$ where *a-* and *d-*positions are hydrophobic residues, adopted a dimeric, trimeric or tetrameric oligomerization state depending on the identity of the residues in the apolar *a-* and *d-*positions. Through the mutation of the four *a-* (Val^9, Asn^{16}, Val^{23}, Val^{30}) and four *d-* (Leu^5, Leu^{12}, Leu^{19}, Leu^{26}) position amino acids in the native GCN4 sequence to either Leu, Val or Ile, the general rules for creating two, three or four stranded coiled-coil assembly were elucidated (**Table 1.1**).

The x-ray crystal structure of GCN4-pI revealed two helical strands packed together to bury their hydrophobic faces in a parallel (both N → C terminus) fashion. The packing of the hydrophobic side chains at the helical interface were shown to participate in Crick's "knobs-in-holes" packing model, first proposed in 1953.[16] In this scheme, *a-* and *d-*position side chains (knobs) are positioned between four residues of the adjacent helix (holes). For example, the GCN4-pI dimer positions the Cα-Cβ bond of the *a-*position side chain between the corresponding *a'-*position partner and the preceding *g'* residue side chain. In a similar manner, the *d-*position side chain packs in a perpendicular fashion against the interhelical *d'* leucine knob and the subsequent *e'* residue (**Figure 1.5**). The side chains of the *a-* and *d-*position residues were determined to be 83% buried in the dimer interface.
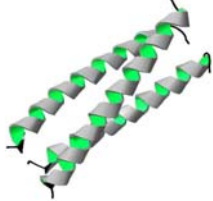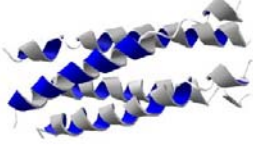
Position		Oligomeric State
_a_	**_d_**	
I	L	2
I	I	3
L	I	4

Table 1.1. Amino acid identity and position determine number of helical strands participating in the formation of the coiled-coil assembly. [1]

Subsequent crystal structures of GCN4 mutant show the coiled-coil oligomeric state is associated with particular side chain-packing geometries across the hydrophobic interface (**Figure 1.5**). In the case of triple-stranded GCN-pII, the Cα-Cβ bond of both *a*- and *d*-position isoleucine side chains occur at an acute angle to the Cα-Cα vector which defines the conjugate hole. Only a minor difference in packing geometries is observed for *a*- and *d*-positions, with a slight 25° difference in angles. In either position, amino acid identity in the acute geometry has no preference between leucine or the β-

branched valine and isoleucine. Dimeric (discussed above) and tetrameric assemblies
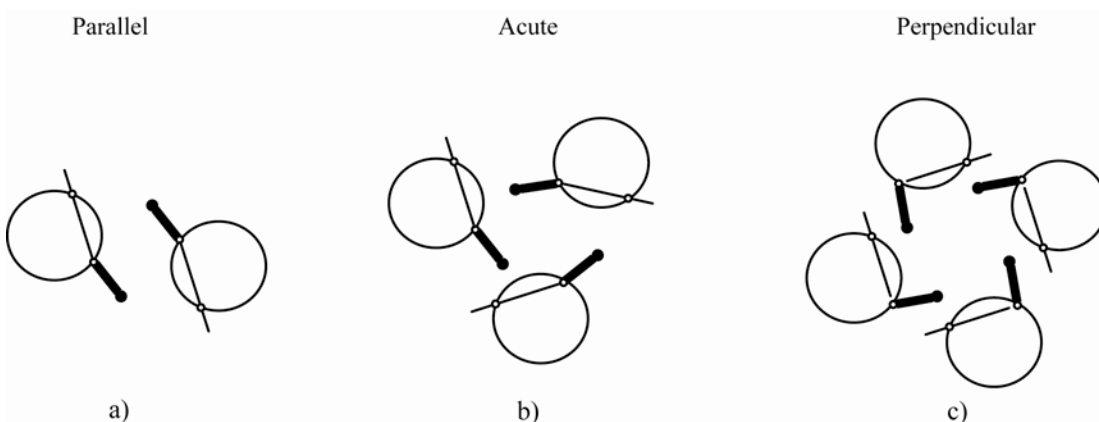
Figure 1.5.   Knobs-in-holes packing variations displayed by synthetic GCN4 coiled-coil assemblies. a.) Parallel sidechain packing orientation via preferred β-branched sidechains, b.) Acute arrangement shows no preference, c.) Perpendicular packing favors leucine.

have a more complicated packing regime, displaying mixed parallel and perpendicular arrangements. For the GCN4-pLI tetramer, the packing arrangement is the reverse of the dimer with the *a*-position leucine positioned in a perpendicular fashion and *d*-layer isoleucine in a parallel arrangement.

Additionally, since the *a*- and *d*-position residues comprise the hydrophobic core of the coiled-coil, the introduction of amino acids which provide novel interactions at defined core positions can specify lateral registry between helices as a consequence of

steric or electronic effects disfavoring alternative helix packing arrangements. Several types of interactions have been reported which demonstrate control over helix-helix orientation through the introduction of buried polar interactions, steric matching of core residues, and segregation between fluoro- versus protio-substituted residues.

1.3.2   *e*- and *g*-position residues

Structural studies of synthetic coiled-coils have shown the *e*- and *g*-position residues in the heptad play a critical role in orchestrating helix-helix interactions and furthermore, as a result of their positions flanking the hydrophobic core, also serve as active participants in knobs-in-holes side chain packing.   In a parallel coiled-coil assembly, the N-terminus of a single helix is in alignment with the N-terminus of its partner helix, thereby placing in close proximity, the core-forming residues with the *g* and *e*+1 positions of neighboring helices.   Therefore, the identity of the residues occupying these important positions, in conjunction with the *a*- and *d*-position amino acids, serve as key design elements in assuring proper folding and thermodynamic stability of the coiled-coil assembly.

Strand orientation and lateral registry of adjacent helices comprise the primary contributions of *e*- and *g*-position residues in the shaping of coiled-coil assemblies. Strand orientation refers to the relative positioning of the N-terminus of a helix with respect to the N-terminus of its partner helix, either parallel (N- to N-terminus) and anti-parallel (N- to C-terminus) arrangements (**Figure 1.6**). Typically, charged residues occupy the *e*- and *g*-positions such that cooperative or repulsive Coulombic interactions

dictate parallel or antiparallel orientation. Lateral registry describes the relative alignment of two adjacent helices. The vast majority of natural and synthetic leucine zippers display an in-register alignment, where the final assembly is a blunt-ended
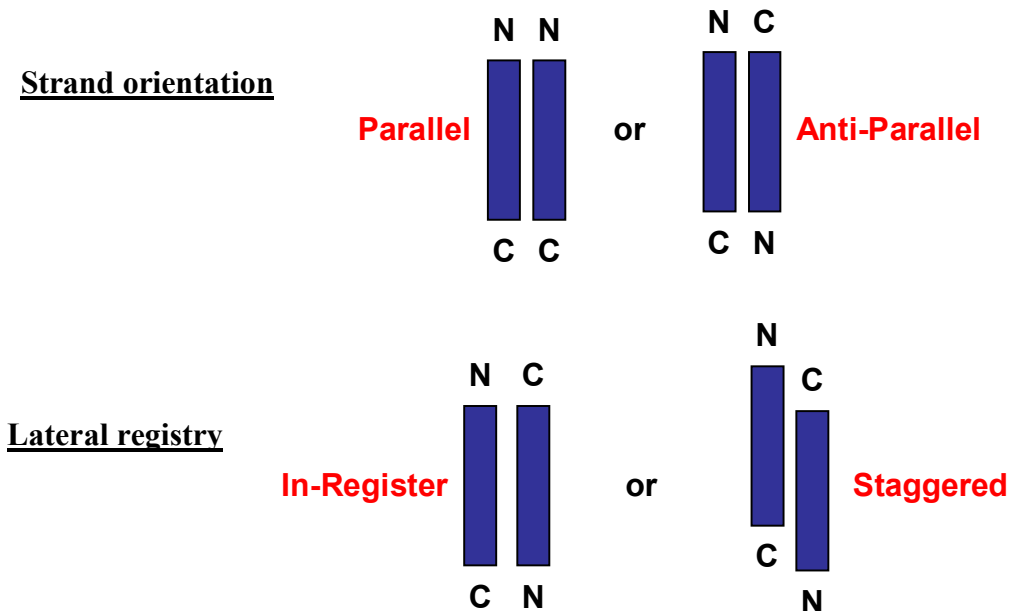
Figure 1.6. An overview of common strand orientation and lateral registry arrangements of helical peptides (represented by blue rectangles). Positions *e* and *g* are occupied by charged residues which allow for the control of these intermolecular associations.

structure. However, fibrillogenic coiled-coil peptides display a unique lateral registry of protomers comprising the fibril, where adjacent helices are packed together with an axial stagger corresponding to an integral number of heptad repeats (**Figure 1.6**). Longitudinal

self-assembly can be accomplished if the offset protomers posses complementary "sticky" ends between adjacent helices.

1.3.3 Solvent-accessible residues

The role core-forming a- and d-position residues play in oligomerization and strand orientation is a continuously active area of research. However, the remaining residues in the canonical heptad motif are also critical components in controlling the overall global fold of the aggregate. Positions b, c and f are unique since they comprise the largest area of the coiled-coil in contact with aqueous solvent. For this reason, these positions are primarily occupied by the polar amino acids Gln, Glu, Tyr, Arg, Lys and less frequently, the helix-forming Ala.

An obvious consequence of f-position residue identity is the encouragement or inhibition of lateral association between proximal fibers. For instance, alternating Lys and Glu residues in the solvent-exposed f-position will provide charge-complementary pairs for neighboring fibers of the same sequence. Alternatively, the presentation of a single charge down one face of the fiber will discourage lateral association due to charge-charge repulsion between fibers. In this way, control over interstrand behavior can be encoded into the primary sequence of the assembly. Finally, since this position is generally not engaged in knobs-in-holes packing or structure stabilization, it can be occupied by a chromophore like Tyr and used for UV absorbance measurements.

ELECTROSTATICS (0.5-4 kJ/mol/bond)   **HYDROGEN BONDING** (4-12 kJ/mol/bond)

A
C
I
D
I
C

(-)

Aspartic Acid (D)   Glutamic Acid (E)

Serine (S)   Threonine (T)

B
A
S
I
C

(+)

Lysine (K)   Arginine (R)

P
O
L
A
R

Asparagine (N)   Glutamine (Q)

HYDROPHOBIC INTERACTIONS (4-8 kJ/mol/bond)

N
O
N

P
O
L
A
R

Alanine (A)   Leucine (L)

A
R
O
M
A
T
I
C

Phenylalanine (A)   Tyrosine (Y)

B

B
R
A
N
C
H
E
D

Valine (V)   Isoleucine (I)

Tryptophan (W)
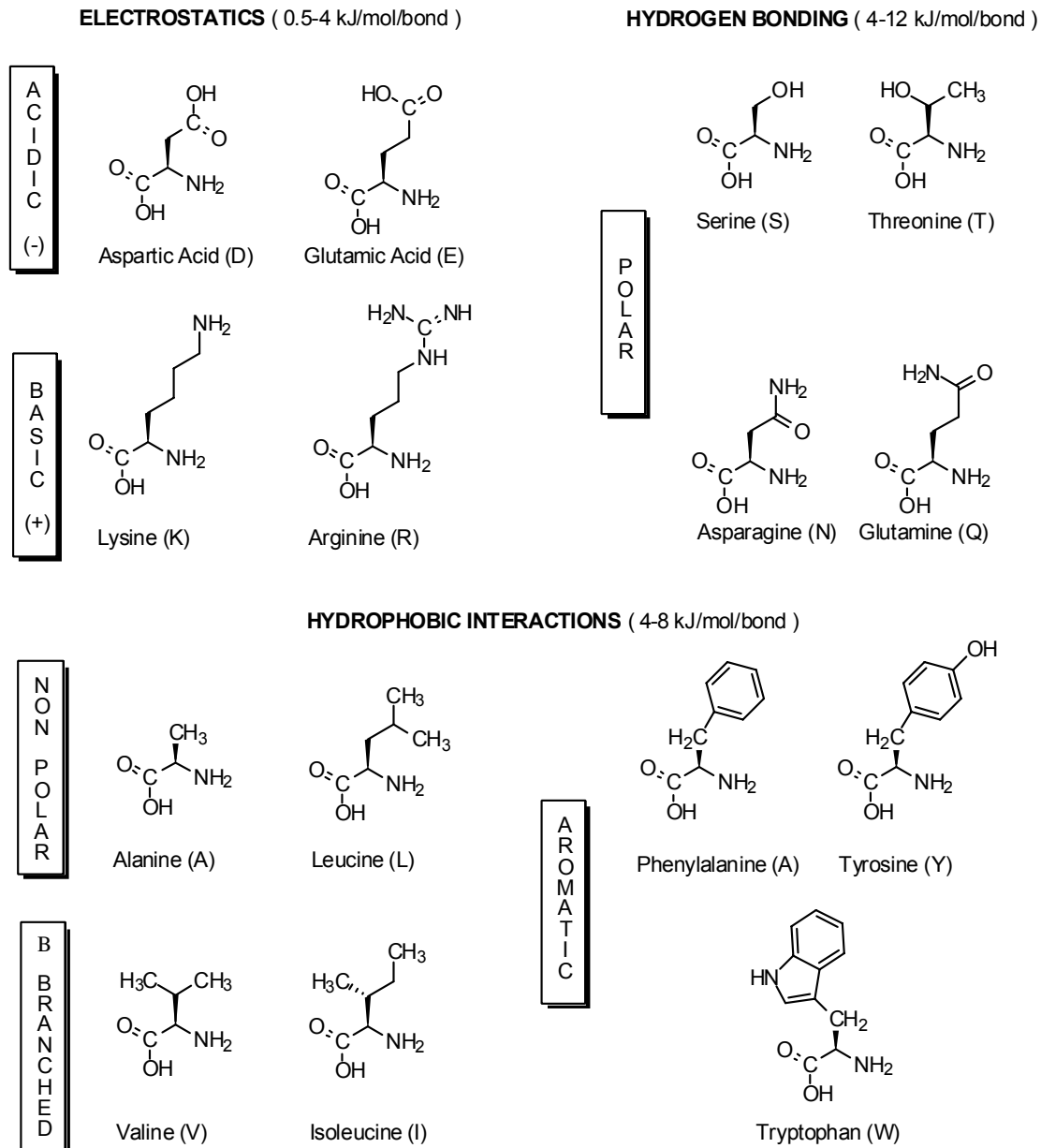
Figure 1.7.   Classification of common amino acids by the properties which dominate interactions occurring in peptides and proteins.

17

1.3.4 Non-covalent interactions in native coiled-coil assembly

Remarkably, self-assembly of complex biological macrostructures, such as coiled-coil assemblies, is orchestrated and maintained by a network of relatively weak, noncovalent interactions such as cooperative / repulsive electrostatics, hydrophobic interactions, steric complementarity and hydrogen bonding, which arise from the amino acid residues comprising the heptad repeat unit (**Figure 1.7**). Control over oligomerization number (*n*) and strand orientation (parallel or antiparallel) in coiled-coil assemblies composed of tandem heptad repeats has been shown to rely on sidechain packing of hydrophobic residues in positions *a* and *d* and electrostatic interactions at positions *e* and *g*. However, model of self-assembly based on native coiled-coil structures extend only to the dimeric, trimeric and tetrameric oligomerization states. More importantly, the utility of this model in generating helical fibers is limited since it describes merely the means for controlling lateral association not axial elongation, a crucial component of biomimetic design strategies for fibrous materials.

1.4 Established strategies for generating fibrous materials from helical peptides

Reported strategies for building fibrous aggregates from the self-assembly of designer helical peptide sequences can be found in the literature as early as 1997. Kojima and coworkers provide the first report of a *de novo* designed α-helical peptide capable of self-assembling into a fibrous structure.[17] This 21-residue peptide sequence, termed α-3,

is composed of three heptad repeat units, (LETLAKA)$_3$. The peptide was designed to form an amphipathic, α-helical structure with the hydrophobic face formed by leucine residues and a hydrophilic surface composed of glutamic acid and lysine. Fiber formation was predicted to be dominated by hydrophobic interactions between *a*- and *d*-position leucine side chains, with an additional contribution to stability by cooperative electrostatic interactions between charged *e*- and *g*-position residues. Although a thorough biophysical description of the system was lacking, the resulting fibers were characterized as possessing fibers of several μM length and 5-10 nm diameters.

The first thoroughly described scheme for the self-assembly of α-helical peptides into helical fibers was the heterodimeric SAF (self-assembling fibre) system developed by Woolfson and coworkers (**Figure 1.8**).[18] Fiber formation in this scheme relies on cooperative electrostatic interactions to encourage a staggered alignment between two different *de novo*-designed leucine zipper peptides. Increased stability of this pairing is achieved through structure-stabilizing hydrogen bonding between asparagines residues, which are possible only when the adjacent peptides align in the desired staggered formation. The resulting fibers are several μM in length and additionally show lateral association resulting in diameters in excess of 40 nm. The addition of charge-screening salts disrupts the fibrous architecture, which emphasizes the role of electrostatic interactions in this design. Subsequent work on the SAF system demonstrated control over the fiber morphology could be achieved through second-generation, rationally-designed peptides which introduced bends, kinks and cross-links to the fiber architecture.

EIDALEYENDALEQKIAALKQKIASLKQEIDALEYENDALEQKIAALKQKIASLKQEIDALEYENDALEQ

KIRALKAKNAHLKQEIAALEQEIAALEQKIRALKAKNAHLKQEIAALEQEIAALEQKIRALKAKNAHLKQ
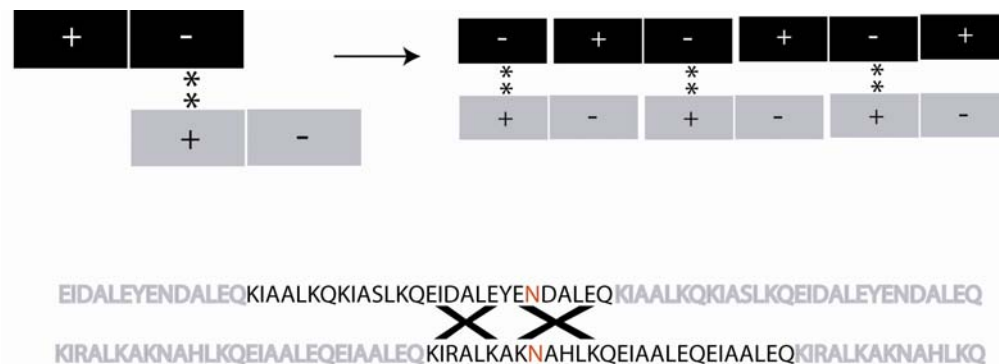
Figure 1.8. Representation of the SAF peptide scheme. (Top) Blocks in black and grey represent peptides 1 and 2, respectively. Cooperative electrostatics enforce a staggered alignment between peptides. The star marks positions occupied by asparagine, which provides enhanced stability of the pairing through the addition of hydrogen bonding between buried polar residues. (Bottom) Cooperative electrostatic interactions are highlighted along with the asparagine position in red.

The SAF scheme is the leading example of a hetero-component system, in which fiber formation arises from the self-assembly of two peptides of different primary sequences. However, Potekhin and coworkers describe a robust single-component structural model for generating axially-elongated α-helical fibrils from identical, short oligopeptide sequences.[19] Using the canonical leucine zipper motif as inspiration, a 34-residue oligopeptide $[Q_cL_dA_eR_fE_gL_a(Q_bQ_cL_dA_eR_fE_gL_a)_4]$ was designed to form a 5-stranded coiled-coil fiber, with α-helical protomers staggered along the axis. On the basis of their model, an oligopeptide sequence composed of L amino acids arranged in

multiple heptad repeats, will assemble into an *n*-stranded helical fiber if the axial stagger between adjacent helices (*Δl*) is defined by a multiple of heptads (**Figure 1.9**). An empirical equation is presented for a set of "magic numbers" which predicts the degree of oligomerization in a self assembled α-helical fiber (**Equation 1.1**).

$$\frac{(L + \delta l)}{n} = \Delta l$$

where
- n = degree of oligomerization of the helical bundle
- L = amino acid residues in the peptide
- δl = space for head-to-tail packing (usually 1)
- Δl = shifts of adjacent helices in residues
  (in multiples of heptads; 7, 14, 21 …)

(Equation 1.1.)

To demonstrate the power of this model, the Potekhin group generated a five-stranded fiber from a 34 residue peptide sequence (L) containing one heptad axial stagger (Δl) with a predicted one residue padding (δl). Most remarkably, the magic number formulation results in the self-assembly of a five-stranded, α-helical fiber despite the lack of design elements in the peptide sequence which were previously thought to be critical in forming coiled-coil assemblies of a specific oligomerization state. For example, the core-forming *a*- and *d*-positions were occupied by leucine, an unconventional choice since this residue is associated with a range of oligomerization states from two through five. Furthermore, the conventional electrostatic element of traditional coiled-coils was neutralized through the selection of alanine to occupy the *e*-position. Placement of an apolar residue near the helical interface can serve to widen the hydrophobic cluster to favor a four- and five-stranded helical bundle.
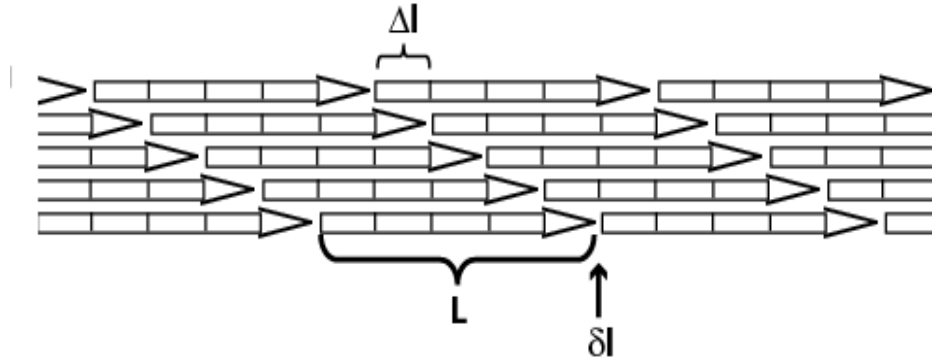
Figure 1.9. Model for fiber growth through axial-staggered peptide sequences. This representation describes a five-stranded fiber from a 34 residue peptide (L) containing a heptad stagger (Δl) with one residue padding (δl).

1.4.1 A hybrid strategy of magic number formulism and native heptad elements

The major supposition of the Potekhin model is that fibrillogenesis and oligomerization determination is strongly dependant on the length of the peptide sequence. However, certain values for peptide length (L) can result in multiple oligomeric states (n) when using **(Equation 1.1)** to solve for heptad stagger (Δl). Therefore, peptide length alone cannot be the sole determinant of the oligomerization state. Similarly, native coiled-coil assembly models are insufficient as sole models of

biomimetic protein fibers since they are primarily concerned with lateral association rather than axial elongation.

Therefore, a hybrid model which combines the formalisms of knobs-in-holes sidechain packing and electrostatic interactions with Potekhin's "magic number" axial-staggering scheme is an obvious solution to generating an axially elongated fiber of a specified oligomerization state. In this hybrid approach, the hydrophobic core-forming *a*- and *d*-position residues and the electrostatic interactions between proximal *e*- and *g*-position amino acids would be chosen to enforce an axial stagger of helical protomers to achieve the magic number formulism of Potekhin.

1.4.2 The rational design of a two-stranded, α-helical fiber

Using a hybrid design strategy as previously described, an oligopeptide **S1** was created in the Conticello group with the goal of generating a two-stranded, α-helical fiber (**Figure 1.10**). The 42-residue peptide sequence is composed of six heptad repeats, with core-forming *a*- and *d*-positions occupied by isoleucine and leucine, respectively. These two parameters, peptide length and isoleucine / leucine core-forming residue choice, conform to the formulations for generating a two-stranded helical assembly expressed by both the knobs-in-holes packing and "magic numbers" axial-stagger models described previously. Furthermore, additional features were programmed into the peptide sequence to favor a three heptad axial staggering required by the Potekhin model for dimeric fiber assembly. For instance, the formation of parallel, in-register homodimeric associations were negatively selected against by placing similarly charged residues at the *e*+1 and *g*

23
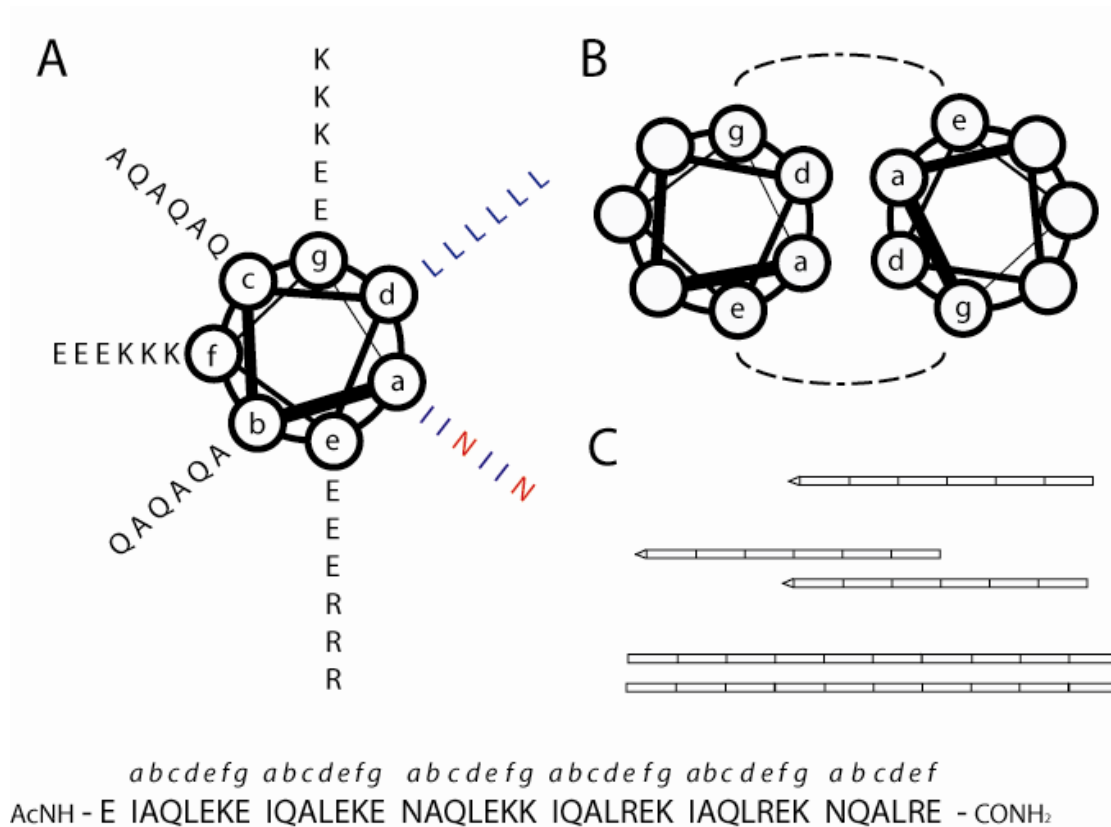
Figure 1.10. General design scheme for assembling a dimeric helical fiber. A.) Helical wheel diagram of S1, B.) Graphical representation of the proposed two-stranded helical association and C.) Scheme for building axially elongated fibers through staggered lateral association starting from monomer to dimeric coiled-coil association and finally aggregation of dimeric protofibrils.

positions which define the helical-strand interface. Additionally, anti-parallel strand orientation was designed to be disfavored due to the resulting packing of a polar asparagine residue with an apolar leucine or isoleucine at the hydrophobic interface. When aligned in the desired three-heptad stagger, the destabilizing effect of the two polar asparagine residues in sequence is neutralized by amide sidechain hydrogen bonds formed between the juxtaposed residues.

Structural studies of the **S1** peptide in aqueous solution established α-helicity and fiber formation of the assembly by circular dichroism (CD) and transmission electron microscopy (TEM) respectively. CD spectroscopy is a critical component of secondary structure evaluation, particularly when the resulting structure is of α-helical character. The CD spectrum of **S1** peptide solution displays a characteristic α-helical spectrum, with distinct minima at 208 and 222 nm. Values for the mean residue ellipticity (θ) ratio of $\theta_{222}/\theta_{208}$, determined by CD, were in agreement with conventional coiled-coil assemblies, giving confidence in the formation of the desired tertiary structure.

Further information about local conformation of core-forming residues was gained through solid-state CP/MAS/NMR spectroscopy of isotopically-labeled **S1** peptide. A leucine residue within the central heptad was labeled at the carbonyl carbon with a ^{13}C isotope. The chemical shift of the labeled **S1** leucine was observed significantly downfield of the average random coil chemical shift of a leucine carbonyl group. Additionally, comparison of the observed chemical shift in the **S1** Leu(19) carbonyl group with an α-helical form of poly-leucine, suggests this residue and **S1** peptide adopt an α-helical form in solid-state.

A final NMR-based structural conformation study was performed by isotopically labeling the carbonyl carbon of leucine(19) and nitrogen atom of isoleucine(23), corresponding to i and $i+4$ core-forming residues. REDOR experiments revealed the distance between these two amino acids was 4.0 ± 0.1 Å, within reason of the expected distance of 4.2 Å for a typical α-helix. Random coil or β-sheet secondary structure at these positions can be ruled out since the distances between two nuclei involved in these conformations exceed the detection limits of REDOR.

Manifestation of the fiber-promoting scheme could be observed by transmission electron microscopy (TEM) and complimentary techniques such as small-angle scattering techniques SAXS and SANS. Although observed diameters by negative-stain TEM were at least one order of magnitude larger than the expected, small-angle neutron scattering (SANS) and synchrotron X-ray (SAXS) scattering experiments of **S1** fibers offered closer approximations of expected diameter measurements at 15.6 ± 1.4 Å and 17.1 ± 0.2 Å respectively. The minimal diameter estimate for a generic double-stranded coiled-coil is 14.8 Å. This value is calculated from the Cα trajectory of the polypeptide chain which does not consider steric contributions originating from amino acid sidechains. Considering sidechain contributions and the relative agreement between the two independent diameter measurements, it is reasonable to conclude that the assembly of **S1** results in a dimeric fiber and therefore the desired lateral stagger has been achieved.

1.4.3 The generation of a triple-stranded α-helical fiber

Extension of the helical fiber scheme to higher-order aggregates was achieved by the Conticello group with the design of a peptide sequence predicted to self-assemble into a three-stranded helical fiber. A 41-residue peptide **S6K** was designed with all isoleucine residues exclusively occupying all core-forming *a*- and *d*-positions, which was shown to favor the formation of a trimeric oligomerization state in the previously described GCN4-pII coiled-coil mutant (Error! Reference source not found.). Without the presence of a polar residue within the hydrophobic core directing helical registry, as was the case in the double-stranded **S1** helical fiber, this peptide relies on cooperative Coulombic interactions at the *e*- and *g*-position to assist in the reinforcement of helical alignment. In this manner, the heptad repeat units were designed such that charge-complementarity between adjacent helices is possible only if the protomers align in a parallel orientation with a two-heptad staggered formation. When arranged in this fashion, all *e* or *g* charges will be neutralized by the partner *e'* or g' residue. By Potekhin's magic number formulation, a two-heptad stagger between adjacent helices should favor a trimeric oligomerization state.

Similar to the dimeric **S1** peptide, the **S6K** peptide solution displayed a CD spectrum with characteristic α-helical character. The peptide assembly was found to be resistant to thermal denaturation when assayed by differential scanning calorimetry (DSC) or CD. Furthermore, TEM images provided conformation of the axial elongation design through the visualization of long-aspect-ratio fibers. However, the fiber diameters observed by TEM were 1-2 orders of magnitude larger than expected. The observed
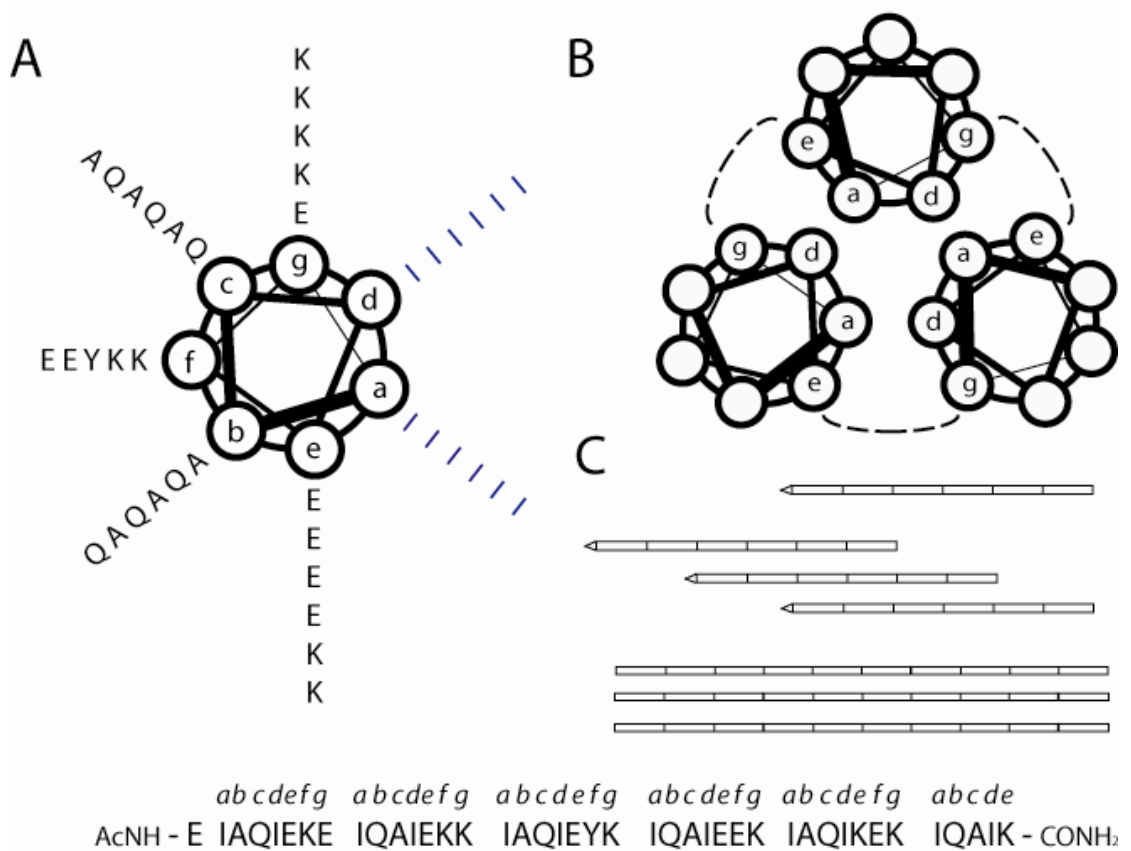
Figure 1.11. General design scheme for assembling a trimeric helical fiber. A.) Helical wheel diagram of S6K all isoleucine core, B.) Graphical representation of the proposed three-stranded helical association and C.) Scheme for building axially elongated fibers through staggered lateral association starting from monomer to dimeric coiled-coil association and finally aggregation of trimeric protofibrils.

aggregation tendencies of the **S6K** helical fibers and the resulting solution clouding inhibited the availability of biophysical characterization techniques, such as NMR and scattering techniques, utilized in characterizing **S1** peptide fibers.

Next-generation designs of the **S6K** fiber system incorporated a hydrophilic $(PEG)_4$-Gly-Gly linker between the peptide and a D-biotinyl moiety at the N-terminus of the monomer to increase solubility. This design modification successfully decreased the extent of fiber thickening and solution clouding, which consequently enabled the measurement of the fiber diameter by SAXS. A fiber diameter of ~ 27 Å was observed, within the expected diameter range of a triple-stranded coiled-coil assembly.

1.5 Summary

The self-assembly of helical peptides shows great potential as a viable fabrication scheme for generating functional materials on the nano- to micrometer scale. Information gained from the structural characterization of functional components in biological systems can be incorporated into *de novo* design strategies for generating synthetic nanoscale materials. A model system particularly useful in the generation of functional peptide fibers is the native coiled-coil assemblies, which are composed of helical peptides whose primary sequence is defined by tandem heptad repeat units. The ruleset, defined by Alber and coworkers, for generating synthetic coiled-coil assemblies of predicted oligomerization states has been previously elucidated. However, this system is primarily concerned with the generation of in-register, discrete coiled-coil assemblies, rather than axially-elongated helical fibers.

Fortunately, a powerful strategy for generating long-aspect-ratio fibers has been described in the literature, which uses the axial staggering of adjacent protomers to achieve elongation along the fiber axis. Using a combination of this synthetic strategy and the natural ruleset of native coiled-coil assembly, a novel rational design strategy for generating an n-stranded helical fiber has been reported by our group. The experiments described above validate this strategy for generating oligopeptides which self-assemble into two- and three-stranded helical fibers.

However, native biological assemblies are known not only for their well-defined structures, but also for their unique functions that arise as a consequence of those structures. In the following chapters, the design, synthesis and characterization of a series of self-assembling peptide systems which are capable of sensing and responding predictably to incremental changes in environmental conditions will be described.

1.6 References

1.   Harbury, P. B.; Zhang, T., A switch between two-, three-, and four-stranded coiled coils in GCN4 leucine zipper mutants. *Science* **1993,** 262, (5138), 1401.

2.   Wright, E. R.; Conticello, V. P., Self-assembly of block copolymers derived from elastin-mimetic polypeptide sequences. *Adv Drug Deliv Rev* **2002,** 54, (8), 1057-73.

3.   Stevens, M. M.; George, J. H., Exploring and Engineering the Cell Surface Interface. *Science* **2005,** 310, (5751), 1135-1138.

4.   Karlsson, A.; Karlsson, M.; Karlsson, R.; Sott, K.; Lundqvist, A.; Tokarz, M.; Orwar, O., Nanofluidic Networks Based on Surfactant Membrane Technology. *Anal. Chem.* **2003,** 75, (11), 2529-2537.

5.   Whitesides, G. M.; Grzybowski, B., Self-Assembly at All Scales. *Science* **2002,** 295, (5564), 2418-2421.

6.   Whitesides, G. M.; Boncheva, M., Supramolecular Chemistry And Self-assembly Special Feature: Beyond molecules: Self-assembly of mesoscopic and macroscopic components. *Proceedings of the National Academy of Sciences* **2002,** 99, (8), 4769-4774.

7.   Janmey, P. A.; Shah, J. V.; Tang, J. X.; Stossel, T. P., Actin filament networks. *Results Probl Cell Differ* **2001,** 32, 181-99.

8.   Au, Y., The muscle ultrastructure: a structural perspective of the sarcomere. *Cell Mol Life Sci* **2004,** 61, (24), 3016-33.

9.   Yonekura, K.; Maki-Yonekura, S.; Namba, K., Growth mechanism of the bacterial flagellar filament. *Res Microbiol* **2002,** 153, (4), 191-7.

10.   Behanna, H. A.; Donners, J. J.; Gordon, A. C.; Stupp, S. I., Coassembly of amphiphiles with opposite peptide polarities into nanofibers. *J Am Chem Soc* **2005,** 127, (4), 1193-200.

11.   Collier, J. H.; Hu, B. H.; Ruberti, J. W.; Zhang, J.; Shum, P.; Thompson, D. H.; Messersmith, P. B., Thermally and photochemically triggered self-assembly of peptide hydrogels. *J Am Chem Soc* **2001,** 123, (38), 9463-4.

12.   Zhang, S.; Holmes, T.; Lockshin, C.; Rich, A., Spontaneous assembly of a self-complementary oligopeptide to form a stable macroscopic membrane. *Proc Natl Acad Sci U S A* **1993,** 90, (8), 3334-8.

13.   Yamada, K. M., Adhesive recognition sequences. *J Biol Chem* **1991,** 266, (20), 12809-12.

14.   Rajagopal, K.; Ozbas, B.; Pochan, D. J.; Schneider, J. P., Probing the importance of lateral hydrophobic association in self-assembling peptide hydrogelators. *Eur Biophys J* **2006,** 35, (2), 162-9.

15.   Woolfson, D. N.; Ryadnov, M. G., Peptide-based fibrous biomaterials: Some things old, new and borrowed. *Curr Opin Chem Biol* **2006,** 10, (6), 559-67.

16.   Crick, F., The packing of [alpha]-helices: simple coiled-coils. *Acta Crystallographica* **1953,** 6, (8-9), 689-697.

17.   Kojima, S. K., Y.; Yoshida, T.; Yazaki, K.; Miura, I., Fibril Formation by an Amphipathic a-Helix-Forming Polypeptide Produced by Gene Engineering. *Proceedings of the Japan Academy. Ser. B: Physical and Biological Sciences* **1997,** 73, (1), 7-11.

18.   Pandya, M. J.; Spooner, G. M.; Sunde, M.; Thorpe, J. R.; Rodger, A.; Woolfson, D. N., Sticky-end assembly of a designed peptide fiber provides insight into protein fibrillogenesis. *Biochemistry* **2000,** 39, (30), 8728-34.

19.   Potekhin, S. A.; Melnik, T. N.; Popov, V.; Lanina, N. F.; Vazina, A. A.; Rigler, P.; Verdini, A. S.; Corradin, G.; Kajava, A. V., De novo design of fibrils made of short alpha-helical coiled coil peptides. *Chem Biol* **2001,** 8, (11), 1025-32.

** Protein Data Bank structure of GCN4-pIL dimer (27TA), GCN4-pII trimer (1GCM) and GCN4-pLI tetramer (1GCL) shown.

Chapter II: A pH-responsive switch for helical fiber formation

2.1 Introduction

The coiled-coil structural motif has been shown to serve as a practical template for the design of novel synthetic peptide systems capable of self-assembling into structurally-defined long-aspect-ratio fibers. Through the incorporation of key structural elements of native biological systems into *de novo* design strategies, several groups have reported the generation of biomimetic fiberous suprastructures of predictable measurements.[3,4,5,7] However, native biomolecular assemblies are recognized not only for their well-defined structures, but also for their capacity to demonstrate an array of vital functionalities.

A particularly tantalizing functionality displayed by native protein complexes is their ability to undergo a significant conformational change upon sensing incremental changes in their physical environment, such as temperature, metal ion concentration, the presence of small molecules or pH shifts.[9,11,13,15,16] Accordingly, the structural determinants which facilitate this behavior in natural systems are hypothesized to provide inspiration for the design of novel responsive mechanisms in synthetic functional materials.

A significant challenge remains in the creation of novel soft materials which exhibit a predictable response upon the sensing of specific stimuli in their surroundings. In native coiled-coil structures, critical determinants of self-assembly between protomers frequently involve specific recognition at the interfaces between the structural elements. For example, the quaternary structure of native coiled-coil assemblies is strongly coupled

to the identities of residues in the canonical heptad motif which comprising the hydrophobic core *a*- and *d*-positions and the charged *e*- and *g*-positions defining the interhelical interface. Control over the nature of these contacts through the introduction of stimuli-responsive amino acids can modify the stabilization of the complex to provide a mechanism for the dynamic control of the assembly.

In this manner, a series of synthetic coiled-coil assemblies have been generated which utilize light, pH, temperature and ionic strength as external stimuli for inducing an observable conformational transition (**Table 2.1**). The use of amino acids which can be ionized under appropriate pH conditions is an approach used in many of these constructs to facilitate dynamic assembly of the coiled-coil structure. For example, glutamic acid residues in the *e*- and *g*-positions destabilize the interhelical interface of a coiled-coil when the complex is assembled under significantly basic pH conditions. This approach has been utilized to assemble gold nanoparticle aggregates upon a pH triggering event and also to initiate fiber disassembly with charge screening upon increasing ionic strength.[17,5]

In this chapter, a pH-responsive mechanism programmed into the hydrophobic core of a trimeric coiled-coil motif is shown to facilitate control over the reversible assembly of a long-aspect-ratio helical fiber. This behavior is coupled to a pH-induced conformational change in the peptide system.

Sequence	Stimuli	Response
SGDLENEVAQLEREVRSLEDEAAELEQ-KVSRLKNEIEDLEAE [2]	pH 4.5 - 11.2	α-helical coiled-coil to random coil
KIAALKQKIASLKQEIDALEYENDALEQ [4, 5]	Ionic strength, [KF]	coiled-coil to random coil
KIRALKAKNAHLKQEIAALEQEIAALEQ	pH (6.5 and 7.5)	α-helical coiled-coil to random coil
AALEKEIAALEQEIAALEKEIAALEYEN-AALEKEIAALEQE [6]		
YIHALHRKAFAKIARLERHIRALEHAA [8]	Zinc(II) ion	coiled-coil to β-hairpin
KIAALKQKIASLKQEIDALEYENDALEQ-KIAALEQ [10]	Ionic strength, [KCl]	coiled-coil to random coil
EIAQLEYEISQLEQ [12]	pH	random coil to coiled-coil
EIAQLEYEISQLEQEIQALES		
KIAQLKYKISQLKWKIQSLKQ		
IGKLKEEIDKLNRDLDDMEDENEQLKQ-ENKTLLKVVGKLTR [14]	Temperature	random coil to α-helix
	(0 ºC at pH 5.75)	
	Ionic strength	

Table 2.1. A compilation of environmentally-responsive peptide systems based on α-helix, random coil and/or coiled-coil structural motifs.

2.2 Results

2.2.1 Design of TZ1H peptide sequence

The amino acid sequence of peptide **TZ1H** was designed with inspiration from the isoleucine zipper peptide GCN4-pII, the latter of which was shown on the basis of crystallographic and analytical ultracentrifugation data to form a triple-stranded coiled-coil assembly.[18] The 41-residue peptide sequence of GCN4-pII is organized into six tandem heptad repeats ([*a-b-c-d-e-f-g*]$_6$), in a fashion reminiscent of the native coiled-coil structural motif. Structural studies of native and mutant coiled-coil complexes have established that the identity of residues occupying the *a*- and *d*-positions in the heptad will strongly direct the oligomerization state of coiled-coil assemblies. Therefore, the incorporation of isoleucine residues into the majority of the core-forming positions of **TZ1H** was hypothesized to favor the formation of a trimeric assembly, as exemplified in the GCN4-pII coiled-coil complex.

A pH-responsive mechanism was engineered into the **TZ1H** peptide through the introduction of histidine residues in core forming *d*-positions of alternate heptads. (**Figure 2.1-Top**). In a cross-sectional diagram of the helical fiber, illustrated in **Figure 2.1-Bottom**, the core histidine residues occupy adjacent positions across the helical interface. It was hypothesized that protonation of the proximally-arranged, imidazole side chains to their charged state will introduce an electrostatic destabilization within the core of the helical fiber. The presence of multiple charged moieties
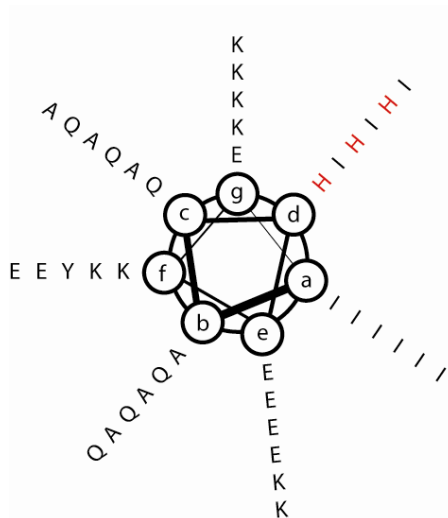
AcNH- E IAQ**H**EKE IQAIEKK IAQ**H**EYK IQAIEEK IAQ**H**KEK IQAIK -CONH2
abcdefg abcdefg abcdefg abcdefg abcdefg abcde
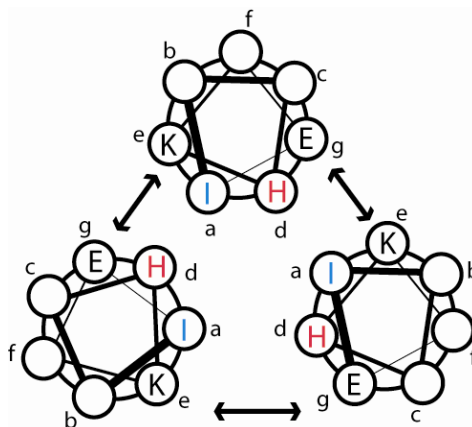
Figure 2.1. **(Top) Helical wheel diagram of a single TZ1H helical peptide and (below) the associated primary sequence. (Bottom) Cross-sectional view of a triple-stranded helical bundle formed through the self-assembly showing core-forming *a*- and *d*-position occupied by isoleucine (blue) or histidine (red). Note, the majority of the hydrophobic core consists of isoleucine residues expect for histidine in the *d*-position of alternate heptads.**

38

within the hydrophobic tunnel of the coiled-coil fiber was predicted to trigger disassembly of the fibrous aggregate. As a consequence, the protonation state of the histidine side chain would determine the stability of the helical fiber and furthermore, provide a mechanism which couples incremental changes in pH near the pK_a of the imidazole group to the self-assembly of the **TZ1H** peptide system.

The amino acid sequence of **TZ1H** peptide was also designed to possess a network of cooperative electrostatic interactions between the *e-* and *g*-position residues which define the solvent-accessible interstrand interface. The placement of these charged residues are fully complementary only in a staggered alignment in which the peptides self-organize with an axial stagger of two heptads, or 1/3 the peptide length, between adjacent helical strands. The enforced staggered regime should generate multiple helical protomers, which are capable of adding lengthwise to generate a helical rope (**Figure 2.2**).

2.2.2 Circular dichroism (CD) spectrometry

CD spectroscopy offers a convenient technique for probing α-helical structure in coiled-coil systems.[19] To investigate the effect of the isoleucine to histidine mutation on the self-assembly of **TZ1H**, CD spectroscopy was performed on 60 μM peptide solutions (10 mM phosphate, 4 °C) prepared at pH 8.1, significantly above the pK_a of the histidine side chains. A characteristic α-helical trace, with negative CD signals at 208 and 222 nm, was observed for **TZ1H** possessing the neutral form of histidine within the hydrophobic core (**Figure 2.3**).

Helical Peptide

Heptad

Trimeric Protomer
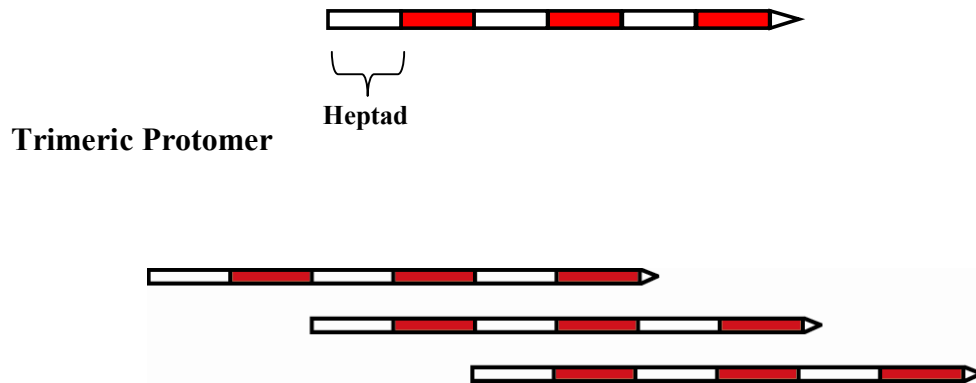
Helical Fiber
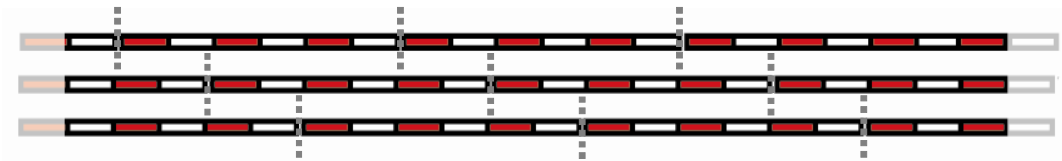
Figure 2.2. Staggering of adjacent monomers is achieved through cooperative Coulombic interactions programmed into the primary sequence at the e- and g-positions within the individual heptads. Note the alignment of histidine (red) containing heptads. (Top) Axial displacement of 2 heptad units results in helical protomer assembly while (Bottom) fiber formation results from the lengthwise addition of protomers.
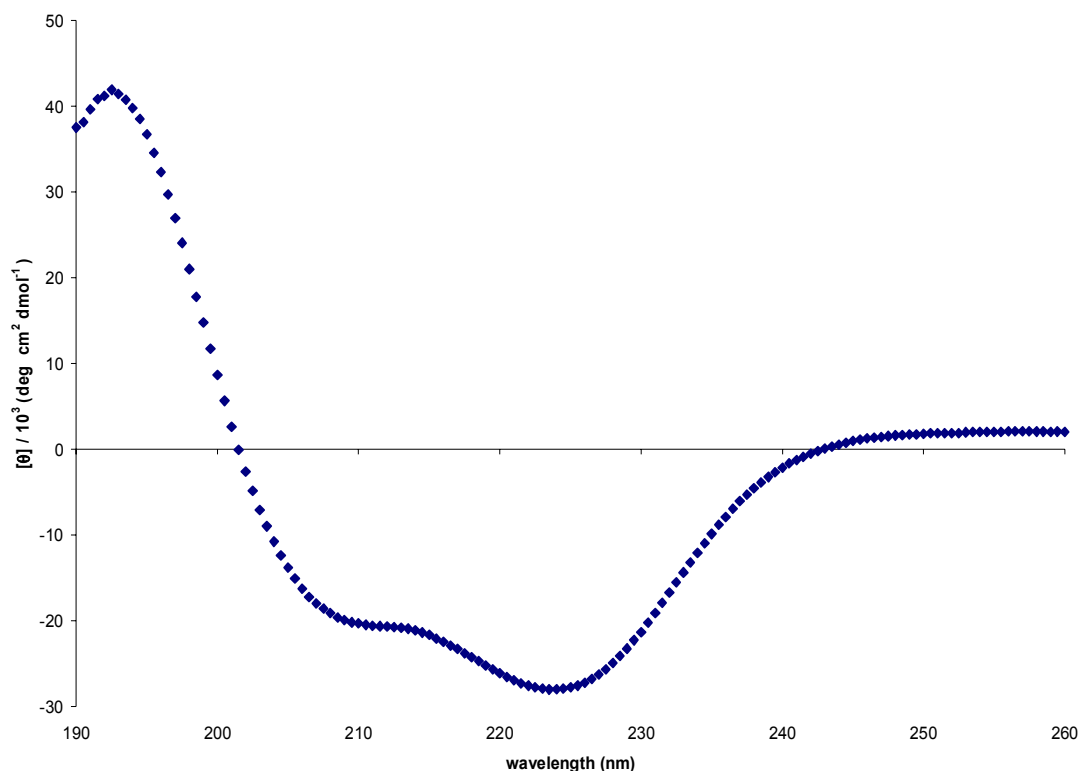
Figure 2.3. **Circular dichroism spectrum of TZ1H peptide (60 μM, 10 mM phosphate, pH 8.1).** **Minima observed at 222 and 208 nm indicate α-helical secondary structure.**

Based on the CD signal at 222 nm ($[\theta]_{222}$), the fractional helicity of the species was determined to be 70% for **TZ1H** assembled at 60 μM peptide concentration. This is in agreement with values reported in synthetic coiled-coil fibrils.[6] However, a particularly striking feature of the CD spectra is observed in the ratio of $[\theta]_{222}$ / $[\theta]_{208}$, a qualitative indicator of helix-helix interactions. The idealized $[\theta]_{222}$ / $[\theta]_{208}$ ratio for a monomeric helix is cited as 0.9, while for coiled-coil assemblies it is approximately 1.1. For **TZ1H** peptide prepared at pH 8.1, the observed $[\theta]_{222}$ / $[\theta]_{208}$ value was 1.43, which

indicates coiled-coil content. However, visual inspection of the CD spectrum suggests this value is impacted by a significant attenuation and shifting to longer wavelength around the 208 nm minimum. This behavior is associated with light-scattering within the solution, presumably caused by the precipitation of peptide. Indeed, visual inspection of **TZ1H** peptide solution prepared under fiber-forming conditions at concentrations ranging between 50 and 100 µM showed clouding when incubated for as little as 1 hour at 5 $^{\circ}$C or room temperature. Evidence of helical fibers localized to the suspended precipitant was obtained by briefly centrifuging the clouded sample and collecting CD spectra on the re-suspended pellet and supernatant.

To investigate the effect of peptide concentration on the extent of precipitation, CD spectrometry was performed on **TZ1H** (10 mM phosphate, pH 8.1) prepared across a range of peptide concentrations from 4 to 61 µM (**Figure 2.4**). Significant attenuation of signal and shifting to a longer wavelength was observed in solutions assembled above approximately 20 µM peptide concentration. On the opposite extreme of the concentration array, the observed value of $[\theta]_{222}$ / $[\theta]_{208}$ for **TZ1H** peptide solutions prepared below 10 µM indicate a loss of helix-helix interactions. Therefore, the optimal working concentration for subsequent experiments was determined to be between 10 and 20 µM.

2.2.3 Conformational changes in peptide TZ1H

To access the pH-dependant self-assembly behavior of **TZ1H**, aliquots of peptide were prepared at 9.85 µM in 10 mM phosphate buffer at across a pH gradient ranging from pH 4.0 – 8.0 in approximately 0.5 pH-unit increments. Circular dichroism

42
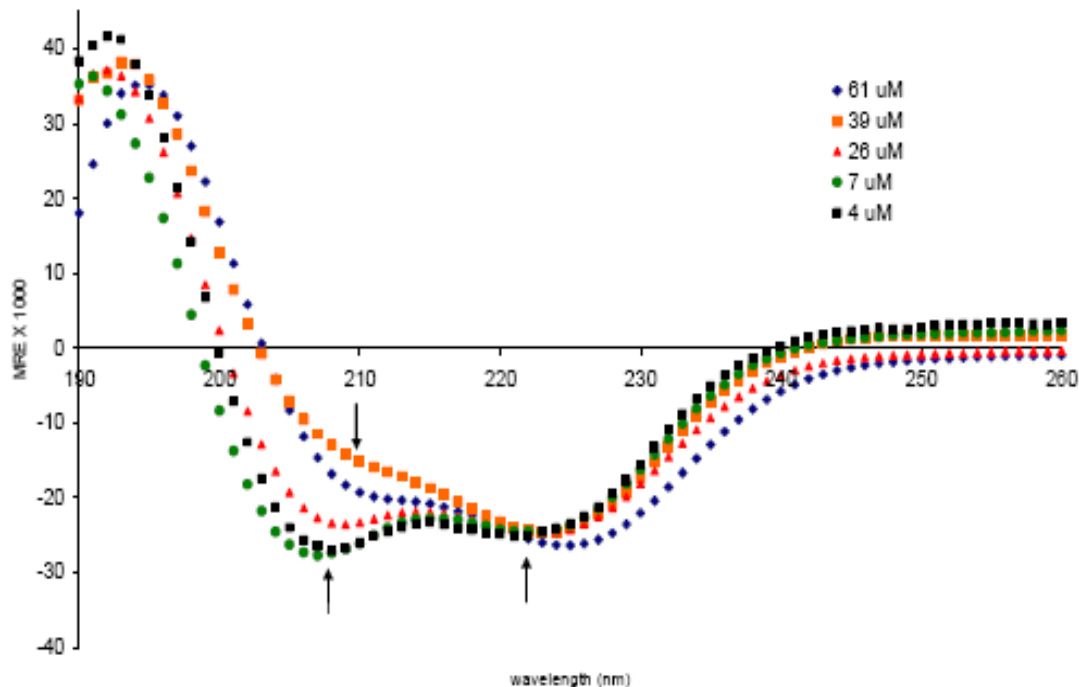
Figure 2.4. Concentration dependence of the circular dichroism spectra of TZ1H in 10 mM phosphate buffer, pH 8.3 at 25 °C. Lower arrows indicate the positions of the characteristic α-helical minima at 208 nm and 222 nm. The upper arrow indicates the effect of increased self-assembly due to higher concentration on the absorption at 208 nm, which results in attenuation of the signal and a shift to longer wavelengths.

spectroscopy performed on **TZ1H** peptide solutions indicated the observed peptide conformation was strongly dependant on the pH of the surrounding buffer solution (**Figure 2.5**).

The role histidine residues play in the pH-induced conformational transition can be better understood in plotting mean residue ellipticity at 222 nm ($[\theta]_{222}$) as a function of pH (**Figure 2.5-inset**). The observed MRE values were weakly negative within the pH range from 4.0 to 5.5, indicating marginal helicity. However, a large change in $[\theta]_{222}$ was observed over the pH range from 5.6 to 6.5, with an inflection point observed at pH 5.8. The limiting value of helicity was observed at higher pH.

Peptide samples prepared at pH values between 6.5 and 8.0 displayed a strongly α-helical CD signature with minima at both 208 and 222 nm. The limiting value for the fraction helicity at pH 8.0 was calculated as 87%. Furthermore, the value of the $[\theta]_{222}$ / $[\theta]_{208}$ ratio at pH 8.0 was 1.07, which was within the expected range for a coiled-coil assembly. In contrast, **TZ1H** peptide solutions at pH values in the range of 5.6 − 4.0 showed a loss of α-helical CD signal with the emergence of a new minimum at approximately 201 nm, which is suggestive of significant content of random-coil conformation. Additionally, a near-isodichroic point was observed at 203 nm across the pH-dependant CD spectra, which is consistent with a helix-coil conformational transition.

Furthermore, this helix-to-coil transition mechanism was determined to be fully reversible as a function of pH by CD spectroscopy. Peptide **TZ1H** prepared in buffer at pH 4.0 showing high coil content could be converted to α-helix by raising the solution pH to 8.0, then immediately returned back to the initial coil conformation by lowering the solution pH to 4.0 (**Figure 2.6**). Similarly, the reversibility of conformational transition from helix-to-coil was also demonstrated.
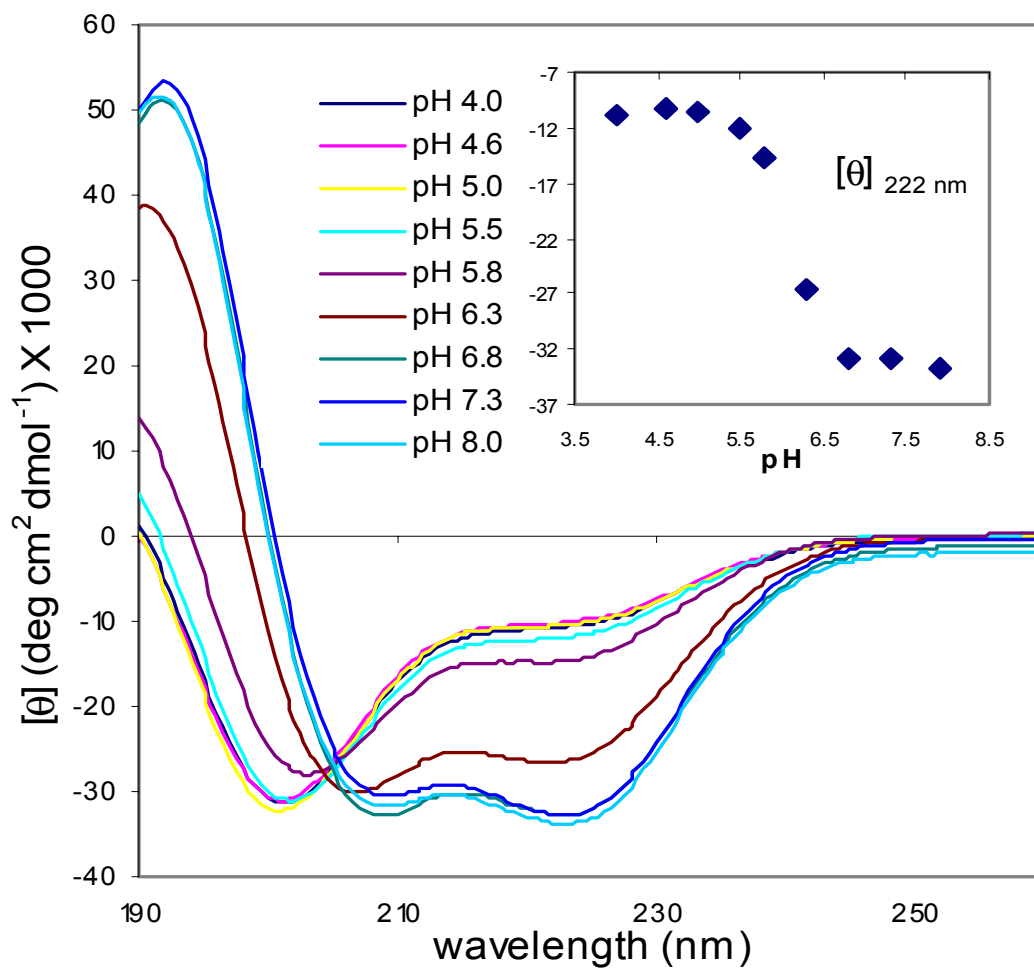
Figure 2.5. CD spectroscopy shows pH-dependence of α-helicity in TZ1H solutions (9.85 μM, 10 mM phosphate, 4 °C) prepared across a pH range of 4.0 - 8.0. (Inset) Mean residue ellipticity at 222 nm for TZ1H as a function of pH.
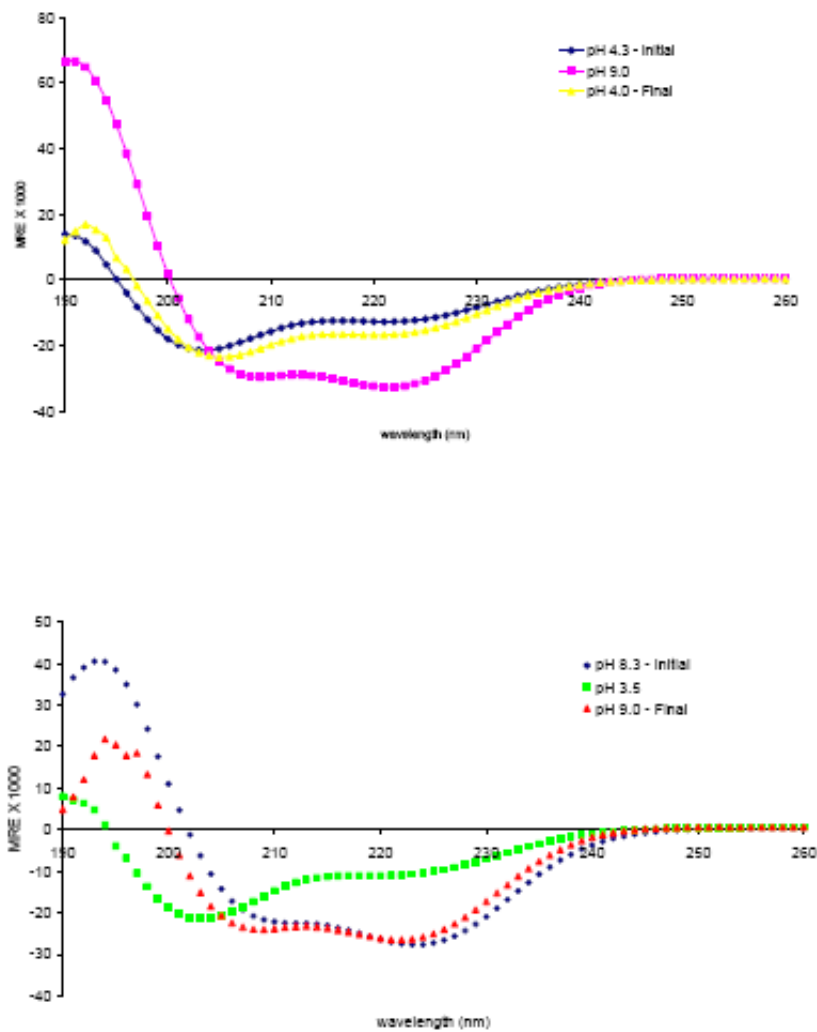
Figure 2.6. Reversibility of the pH-induced conformational transition of peptide TZ1H determined by CD spectrometry. (Top) CD spectra for the coil-helix-coil transition of TZ1H (35 μM, 10 mM phosphate, 25 ºC). (Bottom) CD spectra for the helix-coil-helix transition of TZ1H (30 μM, 10 mM phosphate, 25 ºC).

2.2.4 Transmission Electron microscopy

Conventional transmission electron microscopy (TEM) was utilized in the visualization of **TZ1H** peptide samples prepared at pH 4.0 and 8.2, which define the limits of random coil and helix conformations, respectively. Multiple attempts at imaging **TZ1H** peptides prepared at pH 4.0, using several different negative stains and sample application methods, provided negligible evidence of fiber formation. This observation is in agreement with the hypothesis that α-helical secondary structure is vital to helical fiber formation in the **TZ1H** peptide system.

However, peptide samples prepared under basic conditions (pH 8.2) and at concentrations between 50 – 100 μM, routinely showed an abundance of long-aspect-ratio fibers with diameters ranging between 40 and 100 nm (**Figure 2.7**). However, the observed diameter dimensions were at least one order of magnitude larger than the approximated diameter for a triple-stranded helical bundle. This phenomenon is frequently reported in other helical self-assembling peptide systems and has been attributed to lateral associations between adjacent fibers in a process termed thickening.[20]

2.2.5 Cryo-electron microscopy tomography

Cryo-electron tomography (CET) is a technique which provides access to information concerning the internal structure of large molecules and supramolecular assemblies in their native, hydrated state.[21] This is achieved through recording projection images of a single object from multiple angles and computationally
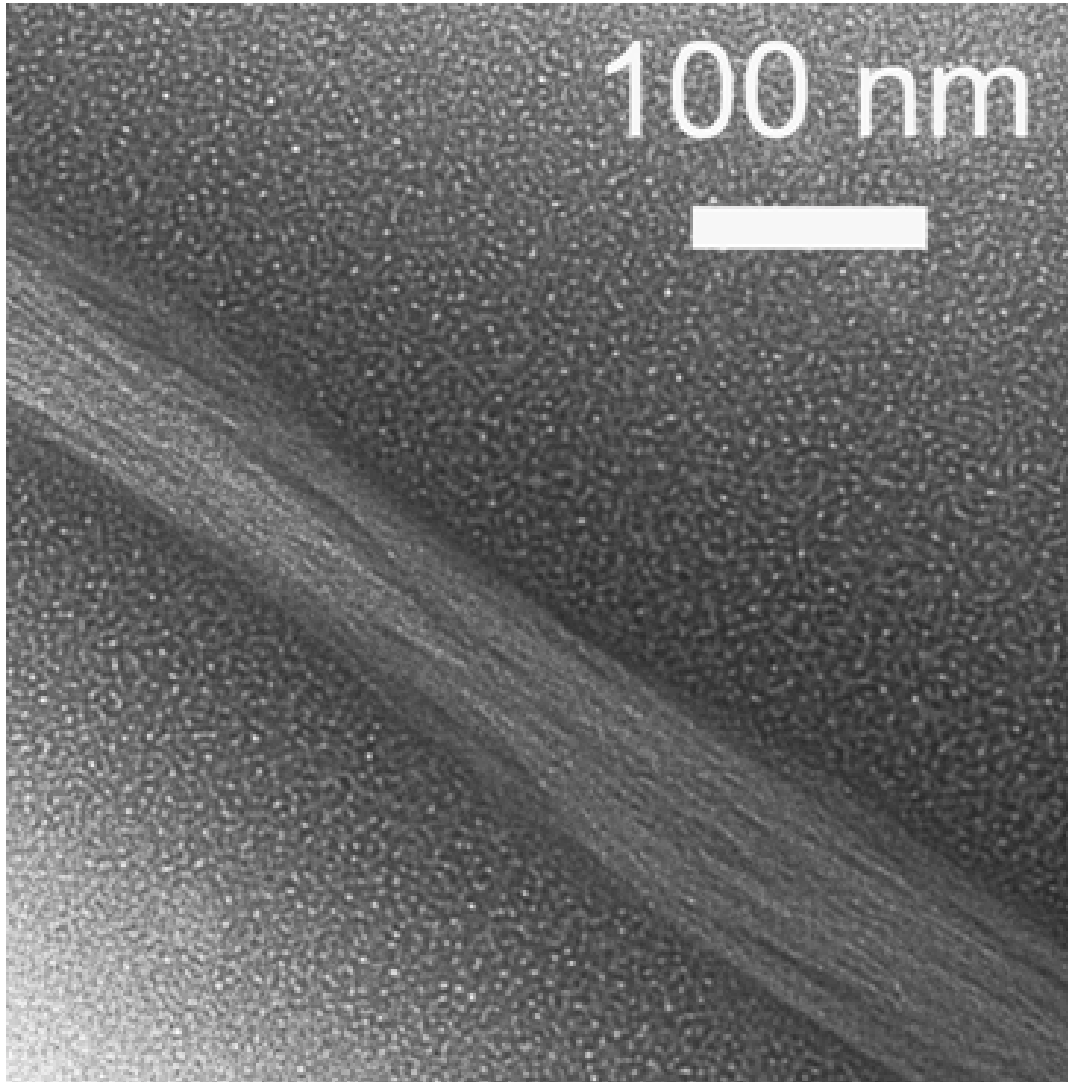
Figure 2.7. Negative-stain TEM image of 100 μM TZ1H peptide assembled at pH

8.2 showing a large-diameter fiber bundle of approximately 100 nm diameter.

recombining the data into a three-dimensional reconstruction. In electron tomography, a collection of two dimensional images are generated by incrementally tilting the sample on one or two axis. Subsequently, a final reconstruction is computationally assembled.

Insight into the internal organization of large-diameter **TZ1H** fibers was provided through the employment of cryo-electron tomography (CET) with Dr. Elizabeth Wright. A three-dimensional image volume was constructed from a single axis tilt series collected from a vitrified thin sample of **TZ1H** fibers. The three-dimensional reconstruction was compiled into a movie from the individual image stacks and cross-sectional images parallel to the fiber axis were obtained as frame captures of the movie. Mid-sample slices suggest large-diameter fibers are composed of interwoven, thinner-diameter fibrils, the later of which possess a range of diameters, from 26-122 nm (**Figure 2.8** and **2.9**). The dimensions of the observed smaller-diameter fibrils closely agree with those reported for isolated fibers in negative-stain TEM images.

2.2.6 High resolution scanning electron microscopy

Low-temperature, high-resolution scanning electron microscopy (LT-HRSEM) was employed in the investigation of **TZ1H** bulk solution morphology. This technique provides topographical information of frozen, hydrated samples in bulk solution without the use of chemical fixatives or stains. Aqueous samples are cryoimmobilized in liquid ethane (-183 ^{o}C) and the surface features of the specimen are exposed through controlled

49
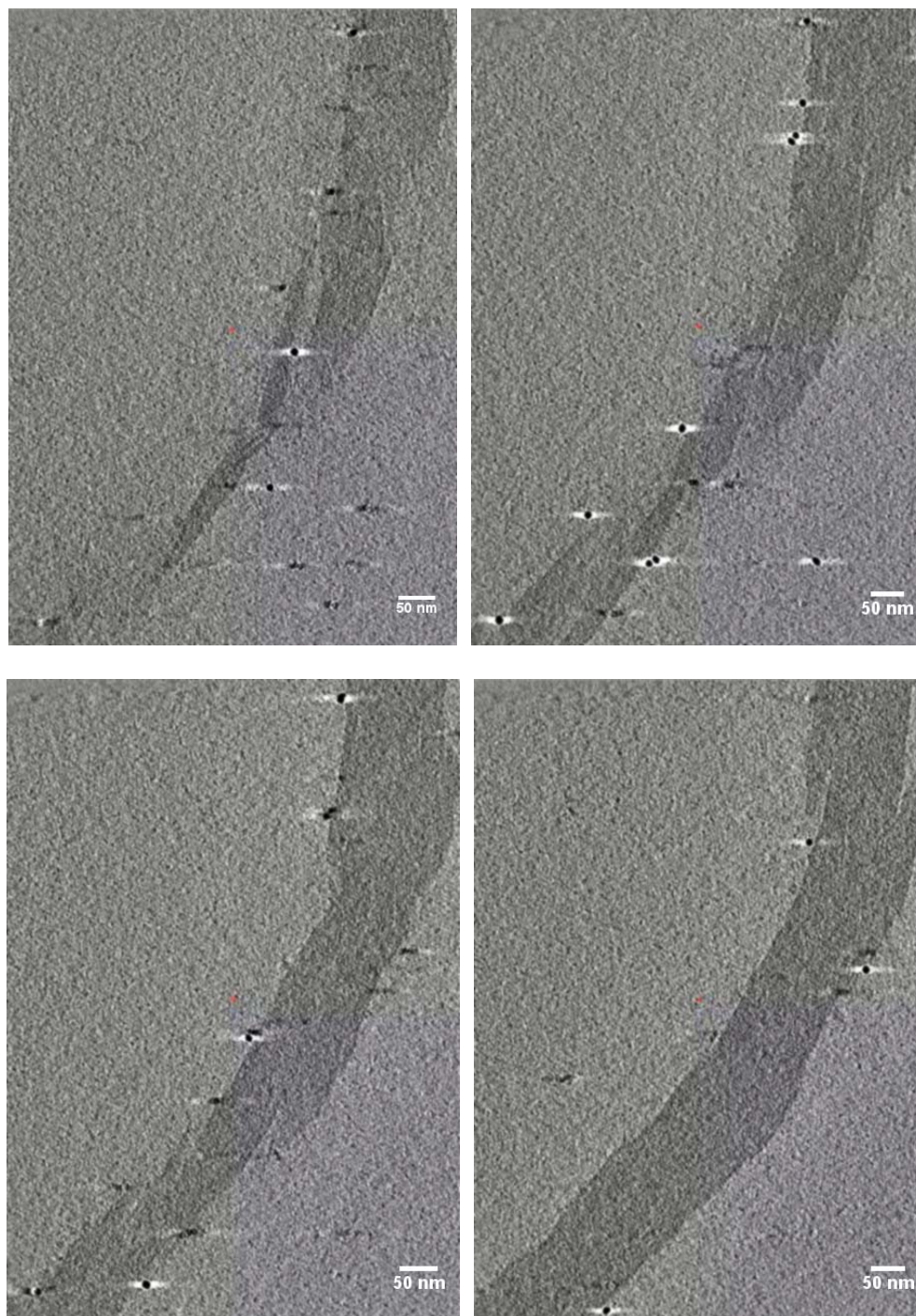
Figure 2.8. Sequential cryoTEM tomography slices through an isolated large-diameter TZ1H peptide fiber. Black spheres are 10 nm gold fiducial markers used to align images during 3-D reconstruction.
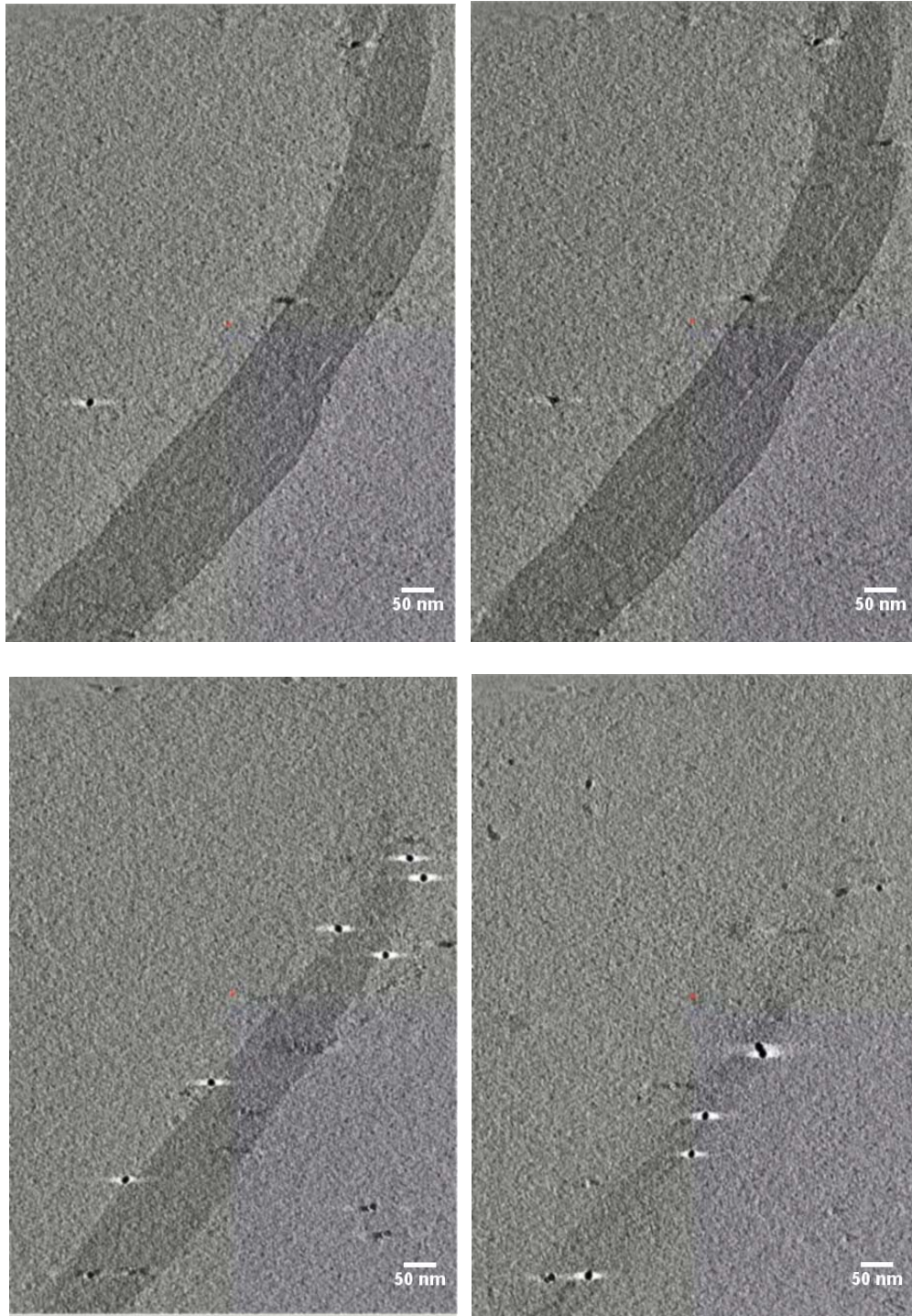
Figure 2.9. CryoTEM tomogram (continued)

s

ublimation of bulk water around the specimen.

At pH 8.1, large-diameter fibers with diameters in excess of 100 nm were served, in agreement with conventional and cryo TEM. However, these images also revealed large helical bundles entangled within a dense network of small-diameter fibrils (**Figure 2.10-Top**). The majority of the fibrils are of uniform diameter and heavily intertwined with one another, such that isolated fibers were seldom encountered in any viewing field. Intermediate and high magnification images confirmed the presence of two distinct species in assembled **TZ1H** samples - either smooth, featureless large diameter fibers (72 ± 2.8 nm) or small-diameter (11.3 ± 0.3 nm) fibrils (**Figure 2.10-Bottom**). Large-diameter fibers were spatially separated and rarely observed in contact with fibers of similar diameter. However, thinner-diameter fibers made extensive contacts with one another, comprising a landscape of proteinatous networks.

Furthermore, the extensive proteinatous meshwork revealed by LT-HRSEM provides visual evidence supporting microrheology data previously collected on the **TZ1H** peptide system by Dr. Yuri Zimenkov. Microrheology is a technique which can determine the storage and dissipation of mechanical energy in soft, nanoscale materials by examining the Brownian motion of sub-micron particles suspended in the solution using optical microscopy.

When assembled under buffer conditions pH 4.0 and pH 8.0, representing random-coil and helical secondary structure respectively, the **TZ1H** peptide system displayed very different microrheological properties. Under fiber forming conditions in buffer pH adjusted to 8.0, the peptide solution exhibited an elastic storage modulus, $G'(\omega)$, higher than the viscous loss modulus, $G''(\omega)$ at all frequencies probed.
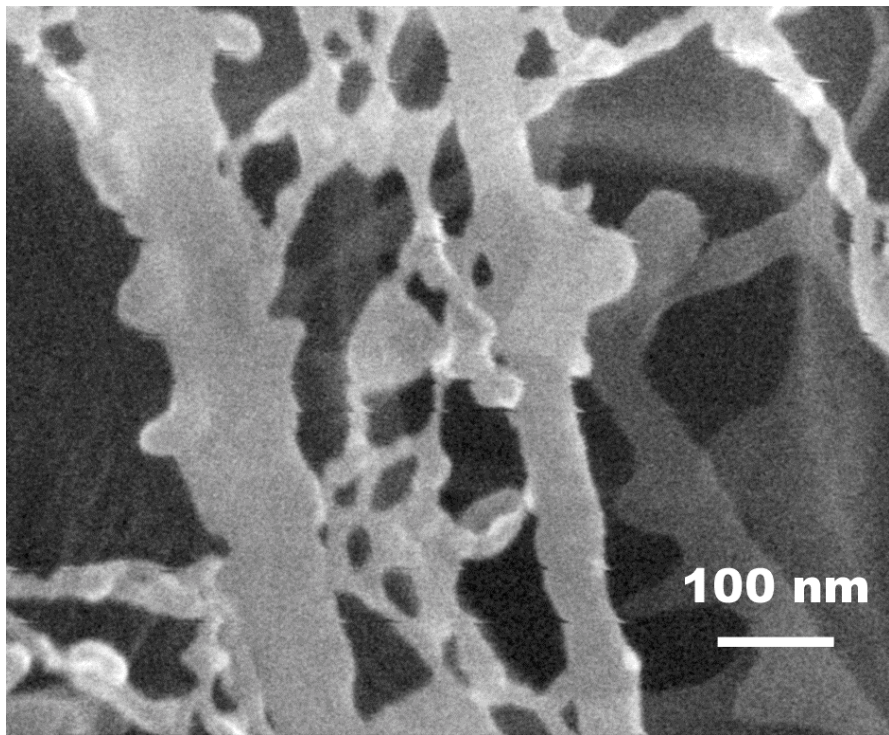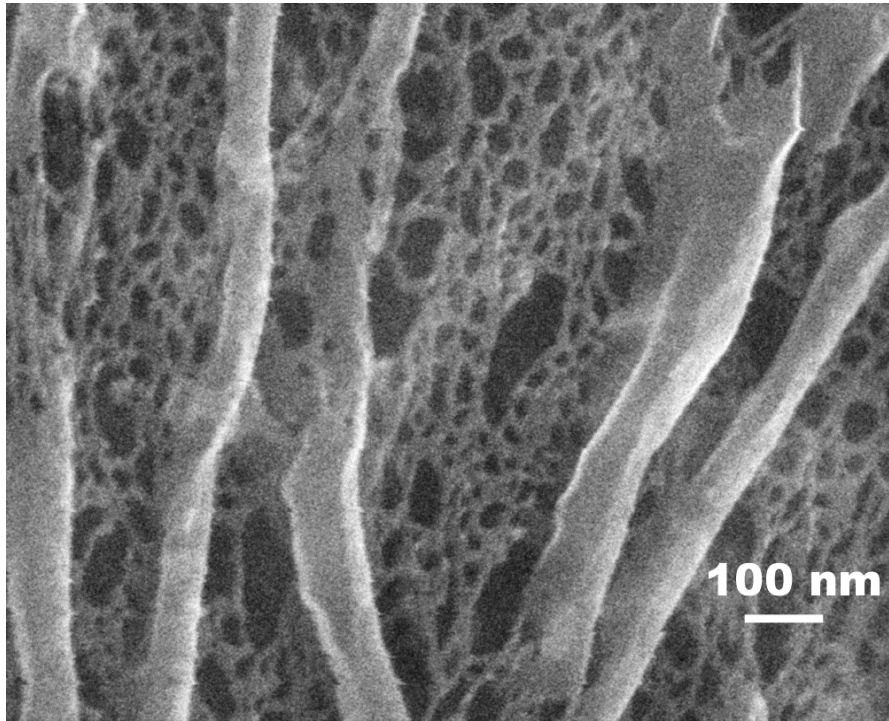
Figure 2.10. Low (Top) and intermediate (Bottom) magnification HRSEM image reveals fine, proteinatous mesh of fibers intertwined with large diameter bundles.

Conversely, the viscous modulus of **TZ1H** peptide prepared at pH 4.0, corresponding to conditions which result in random coil conformation, closely resembled that of water (**Figure 2.11**). This observation suggests little association between monomeric **TZ1H** peptides when assembled at lower pH, thereby supporting our proposal that helical secondary structure is linked to fiber formation.
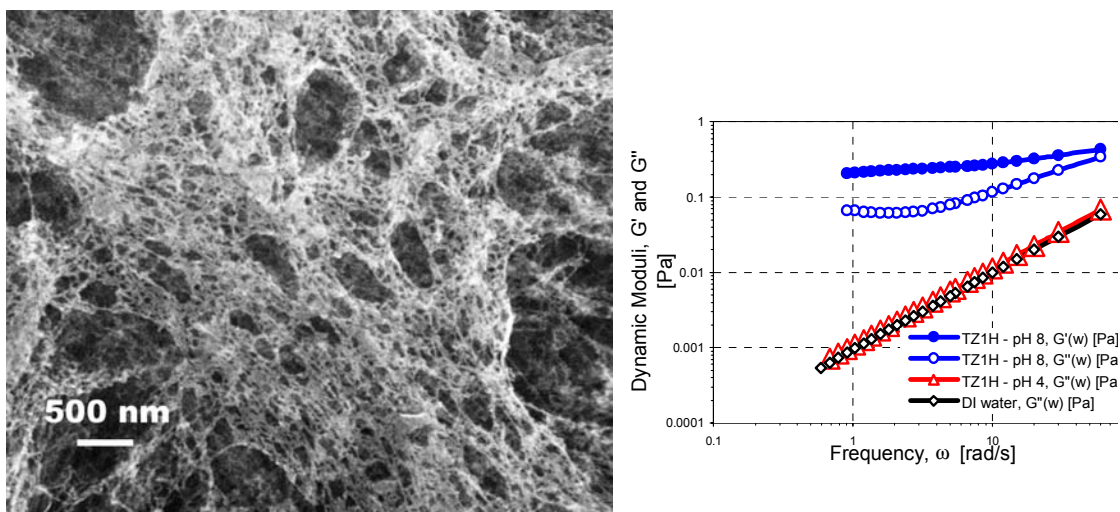
Figure 2.11. (Left) Low magnification SEM image shows entangled fibrils make extensive contacts. (Right) Sharp differences in pH-responsive behavior demonstrated by microrheology.[1]

2.2.7 Modifications to TEM protocols

Previous TEM imaging show only fibers possessing diameters in excess of 100 nm, while supplementary electron microscopy techniques suggested smaller diameter fibers were represented in the self-assembled system. Attempts to modify the existing TEM sample preparation protocol, including longer staining with alternate stains, proved

to be critical in revealing the small diameter fibers. Negative stains are reagents composed of heavy atoms, which are used in transmission electron microscopy to provide a uniform, electron-dense background. A mixture of two negative stains with complementary qualities was utilized. Methylamine vanadate has a low atomic number (23) relative to conventional negative stains such as uranium (92) and tungsten (74). It is frequently used to visualize small diameter objects, such as 1.4 nm gold markers, since it does not obscure small objects like heavier atom stains. Mixed 1:1 with methylamine vanadate was a methylamine tungstate solution, the later being an organotungsten compound known for excellent spreading quality and providing high density contrast.

With the assistance of this alternative negative stain and higher magnification imaging, TEM images were obtained revealing the presence of much thinner fibrils, possessing diameters of 3.3 ± 0.7 nm (**Figure 2.12** and **2.13**). This value is more closely aligned with estimated lateral dimensions of trimeric helical bundles. These species were imaged either in isolation, in loose association with each other or within larger diameter fiber bundles. Furthermore, close inspection of the large diameter fibers revealed longitudinal striations with diameters of 2.5 ± 0.3 nm, reminiscent of isolated fibrils. This suggests the large diameter fibers are composed of associated bundles of smaller diameter fibrils.

Figure 2.12. Higher magnification TEM image of large diameter bundles reveals longitudinal striations displaying diameters reminiscent of isolated small diameter fibrils.
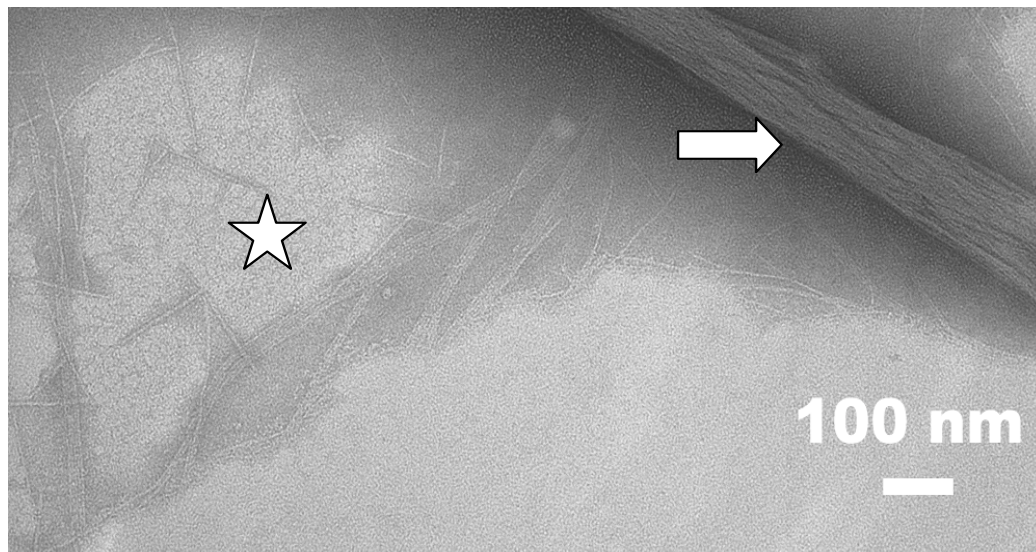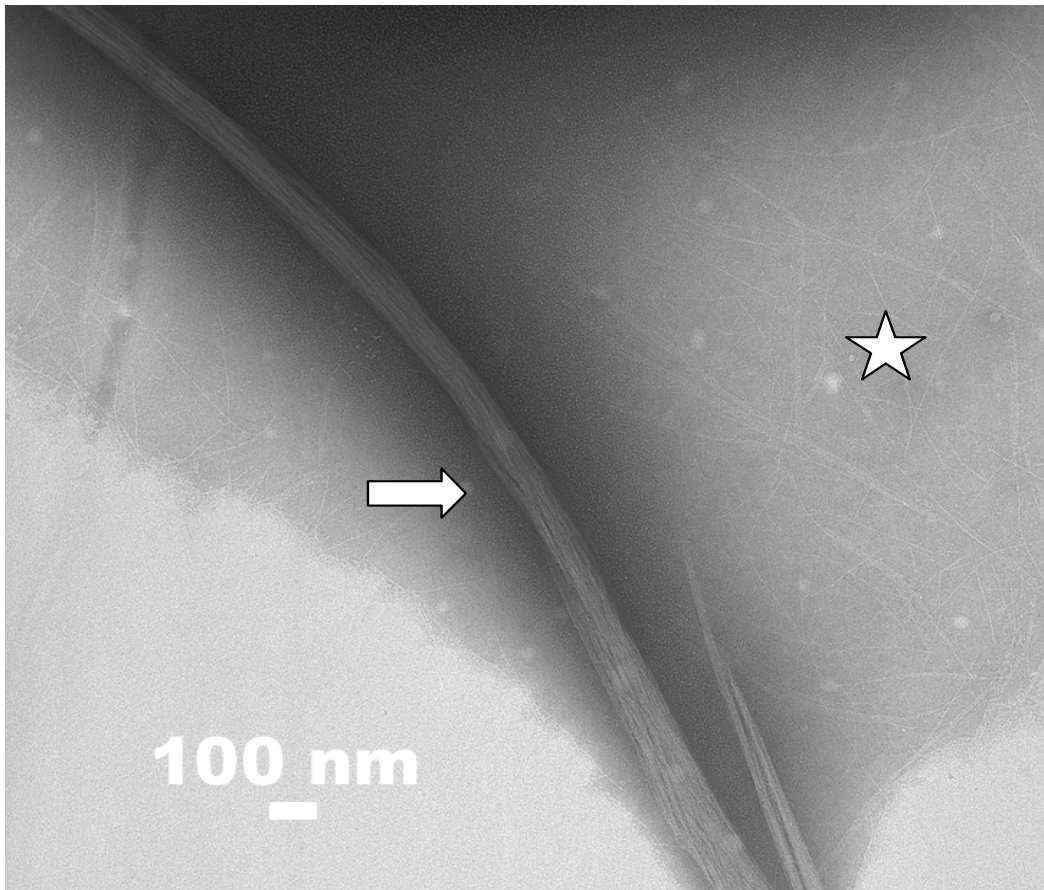
Figure 2.13. Conventional TEM imaging showing approximately 3 nm fibrils mixed with large-diameter helical bundles. Stars mark an area containing thin-diameter fibrils and arrows large helical bundles.

2.3 Summary

The rational design scheme described in this chapter provides a straightforward approach to producing novel nanoscale materials capable of responding predictably to distinct environmental cues. The self-assembly of a synthetic peptide into a well-defined, fibrous material was shown to proceed through a mechanism coupling peptide conformation to the protonation of core-forming residues.

2.3.1 A depressed pKa value for the buried histidine side chain

In our working model for the pH-dependant conformational switch, a secondary structure transition occurs in response to the protonation state of d-layer histidine side chains, thereby coupling the pK_a of the imidazole sidechain to fiber formation. In the **TZ1H** peptide system, a sharp coil-helix transition was observed by circular dichroism to occur within a very narrow pH range, displaying a prominent inflection point at pH 5.8.

However, the commonly cited value for the pK_a for a free imidazole ring is near physiological pH, where side chain ionization can be easily modulated by the aqueous environment. This is particularly useful in enzymes which utilize histidine residues on the protein surface as critical nucleophiles or electrophiles in substrate transformations. For example, in staphylococcal nuclease (SNase) the pK_a values for a solvent-exposed histidine was measured as 6.53.[22] A similar value was reported in synthetic model system, in which the pK_a for a solvent-exposed histidine in a small, non-helical peptide (Ac-AAHA-NH$_2$) was observed to be 6.88. [23] Intriguingly, the experimentally-deduced

value for the pK_a of core-forming histidine side chains in the **TZ1H** system was 5.8, which is significantly lower than examples cited above.

However, pKa values for histidine residues have been shown to vary greatly, depending on the identity and spatial proximity of neighboring amino acids. In fact, depressed pK_a values have been reported for histidine residues in hydrophobic environments, such as within folded proteins. A particularly relevant example of lower histidine pK_a values can be found in a series of synthetic four-helix bundles where *d*-layer histidines pK_a values were measured between 5.2 and 6.0.[24] Likewise, in the SNase experiment above, the pKa values for two histidine residues buried in hydrophobic microenvironments within the protein were depressed by at least one pKa unit, between 5.90 and 5.31. These literature values coincide with the experimentally determined pH range observed in the helix-to-coil conformational transition of the **TZ1H** system.

2.3.2 Polar residues and thermostability of the TZ1H system

The substitution of the polar histidine residue for isoleucine in alternate heptad *d*-positions greatly influences the stability of the overall helical assembly. Under basic buffering conditions, the engineered histidine mutation did not prohibit α-helical fiber formation but decreased the T_m of the system lower from >100 °C for the all-isoleucine hydrophobic core to 63 °C for a 15 μM **TZ1H** peptide solution. This destabilizing effect is critical to pH-induced conformational change since the increased stability observed in the majority aliphatic core would most likely preclude the fiber's ability to participate in the reversible interhelical interactions desirable in functional helical assemblies. The

somewhat counterintuitive approach of engineering destabilization into coiled-coil assemblies proved to be vital in transitioning our static fibrous assembly to a dynamic, functional material.

2.3.3   pH titration of *e*- and *g*-positions

Finally, it should be noted that glutamic acid residues occupying *e*- and *g*-positions in the primary sequence of **TZ1H,** possess sidechains with pKa values close to the observed pH 5.8 inflection point. Specifically, the γ-carboxyl side chain of Glu displays a pKa value near 4.0. Therefore, it was necessary to probe whether protonation of the Glu residues, tasked with providing the Coulombic interactions directing peptide registry, could influence fiber assembly. To answer this question the triple-stranded **S6K** parental peptide, possessing an identical sequence to **TZ1H** except with all core His residues mutated to Ile, was assembled across a gradient from pH 4-9. At all assayed pH conditions, strong α-helicity and fiber formation was observed by CD spectrometry and TEM, respectively. Therefore, this suggests the conformational transition observed in the **TZ1H** peptide system is associated with the protonation of the histidine residues, not the *e*- and *g*-position glutamic acids.

2.4   Materials and Methods

2.4.1   Peptide Synthesis and Purification

Peptide **TZ1H** was synthesized on a Symphony Quartet SPPS peptide synthesizer (Peptide Technologies, Tucson, AZ) via standard Fmoc chemistry. Reverse-phase HPLC purification was performed using the Waters 600 purification system (Waters Corp., Milford, MA) with a Waters 996 photodiode array and a reverse phase C-18 column (Atlantis dC18, 10 μm, 19 x 256 mm). The flow rate was held constant at 10 mL / min. The solvent gradient was started with 90% water / 10% acetonitrile in the presence of 0.1% trifluoracetic acid, and increased to 30% water/ 70% acetonitrile over 65 minutes. The average elution time was 26 minutes. A M/Z value for **TZ1H** was obtained by MALDI-TOF mass spectrometry on a Voyager-DE STR instrument (Perseptive Biosystems, Framingham, MA). The calculated value was 4905.6 and observed value 4904.15 which is approximately $\pm$ 1 Da. Peptide concentration measurement was obtained in 6M guanidinium chloride solution utilizing the UV absorbance at 280 nm of the single tyrosine residue in **TZ1H** where c = Molecular Weight x A_{280} / 1280. The expected mass for **TZ1H** peptide is 4905.6 Da and the observed peak by MALDI was 4904.15.

2.4.2   Circular Dichroism

CD spectra were obtained from JASCO J-810 CD spectropolarimeter (Jasco Inc., Easton, MD) equipped with a PFD-425S Peltier temperature control unit, using a 1 mm

quartz cell. Peptide solutions were prepared in 10 mM sodium phosphate buffer. The pH was adjusted with 3N HCl or 5N NaOH solutions. Total sample volume in CD measurements was 300 μL. For pH-dependent CD studies, spectra were acquired at 4 °C or 25 °C using 1 nm intervals, 1 nm bandwidth, 20 nm min^{-1}, and 8 second response time. Spectra were baseline corrected before converting to mean residue ellipticities. Fractional helix content was calculated from MRE using equation F_{helix} = *[θ]*$_{obs}$ - *[θ]*$_{coil}$ / *[θ]*$_{helix}$ - *[θ]*$_{coil}$' where *[θ]*$_{helix}$ and *[θ]*$_{coil}$ in MRE are described as (-42,500 * (1-3 / (# residues))) and +645, respectively.

CD melting curves were generated by monitoring the absorbance at 222 nm of a stirred solution of **TZ1H** (15 μM, 10 mM sodium phosphate buffer, pH 8.3) in a 1 cm quartz cuvette. Spectroscopic data were acquired within the temperature range from 20 °C to 100 °C with equilibration for 5 min at each degree unit. The value of the T_m was determined from the first derivative of the CD melting curve.

For determination of the pH-dependent reversibility of the helix-coil transition, solutions of peptide **TZ1H** were prepared at the indicated concentrations in 10 mM sodium phosphate buffer and the pH was adjusted with 3 N HCl or 5 N NaOH to the appropriate value. CD spectra were recorded at 4 °C and 25 °C as described above.

2.4.3 Electron Microscopy

For low-temperature scanning electron microscopy, a 10 μL aliquot of **TZ1H** peptide solution (1 mg / mL, 10 mM phosphate buffer, pH 7.0) was applied to a 200 mesh, carbon-coated copper grid (Electron Microscopy Sciences, Hatfield, PA). Excess

solution was wicked away with a triangle of filter paper, leaving a thin aqueous film (~ 100 nm) on the grid. Cryo-immobilization was achieved by plunging the sample in liquid ethane (-183.3 ^{o}C). The grid was then rapidly loaded into a Gatan CT 3500 cryostage which was pre-chilled to -170 ^{o}C and subsequently transferred into the Denton DV-602 chromium coater. After achieving a vacuum of $4x10^{-7}$ torr, the sample temperature was raised to -85 ^{o}C in a controlled fashion and held for 5 minutes to sublime bulk, low temperature water past the hydration shell. Finally, a thin (2 nm) continuous coating of chromium metal was sputter-coated onto the sample and the stage was rapidly transferred from the coater to the upper stage of a TOPCON / ISI (Tokyo, Japan) DS-130 field-emission SEM for imaging.

TEM imaging was performed on a JEOL (Tokyo, Japan) JEM-1210 with a LaB$_6$ electron beam source at 90 kV accelerating voltage or a Philips 410 with a tungsten filament source at 80 kV accelerating voltage. Negative stains (Nanoprobes, Yaphank, NY) utilized were methylamine vanadate (NanoVan) and tungstate (NanoW) in a 1:1 ratio following the manufacturer's protocol. Briefly, a 1:1 ratio of each stain was mixed on parafilm and allowed to set for five minutes. After applying 10 mL of peptide sample to the TEM grid, excess solution was wicked from the grid surface with a triangle of filter paper, leaving a thin film of peptide behind. The grids were subsequently washed once with deionized water and the excess liquid was once again wicked away. Next, the 1:1 NanoV / NanoW mixture was applied to the grid surface and allowed to set for two minutes. Next, the stain was wicked from the surface to leave behind a thin film of stain and sample. Finally, one last application of the negative stain mixture was performed and allowed to sit on the grid for one minute before wicking the surface dry. All grids

containing sample and stain were stored in a vacuum desiccator for a minimum of 12 hours before viewing in the microscope.

For electron tomography, **TZ1H** peptide solutions were prepared at 100 μM concentration in 10 mM phosphate buffer pH 7.2 and subsequently flash-frozen onto glow discharged Quantifoil grids (Quantifoil, Jena, Germany) in liquid ethane using a Vitrobot (FEI, The Netherlands). Colloidal gold (10 nm) was both combined with the peptide solutions and applied separately on the grids before freezing. All images were captured on the GIF CCD (Gatan) using slit width of 20 eV, a defocus range of 4–8 μm under focus (first CTF zero between 1/2.8 and 1/4 nm, respectively), a total electron dose of 120 e/Å^2 or less, liquid nitrogen cooling, and CCD pixel size of 0.46 or 0.56 nm on the specimen. Tilt series were collected from approximately -70$^{\text{o}}$ to +70$^{\text{o}}$ with 1$^{\text{o}}$ and 2$^{\text{o}}$ tilt steps automatically using the predictive UCSF tomography package.[25]

Digital micrograph image measurements were performed using the software ImageJ, version 1.36b, freely available from U.S. National Institutes of Health, Bethesda, Maryland, USA (http://rsb.info.nih.gov/ij/). Briefly, the spatial scale was set to a known distance in the image and the distance in pixels. The segmented line tool was used to trace the diameter of fibrils or fiber segments that displaced well defined edges. Fifteen independent diameter measurements were made from fibers spanning every quadrant of the image. Errors in the distance measurements are reported as standard error of the mean.

2.5 References

1.   Zimenkov, Y.; Dublin, S. N.; Ni, R.; Tu, R. S.; Breedveld, V.; Apkarian, R. P.; Conticello, V. P., Rational design of a reversible pH-responsive switch for peptide self-assembly. *J Am Chem Soc* **2006,** 128, (21), 6770-1.

2.   Stevens, M. M.; Allen, S.; Sakata, J. K.; Davies, M. C.; Roberts, C. J.; Tendler, S. J.; Tirrell, D. A.; Williams, P. M., pH-dependent behavior of surface-immobilized artificial leucine zipper proteins. *Langmuir* **2004,** 20, (18), 7747-52.

3.   Benzinger, T. L.; Gregory, D. M.; Burkoth, T. S.; Miller-Auer, H.; Lynn, D. G.; Botto, R. E.; Meredith, S. C., Two-dimensional structure of beta-amyloid(10-35) fibrils. *Biochemistry* **2000,** 39, (12), 3491-9.

4.   Lamm, M. S.; Rajagopal, K.; Schneider, J. P.; Pochan, D. J., Laminated morphology of nontwisting beta-sheet fibrils constructed via peptide self-assembly. *J Am Chem Soc* **2005,** 127, (47), 16692-700.

5.   Pandya, M. J.; Spooner, G. M.; Sunde, M.; Thorpe, J. R.; Rodger, A.; Woolfson, D. N., Sticky-end assembly of a designed peptide fiber provides insight into protein fibrillogenesis. *Biochemistry* **2000,** 39, (30), 8728-34.

6.   Ryadnov, M. G.; Ceyhan, B.; Niemeyer, C. M.; Woolfson, D. N., "Belt and braces": a peptide-based linker system of de novo design. *J Am Chem Soc* **2003,** 125, (31), 9388-94.

7.   Potekhin, S. A.; Melnik, T. N.; Popov, V.; Lanina, N. F.; Vazina, A. A.; Rigler, P.; Verdini, A. S.; Corradin, G.; Kajava, A. V., De novo design of fibrils made of short alpha-helical coiled coil peptides. *Chem Biol* **2001,** 8, (11), 1025-32.

8.   Cerasoli, E.; Sharpe, B. K.; Woolfson, D. N., ZiCo: a peptide designed to switch folded state upon binding zinc. *J Am Chem Soc* **2005,** 127, (43), 15008-9.

9.   Wright, E. R.; Conticello, V. P., Self-assembly of block copolymers derived from elastin-mimetic polypeptide sequences. *Adv Drug Deliv Rev* **2002,** 54, (8), 1057-73.

10.   A. M. Smith, E. F. B. W. R. E. M. J. P. D. N. W., Engineering Increased Stability into Self-Assembled Protein Fibers. *Advanced Functional Materials* **2006,** 16, (8), 1022-1030.

11.   Reiersen, H.; Rees, A. R., An engineered minidomain containing an elastin turn exhibits a reversible temperature-induced IgG binding. *Biochemistry* **1999,** 38, (45), 14897-905.

12.   Dong, H.; Hartgerink, J. D., Short homodimeric and heterodimeric coiled coils. *Biomacromolecules* **2006,** 7, (3), 691-5.

13.   Zirah, S.; Kozin, S. A.; Mazur, A. K.; Blond, A.; Cheminant, M.; Segalas-Milazzo, I.; Debey, P.; Rebuffat, S., Structural changes of region 1-16 of the Alzheimer disease amyloid beta-peptide upon zinc binding and in vitro aging. *J Biol Chem* **2006,** 281, (4), 2151-61.

14.   Dutta, K.; Alexandrov, A.; Huang, H.; Pascal, S. M., pH-induced folding of an apoptotic coiled coil. *Protein Sci* **2001,** 10, (12), 2531-40.

15.   Yadav, M. K.; Redman, J. E.; Leman, L. J.; Alvarez-Gutierrez, J. M.; Zhang, Y.; Stout, C. D.; Ghadiri, M. R., Structure-based engineering of internal cavities in coiled-coil peptides. *Biochemistry* **2005,** 44, (28), 9723-32.

16. Schneider, J. P.; Pochan, D. J.; Ozbas, B.; Rajagopal, K.; Pakstis, L.; Kretsinger, J., Responsive hydrogels from the intramolecular folding and self-assembly of a designed peptide. *J Am Chem Soc* **2002,** 124, (50), 15030-7.

17. M. M. Stevens, N. T. F. C. W. D. A. T. R. L., Coiled-Coil Peptide-Based Assembly of Gold Nanoparticles. *Advanced Materials* **2004,** 16, (11), 915-918.

18. Harbury, P. B.; Kim, P. S.; Alber, T., Crystal structure of an isoleucine-zipper trimer. *Nature* **1994,** 371, (6492), 80-83.

19. O'Shea, E. K.; Rutkowski, R.; Kim, P. S., Evidence that the leucine zipper is a coiled coil. *Science* **1989,** 243, (4890), 538-42.

20. Wagner, D. E.; Phillips, C. L.; Ali, W. M.; Nybakken, G. E.; Crawford, E. D.; Schwab, A. D.; Smith, W. F.; Fairman, R., Toward the development of peptide nanofilaments and nanoropes as smart materials. *Proc Natl Acad Sci U S A* **2005,** 102, (36), 12656-61.

21. Adrian, M.; Dubochet, J.; Lepault, J.; McDowall, A. W., Cryo-electron microscopy of viruses. *Nature* **1984,** 308, (5954), 32-6.

22. Mehler, E. L.; Fuxreiter, M.; Simon, I.; E, B. G.-M., The role of hydrophobic microenvironments in modulating pKa shifts in proteins. *Proteins: Structure, Function, and Genetics* **2002,** 48, (2), 283-292.

23. Armstrong, K. M.; Baldwin, R. L., Charged Histidine Affects {alpha}-Helix Stability at all Positions in the Helix by Interacting with the Backbone Charges. *PNAS* **1993,** 90, (23), 11337-11340.

24.   Broo, K. S.; Brive, L.; Sott, R. S.; Baltzer, L., Site-selective control of the reactivity of surface-exposed histidine residues in designed four-helix-bundle catalysts. *Fold Des* **1998,** 3, (4), 303-12.

25.   Zheng, Q. S.; Braunfeld, M. B.; Sedat, J. W.; Agard, D. A., An improved strategy for automated electron microscopic tomography. *J Struct Biol* **2004,** 147, (2), 91-101.

Chapter III: Extending the TZ1H peptide - A silver (I) ion-induced conformational switch

3.1 Introduction

Metal ions are known to facilitate proper fold and function of many naturally occurring proteins. In fact, nearly 1/4 of all structurally characterized proteins are known to possess prominent metal ion-binding sites.[1] The roles these metals play are numerous and diverse, serving to stabilize protein structure, induce conformational transitions, facilitate electron transfer, participate in ligand transport and enzymatic catalysis. What is most impressive about native metal ion-binding sites is not only the impressive array of functionality displayed but the efficiency in which challenging transformations are performed. Consequently, the field of metallo-protein engineering has developed around the goal of designing biomimetic metal ion-binding site in polypeptide structures.[2] These synthetic models provide valuable information for understanding the mechanism of action utilized in native structures and simultaneously inspire the design of novel biomaterials with unique catalytic or environmental sensing functionalities.

3.1.1 Native metal ion-binding sites are classified by pre-organization of ligands

Two main classifications for metal ion-binding sites are commonly referred to as either preorganized or non-preorganized sites. Preorganization refers to the prior

positioning of protein ligands in the optimal binding conformation in the absence of metal ion. Frequently, the "blue copper" protein, a type I copper protein named for its strong electronic absorbance near 600 nm, is cited as an example of preorganized metal-binding sites. These proteins are considered an extreme example of preorganized metal-binding sites since they are fully folded in the absence of metal ions.[3] Specifically, the copper-binding site is mononuclear and defined by three primary ligands – the Nδ of two histidines, the Sγ of cysteine, and an additional weak axial ligand, usually the Sδ of methionine. This distorted tetrahedral geometry is not preferred by either Cu(I) or Cu(II), which leads to the unique spectroscopic qualities arises.

The other major category of metal-binding sites is termed non-preorganized and it is best understood in the classic example of zinc finger proteins. Functionality of these DNA-binding proteins is dependant on the metal ion-induced folding of zinc finger domains. Zinc fingers are considered an extreme example of metal-induced protein folding since the absence of metal ion renders the protein entirely unfolded. Four residues, two cysteines and two histidines, were shown by extended X-ray absorbtion fine structure (EXAFS) to be the protein ligands responsible for strongly binding zinc ions. Other divalent metal ions, including Cd^{2+}, Co^{2+}, Ni^{2+} and Fe^{2+}, are also bound by this motif, but with much lower affinity.

3.1.2   Engineered metal-binding sites in polypeptide complexes

Several peptide models have been developed in hopes of replicating the native functional roles of metal ions defined within the context of a polypeptide structure. [2,4-7]

One significant revelation which materialized from these studies is the observation that metal ions are capable of inducing conformational transitions from the unfolded to folded state[8-12] or between two independent folded states.[13, 14]

Early studies showed energetically unfavorable secondary structures within a synthetic peptide could be stabilized through the binding of a metal ion. Unprecedented stabilization of short (< 20 amino acids), monomeric helical peptides in water was achieved through the introduction of metal-coordinating histidine and cysteine sidechain residues in i and $(i + 4)$ positions of a peptide, where i and $(i + 4)$ residues comprise one turn on the helix.[15] Monomeric helical peptides do not form in aqueous solution due to the high energetic penalty involved in forming the first nucleating turn. Yet, coordination of a single transition metal ion, such as Cd^{2+}, Zn^{2+} or Cu^{2+} was shown to provide sufficient stabilization energy to fix the peptide backbone in an α-helical conformation. In essence, the metal ion serves as a crosslinker between the i and $(i + 4)$ residues, thereby reducing the entropy of the system when comparing the unfolded state relative to the folded state. An impressive 90% helicity was obtained for a monomeric helical peptide in water using this design element.

Higher-order assemblies can similarly be engineered to be stabilized exclusively in the presence of metal ions. Hodges et al. reported the design of a two-stranded, disulfide-linked coiled-coil peptide assembly which undergoes a metal-induced transition from random coil to α-helix upon binding of lanthanide ions. [16] Two independent metal-binding sites were engineered into the peptide through the addition of γ-carboxyglutamic acid (Gla) residues in the solvent-accessible e- and g-positions of a single heptad. Since these positions govern interstrand electrostatic interactions, the presence of four

carboxylate groups projected across the interface results in an interhelical Gla-Gla repulsion. This destabilizes the coiled-coil assembly and instead favors the unfolded state of the peptide. However, in presence of metal, the negatively charged carboxylate groups, which would normally repel each other, instead participate in the binding of lanthanide ions. The engineered peptide displays dissociation constant (K_d) values for La^{3+} and Yb^{3+} of 0.6 ± 0.3 μM and 0.4 ± 0.2 μM, respectively. These values are comparable with native Gla-containing proteins, such as the 12 - 44 fragment of prothrombin, which has a high-affinity Gd^{3+} binding site displaying reported K_d values of 0.55 μM.

Whereas the previous example of metal-induced coiled-coil assembly involved controlling the electrostatic repulsion of like-charged *e*- and *g*- heptad positions, strategies for engineering metal-binding sites have also utilizing the hydrophobic core-forming *a*- and *d*-position residues. Pecoraro and coworkers reported a three-stranded coiled-coil assembly stabilized through the binding of Hg(II) to residues located in the hydrophobic core.[17] A single Leu->Cys mutation in the *a*-position of a central heptad generates a three-coordinate thiolate site capable of binding soft metals such as Hg(II). When the peptides assemble in a parallel fashion, all N→C oriented, a single layer of a-position cysteine residues are arranged to form a 3-fold symmetrical binding site. This complex was shown to bind free Hg(II) in a 1:3 metal:peptide ratio, as predicted for a three-stranded coiled-coil in which each strand contributes a single metal-binding ligand.

Lastly, a triple-stranded coiled-coil assembly designed by Tanaka and coworkers was shown to form a higher-order assembly only when a transition metal ion is bound

within the hydrophobic core.[8] In this strategy, two isoleucine residues in an all isoleucine core peptide were mutated to histidine. The resulting monomeric α-helix was stabilized by the binding of a metal ion to the resulting His-X$_3$-His coordination site in a 2-coordinate. Assuming an octahedral geometry, four metal-binding sites were available to recruit an additional two helical strands to form the trimeric complex. Metal-binding affinities were determined by monitoring the fraction folded by circular dichroism. Typical dissociation constants were observed, where K$_d$ values of 5 − 35 μM were observed, depending on metal identity.

In this chapter, we report the ability of silver (I), a non-native metal ion, to selectively drive a conformational transition that triggers the self-assembly of a de novo designed peptide into a structurally defined nano-scale material through complexation to an engineered binding site.

3.2   Results

3.2.1   Design of TZ1H peptide sequence

In Chapter II, peptide **TZ1H** was shown to assemble into long aspect-ratio helical fibers at buffer pH values above the pK_a of the histidine residue sidechains which occupied positions in the hydrophobic core critical to structural formation (**Figure 3.1**). The successful design of a pH-triggered, self-assembled helical fiber validated the structural principles underlying the design of **TZ1H**. However, we also recognized that
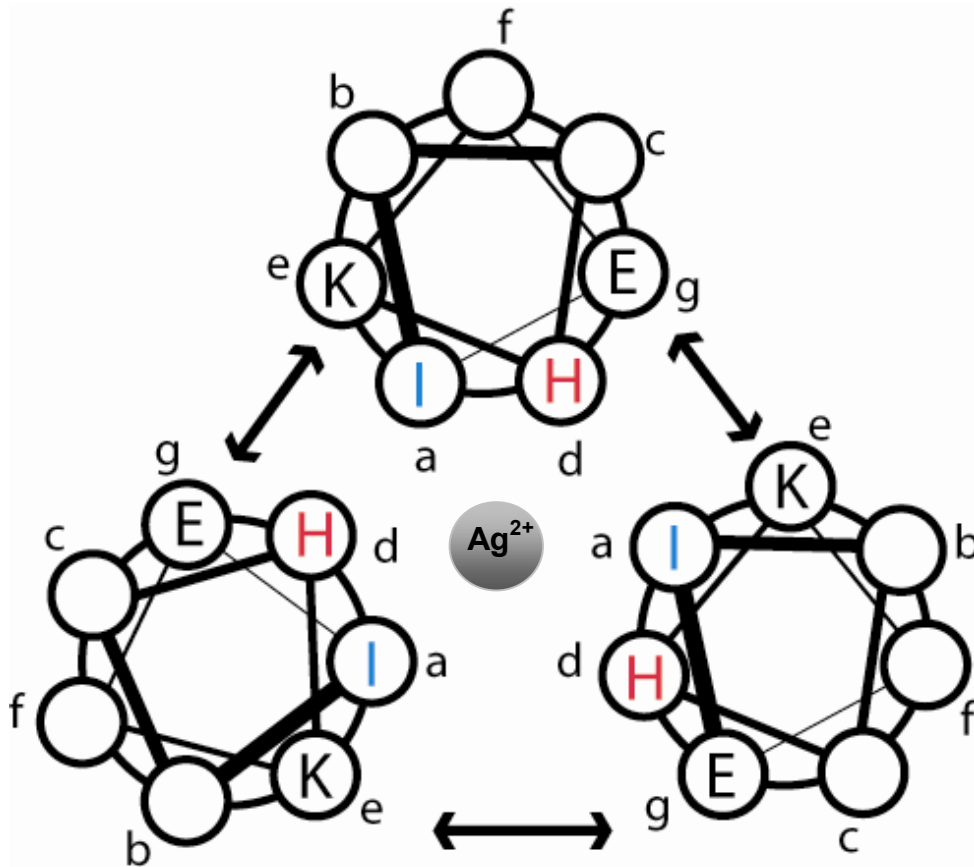
AcNH- E IAQHEKE IQAIEKK IAQHEYK IQAIEEK IAQHKEK IQAIK -CONH2
       abcdefg abcdefg abcdefg abcdefg abcdefg abcde

Figure 3.1. **Helical wheel diagram of TZ1H depicting the cross-sectional view of a triple-stranded helical bundle formed through self-assembly. Below, the primary sequence of TZ1H shows core-forming *a*- and *d*-position occupied by isoleucine (blue) or histidine (red). Note, the majority of the hydrophobic core consists of isoleucine residues except for histidine in the *d*-position of alternate heptads.**

the layers of three proximal histidine residues within the suppositious fibril structure could provide a potential metal ion-binding site and, therefore, a mechanism for coupling a metal ion-induced conformational transition to peptide self-assembly. The purposed trigonal planar geometry within the engineered metal ion-binding site, while not common, does have precedence for some electron-rich late transition metal ions with minimal deviations from ideal geometry in sterically unconstrained systems. Specifically, silver (I) ions have been shown to accept trigonal planar coordination with soft-donor nitrogen ligands, such as imidazoles, pyrazoles and pyridines, in unconstrained systems.[18] Therefore, we predicted the **TZ1H** peptide could accommodate the silver (I) ion which possesses a r_{ion} value of 1.29 Å within the core of the proposed triple-stranded metal binding site. This supposition is supported by reports of ions as large as the chloride anion (r_{ion}, 1.81 Å) observed within a cavity generated between similarly sized glutamine residues in a trimeric coiled-coil.[19]

Elemental silver possesses a single s electron residing outside of a completed d shell, similar to copper and gold. However, only Ag^+ is known to exist as a stable cationic species. The silver (II) and silver (III) oxidation states are unstable in water or are known to exist as insoluble compounds or complexed species. In the case of silver (I) (d^{10}), coordination numbers 2, 3 and 4 are reported with linear, trigonal and tetrahedral geometries respectively. Coordination geometry for silver (I), in particular, is sensitive to the ligand identity and the most commonly observed geometries are linear and tetrahedral.

3.2.2 Circular dichroism of TZ1H in the presence of silver ion at pH 5.6

To test the hypothesis, circular dichroism (CD) spectroscopy was utilized to probe the effect of silver (I) ion titration on the secondary structure of **TZ1H** peptide in aqueous solution. The buffering solution pH value was prepared below the pK_a of the core histidine imidazole sidechain to ensure maximal initial random coil content. Peptide **TZ1H** was prepared to a concentration of 50 μM peptide in 10 mM phosphate buffer (pH 5.6) and titrated with silver (I) triflate in a concentration range between 0 μM to 55 μM. The CD spectrum of **TZ1H** peptide in the absence of silver ion displays a minimum at approximately 201 nm, which is characteristic of random coil content. This confirms the results of the pH-trigger experiments in which a protonated imidazole sidechain inhibits formation of an α-helical secondary structure conformation.

However, an increase in silver ion concentration is accompanied by an observed conformational transition in the CD spectroscopic manifold in which the CD spectra develop minima at 208 nm and 222 nm with a corresponding positive peak at 190 nm (**Figure 3.2**). These spectroscopic features are standard indicators of α-helical secondary structure. Furthermore, the well defined isodichroic point observed at 204 nm is consistant with a quasi-two-state, coil-to-helix conformational transition. Therefore, these data points suggest a conformational transition occurs in this system as a function of silver ion (I) concentration.

Insight into the nature of the conformational switch can be more easily obtained by observing the dependence of the mean residue ellipticity for the α-helix ($[\theta]_{222\ nm}$) on silver (I) ion concentration. Following the resulting titration curve, maximal helicity is achieved with an equimolar ratio of peptide to silver (I). Further addition of silver (I) ion
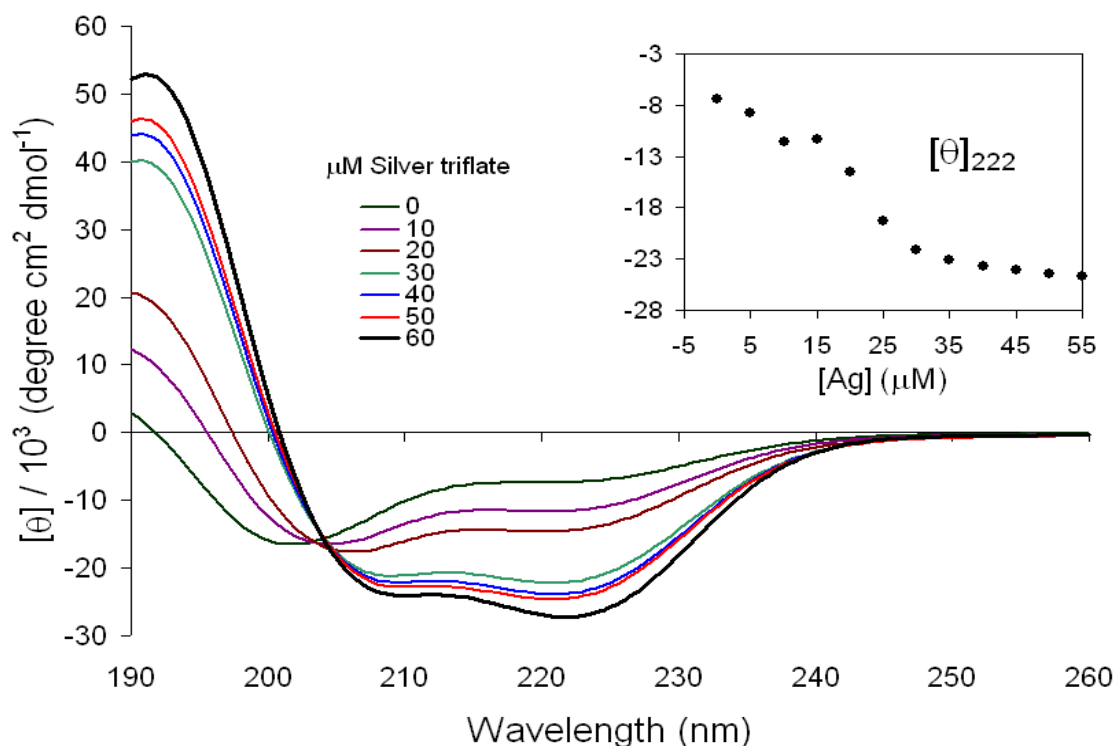
Figure 3.2. Dependence of the CD spectra (50 μM TZ1H peptide, 10 mM NaH$_2$PO$_4$, pH 5.6, 4 °C) on silver (I) ion concentration. Inset: Mean residue ellipticity at 222 nm for TZ1H as a function of silver ion concentration.

offered no further change in helicity of **TZ1H**, implying the available metal ion-binding sites are saturated under these conditions. The limiting value for the fraction helicity for the species (50 μM **TZ1H**, 55 μM silver (I), pH 5.6) was calculated to be 71%.

The **TZ1H** : silver (I) complex exhibits characteristics similar to other coiled-coil assemblies, based on benchmarks from the literature. An agreed value for the observed ratio of $\theta_{222\,nm}$ / $\theta_{208\,nm}$ in coiled-coil assemblies is >1, and the ideal value is often referenced as 1.07.[20] Typical metal-induced α-helical spectra observed in these studies

averaged 1.1, well within the expected range for similar coiled-coil structures. Thermal unfolding of the helical state of **TZ1H,** in the presence of silver ions, was followed by CD spectropolarimetry and was shown to be fully reversible within the temperature range from 30 – 98 $^\circ$C. (**Figure 3.3**) The transition midpoint (T_m) was calculated as 69 $^\circ$C for 70 μM peptide by taking the first derivative of the thermal melting curve.
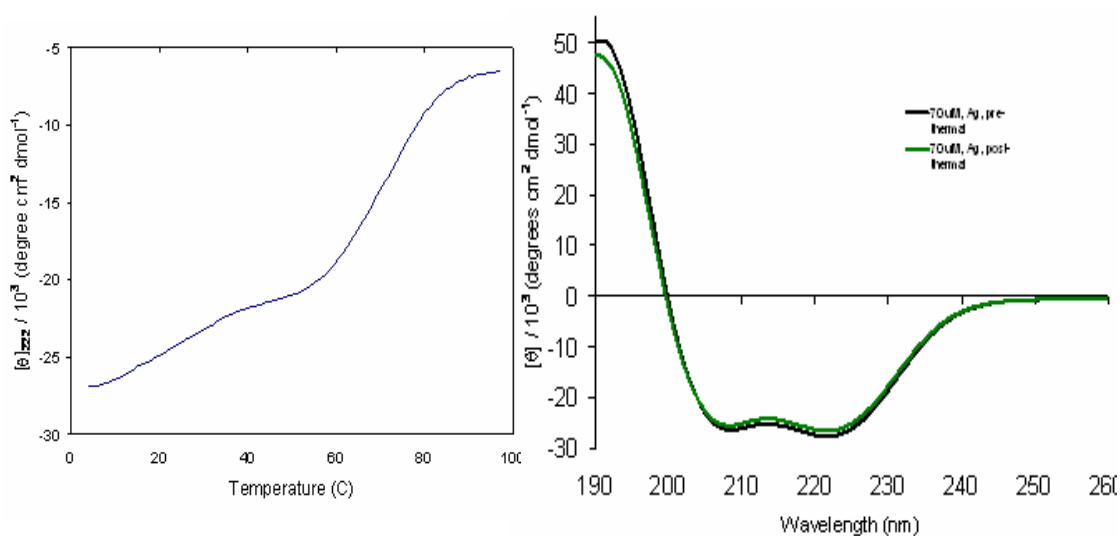
Figure 3.3. **(Left) CD thermal denaturation for peptide TZ1H (70 μM, 10 mM phosphate buffer, pH 5.6) in the presence of equimolar silver (I) ion. The T_m for the helical state was calculated to be approximately 69 $^\circ$C. (Right) CD spectropolarimetric analysis of the reversibility of thermal denaturation for peptide TZ1H (70 μM, 10 mM phosphate buffer, pH 5.6).**

3.2.3 CD spectrometry of TZ1H peptide in the presence of sodium thiosulfate and EDTA

Evidence for the specificity of the silver (I) ion involvement in fiber formation was investigated through the loss of α-helical content via the selective removal of the silver (I) ion through complex formation of silver (I) ion with the thiosulfate anion. The terminal sulfur of the thiosulfate ion is known to bind soft metals with high affinity. Most commonly, sodium thiosulfate is used in photographic processing for its ability to dissolve silver halides.

Circular dichroism spectropolarimetric titration of peptide **TZ1H** (35 μM) with sodium thiosulfate to an approximate three-fold molar excess over the initial peptide concentration shows an immediate effect on the initial α-helical CD spectrum. The CD spectroscopic manifold displays the gradual disappearance of the existing minima at 208 and 222 nm with increasing sodium thiosulfate concentration (**Figure 3.4**). Therefore, these data points suggest a conformational transition occurs in this system as a function of silver ion (I) concentration. Following the mean residue ellipticity at 222 nm as a function of thiosulfate concentration suggests the maximal binding of thiosulfate and silver ion is reached at the respective ratio of approximately 2:1 peptide-to-thiosulfate ratio. Further titration of thiosulfate solution did not significantly change the values for $[\theta]_{222 \, nm}$.
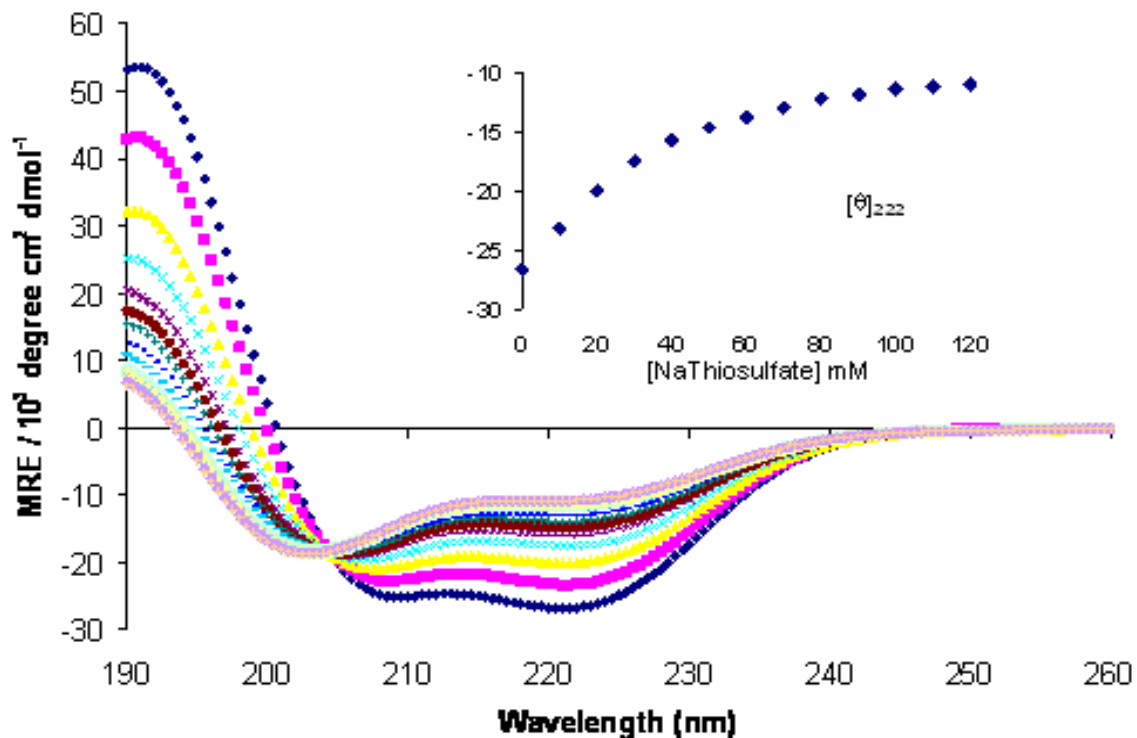
Figure 3.4. Circular dichroism spectropolarimetric titration of peptide TZ1H (35 μM) with sodium thiosulfate to an approximate three-fold molar excess over the initial peptide concentration. Inset: $[\theta]_{222\ nm}$ of peptide TZ1H as a function of thiosulfate concentration. Minima at 208 and 222 nm gradually disappear with increasing thiosulfate concentration.

However, the addition of excess EDTA to the **TZ1H** : silver(I) complex showed little effect on the helicity of the species as monitored by CD spectroscopy (**Figure 3.5**). This can be explained by the low formation constant (10^7 M^{-1}) of silver (I) and the EDTA ion (**Figure 3.6**).[21] The CD spectrum showed little decrease in helicity upon the addition of EDTA to 4-fold excess, where titration was halted.
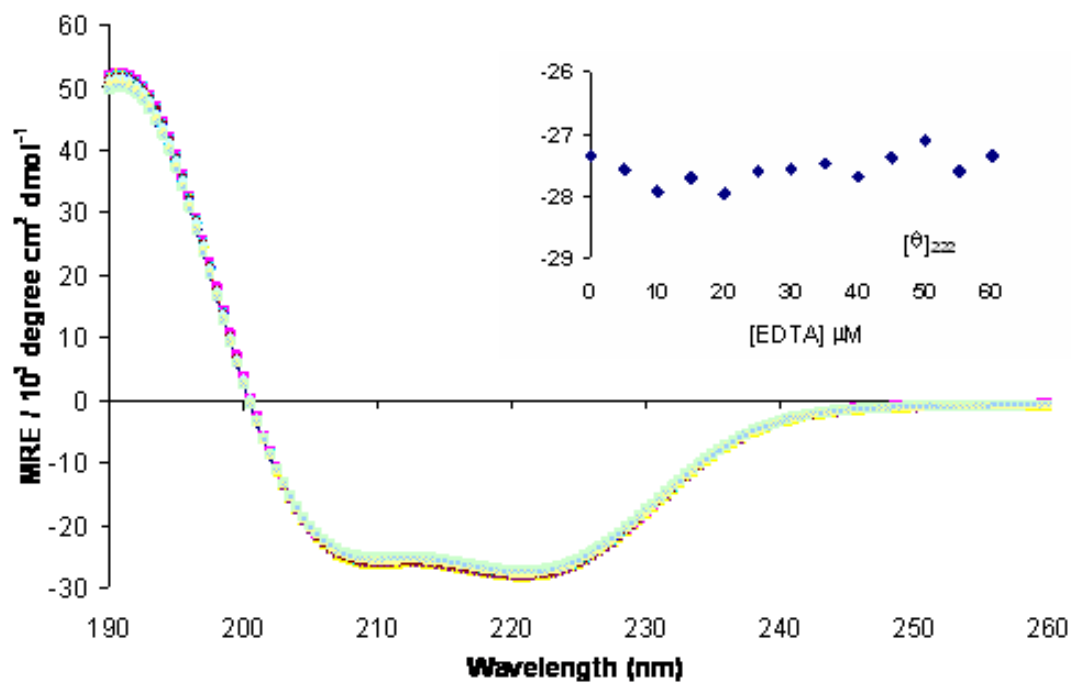
Figure 3.5. Circular dichroism spectropolarimetric titration of TZ1H (44 μM) with excess concentration of EDTA. Inset: $[\theta]_{222\,nm}$ of peptide TZ1H as a function of EDTA concentration. Minima at 208 and 222 nm remain unchanged in the presence of increasing thiosulfate concentration.

$$Ag^+ + 2\ S_2O_3{}^{2-} \longrightarrow Ag(S_2O_3)_2{}^{3-}$$

$$K_f = 2.9 \times 10^{13}\ M^{-1}$$

Thiosulfate anion

$$Ag^+ + EDTA^{4-} \longrightarrow Ag(EDTA)^{3-}$$

$$K_f = 10^7\ M^{-1}$$

Ethylenediaminetetraacetate (EDTA)
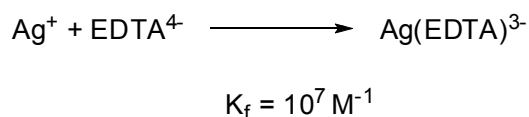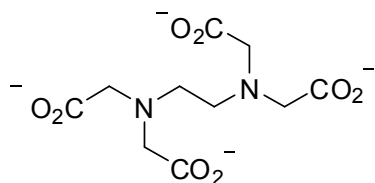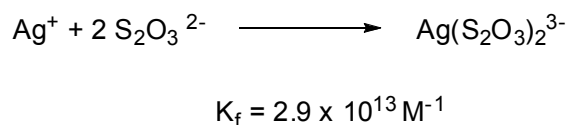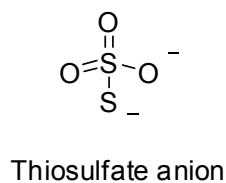
Figure 3.6. **Illustrations of the metal chelating thiosulfate anion and ethylenediaminetetraacetate (EDTA) with their observed formation constant values (K_f) for the formation of silver:chelator complex.**

3.2.4 Histidine residues are involved in the binding of silver (I) ion

The direct role of the histidine residues in silver ion-binding activity can be indirectly ascertained through the effect of pH on the silver ion-induced conformational change. Specifically, the influence of pH on the metal-induced conformational change for the **TZ1H** system can be assayed by CD spectropolarimetry. Aliquots of peptide **TZ1H** (50 μM) solutions in 10 mM phosphate buffer were prepared across a pH gradient

range of 4.4 – 6.0 in 0.3 pH-unit increments. Silver (I) triflate was added to each sample to attain a final concentration of 25 µM silver, resulting in a 1:2 metal:peptide molar ratio. In this manner, the concentration of peptide and pH were identical across the sample set. The only difference between each sample was the buffer pH. After 5 minute incubation at 4 °C, the CD spectrum was obtained and the resulting mean residue ellipticity at 222 nm plotted as a function of pH (**Figure 3.7**).

The observed MRE values were weakly negative within the pH range from 4.0 to 5.0, indicating marginal helicity (< 25% helical content) in this subset of **TZ1H**:silver (I) complexes. However, a large decrease in observed values of $[\theta]_{222}$, associated with increased helical content, was observed over the pH range from 5.2 to 5.8. A sharp drop in $[\theta]_{222\ nm}$ is observed at pH 5.1, where the sigmoidal curve then begins to approach a limiting value at higher pH.

In addition, at pH conditions significantly below the pKa of the histidine side chain, a much higher concentration of silver (I) ion was required to induce a coil-to-helix conformational transition equivalent to that observed at pH 5.6 (**Figure 3.8**). For example, at pH 5.3, a four-fold molar excess of silver (I) ion was required to induce a fractional helicity value for **TZ1H** that was comparable to that observed for a 1:1 silver:peptide complex at pH 5.6. These data suggest that the silver (I) ions are in direct competition with protons for the basic lone-pairs of the free imidazole nitrogen atoms of the histidine residues, and that silver coordination is the driving force for the conformational transition observed for **TZ1H**.
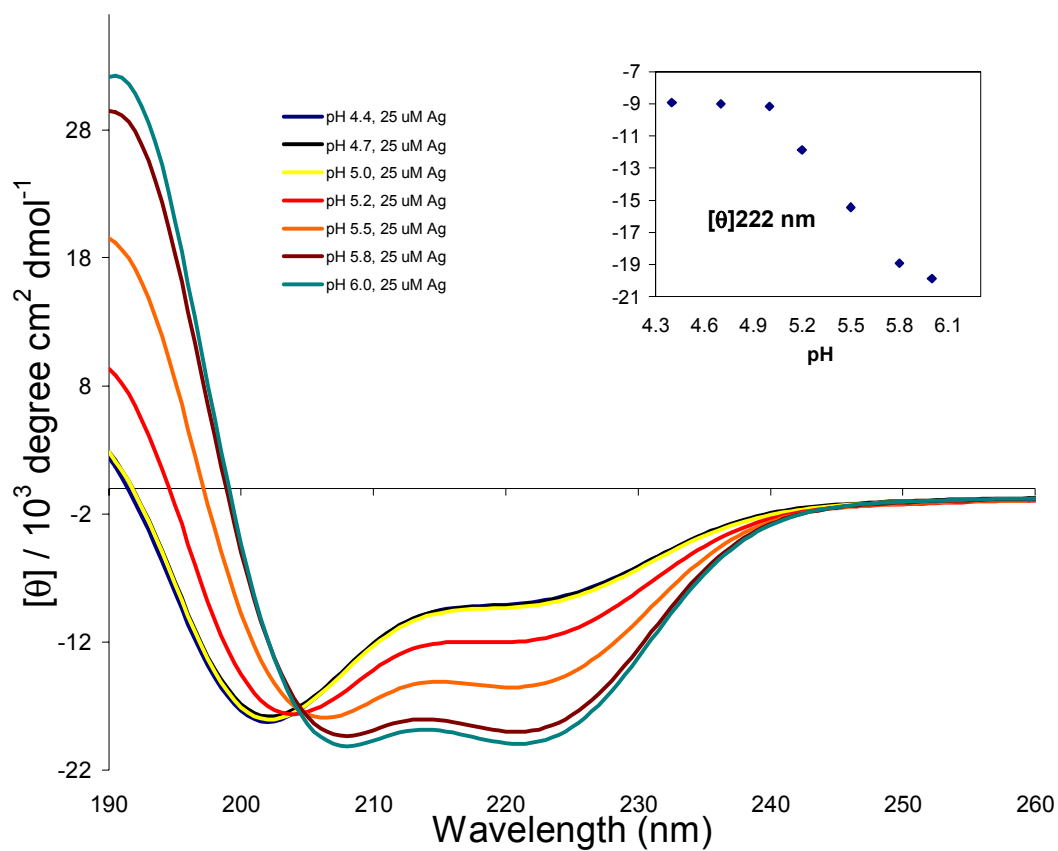
Figure 3.7. Circular dichroism spectra depicting the pH dependence of metal binding for TZ1H in 10 mM phosphate buffer. Aliquots of peptide TZ1H (50 µM) in 10 mM phosphate buffer were prepared across a pH gradient that ranged from 4.4 - 6.0 in 0.3 pH-unit increments in the presence of 25 µM silver. Inset: $[\theta]_{222\ nm}$ of peptide in the presence of half-maximal silver concentration is plotted as a function of pH.
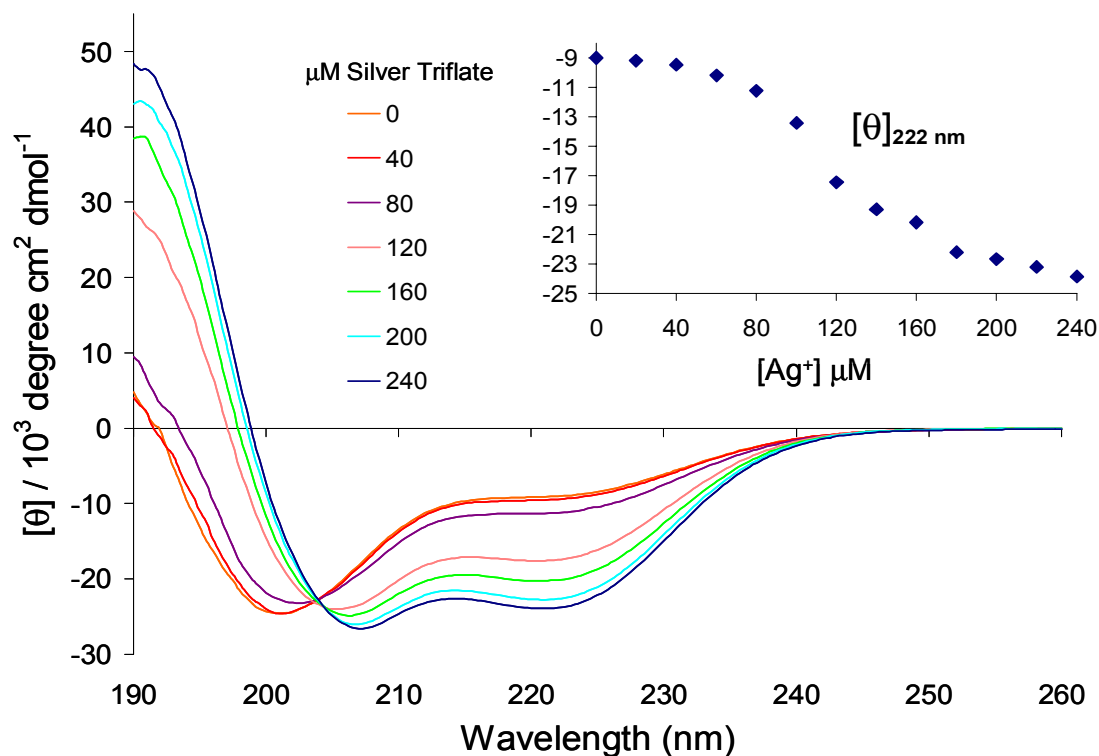
Figure 3.8. Dependence of the CD spectra of TZ1H (60 μM, 10 mM Na₂HPO₄, pH 5.3) on silver (I) ion concentration at 4 °C. Inset: Dependence of $[\theta]_{222\ nm}$ on silver (I) ion concentration. Note that a four-fold higher concentration of silver (I) ion is required to elicit a value of $[\theta]_{222\ nm}$ that is equivalent to the effect of equimolar silver (I) ion on the CD spectrum of peptide TZ1H at pH 5.6.

3.2.5 Isothermal titration calorimetry (ITC)

Isothermal titration calorimetry was employed to gain a quantitative determination of the binding energetics of silver (I) ion to peptide **TZ1H** under conditions that coincided with the conformational transition. Direct measurement of heat exchange resulting from the binding of silver ion, reveals the components of Gibb's free energy of binding (ΔG), enthalpy (ΔH) and entropy change (ΔS). Values for ΔH can be acquired directly from the ITC experiment, whereas the binding constant K_a and number of binding sites, *n*, are solved for by a least squares fitting of the binding isotherm fit to an assumed binding model.   Using K_a and the general thermodynamic equation $\Delta G = - RT \ln K_a$, the value for ΔG of the system can be solved for.   Finally, ΔS is known through the equation $\Delta G = \Delta H - T\Delta S$.

Silver (I) triflate was titrated into solutions of peptide **TZ1H** (70 μM) in phosphate buffer (10 mM, pH 5.6) at 5 °C. The reaction was exothermic under these conditions as indicated by negative kcal / mol of injectant values for the enthalpy of addition of the silver ion (**Figure 3.9**). The resulting titration curves were fitted to a single-binding site model where fitting parameters were free floating. The resulting titration curve fitting resulted in a binding constant (K_b) of (6.49 ± 0.523) x 10^4 M^{-1}. The value for the number of binding sites (*n*) was experimentally determine to be 0.91 ± 0.02, which most closely corresponded to a situation in which one silver (I) ion was bound to a peptide. Theoretically, each **TZ1H** peptide can contribute three histidine residues for coordination to a silver ion. However, in a trimeric coiled-coil structure, each histidine forms one-third of the trigonal planar binding site for a net contribution of one binding
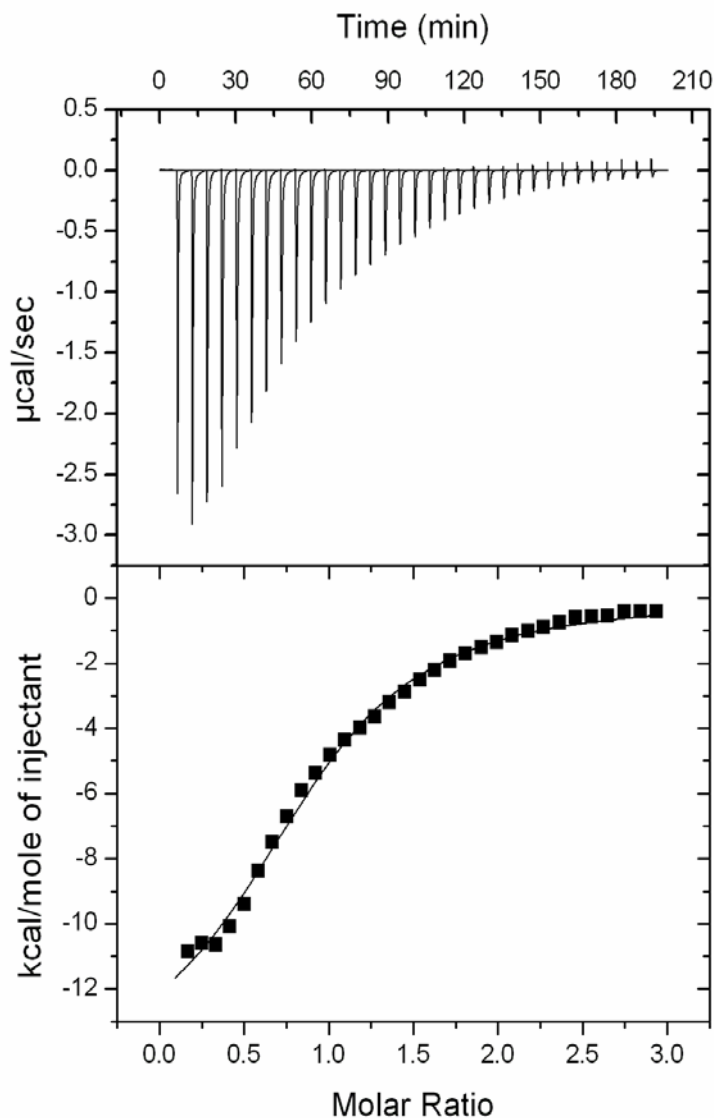
Figure 3.9. Isothermal titration calorimetry analysis for addition of a silver (I) triflate solution (10 mM) to a solution of peptide TZ1H (70 μM in 10 mM phosphate buffer pH 5.6). The data were fit to a single-site binding model, which yielded a value of 0.908 ± 0.0203 for the number of binding sites (n) per TZ1H peptide and a binding constant (K_b) of $(6.49 \pm 0.523) \times 10^4$ M^{-1}. The values of the corresponding thermodynamic parameters ΔH and ΔS were determined to be $(1.4794 \pm 0.462) \times 10^4$ cal/mole and -31.2 cal/Kmole, respectively.

site per peptide. Thus, the experimental value of *n* coincides with the results from CD spectropolarimetry, in which an equimolar ratio of silver (I) ion to peptide was observed to have the maximal effect on the coil-to-helix transition.

Additionally, the effect of histidine sidechain protonation on silver ion binding was observed by ITC. Peptide **TZ1H** solutions prepared in 10 mM phosphate buffer at pH 5.3 and 6.0, representing the limiting pH values of random coil and α-helical conformation, respectively, were titrated with silver triflate solution (**Figure 3.10** and **Figure 3.11**). Previously, we have shown **TZ1H** begins to form α helical secondary structure in buffering conditions above the pKa of the histidine side chain imidazole. Accordingly, the titration of peptide **TZ1H** (10 mM phosphate, pH 6.0) with silver (I) triflate yielded the (n) value of 0.239 ± 0.0744 for the number of binding sites per **TZ1H** peptide (**Table 3.1**).
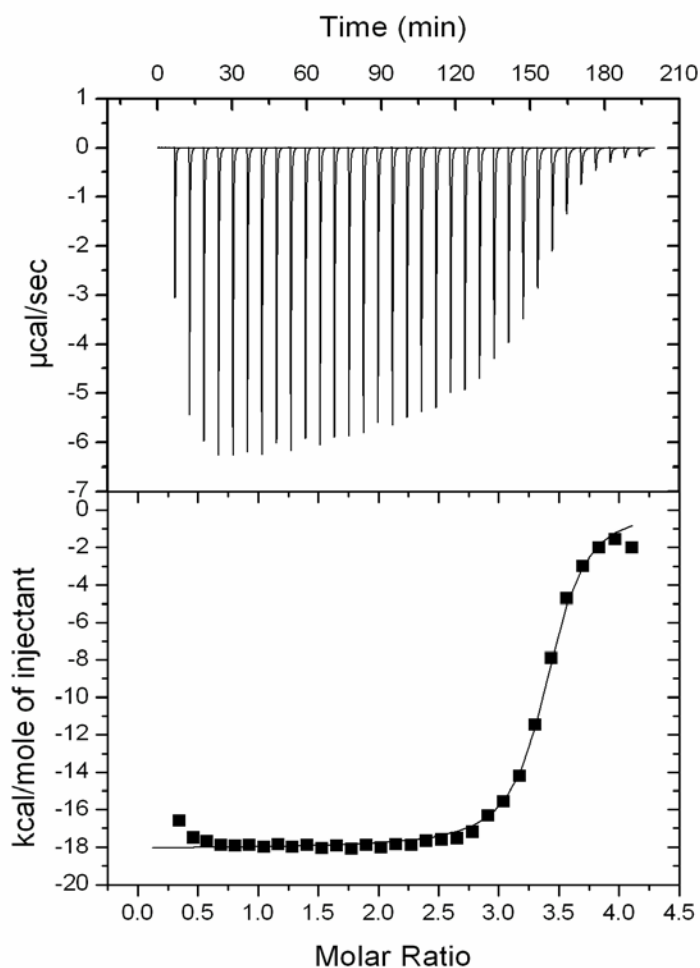
Figure 3.10. Isothermal titration calorimetry analysis for addition of a silver (I) triflate solution (10 mM) to a solution of peptide TZ1H (50 μM in 10 mM phosphate buffer pH 5.3). The data were fit to a single-site binding model, which yielded a value of 3.35 ± 0.00994 for the number of binding sites (*n*) per TZ1H peptide and a binding constant (K_b) of (2.97 ± 3.43) x 10^6 M^{-1}. The values of the corresponding thermodynamic parameters ΔH and ΔS were determined to be (1.807 ± 100.5) x 10^4 cal/mole and -35.3 cal/Kmole, respectively.
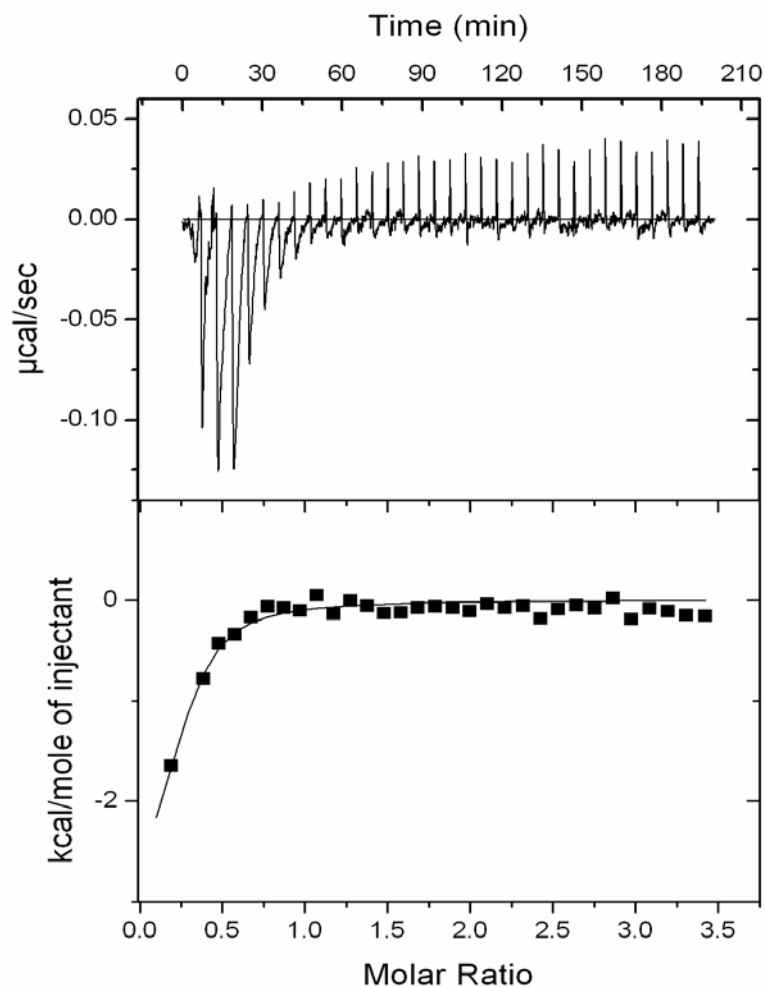
Figure 3.11. Isothermal titration calorimetry analysis for addition of a silver (I) triflate solution (10 mM) to a solution of peptide TZ1H (60 μM in 10 mM phosphate buffer pH 6.0). The data were fit to a single-site binding model, which yielded a value of 0.239 ± 0.0744 for the number of binding sites (*n*) per TZ1H peptide and a binding constant (K_b) of (2.08 ± 1.02) x 10^5 M^{-1}. The values of the corresponding thermodynamic parameters ΔH and ΔS were determined to be – (3198 ± 1233) cal/mole and 12.8 cal/Kmole, respectively.

pH	N	K_b	ΔH	ΔS
5.3	3.35 ± 0.00994	2.97E6 ± 3.43E5	-1.807E4 ± 100.5	-35.3
5.6	0.908 ± 0.0203	6.49E4 ± 5.23E3	-1.479E4 ± 462.6	-31.2
6.0	0.239 ± 0.0744	2.08E5 ± 1.02E5	-3198 ± 1233	12.8

* Where N = number of binding sites, K_b = binding constant in M^{-1}, ΔH = heat change in cal / mole, and ΔS = heat change in cal / mole.

Table 3.1. Summary of ITC values obtained from silver (I) ion titration into TZ1H peptide at three different pH values *

3.2.6 Transmission electron microscopy (TEM) confirms fiber formation of the silver (I) ion-TZ1H complex

Conventional transmission electron microscopy was utilized to investigate the presence of fiber formation resulting from self-assembly of **TZ1H** in the presence or absence of silver. Previously described studies of the pH-triggered self-assembly of **TZ1H** showed fiber formation coincides with the coil-to-helix conformational transition. Attempts at imaging **TZ1H** samples prepared at pH values below the pK_a of the histidine residues provided negligible evidence of fiber formation. However, samples prepared at pH values higher than the pK_a of histidine revealed that **TZ1H** self-assembled into long aspect-ratio helical fibers. Similarly, in the absence of silver (I) ion, no evidence for the formation of fibers was obtained when the peptide was prepared in 10 mM phosphate

buffer at pH 5.6. However, TEM micrographs showed **TZ1H** self-assembled into long-aspect-ratio fibers under equivalent conditions in the presence of equimolar silver (I) ion (**Figure 3.12**).
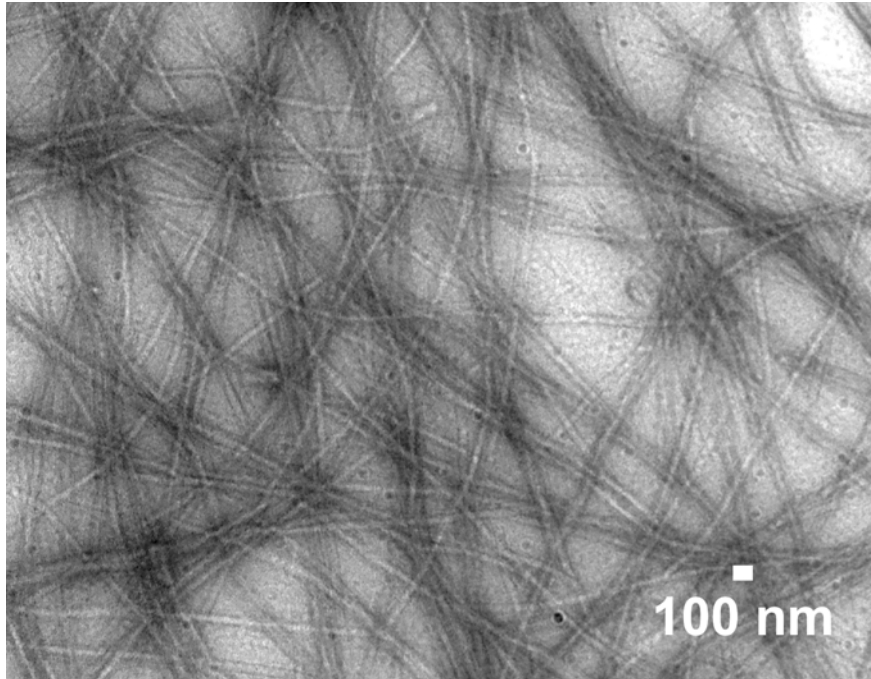
Figure 3.12. TEM image of 100 μM TZ1H peptide prepared in 10 mM phosphate buffer (pH 5.6), in the presence of equimolar silver (I) ion. These images are obtained without the aid of conventional negative stains.

Peptide samples prepared in the presence of silver ion displayed an abundance of fibers with diameters, measured between 6 – 60 nm. Higher magnification images show the presence of smaller diameter fibers with average diameter of 6.5 $\pm$ 0.2 nm, approximately twice the expected lateral dimension of a trimeric helical assembly (**Figure 3.13**). Individually isolated fibers of this minimal diameter could be located either in isolation or integrated into larger fiber bundles. Visual inspection of the large

fiber topography revealed long-axis striations of 5.8 ± 0.2 nm diameters, similar to measurements associated with isolated small-diameter fibers.
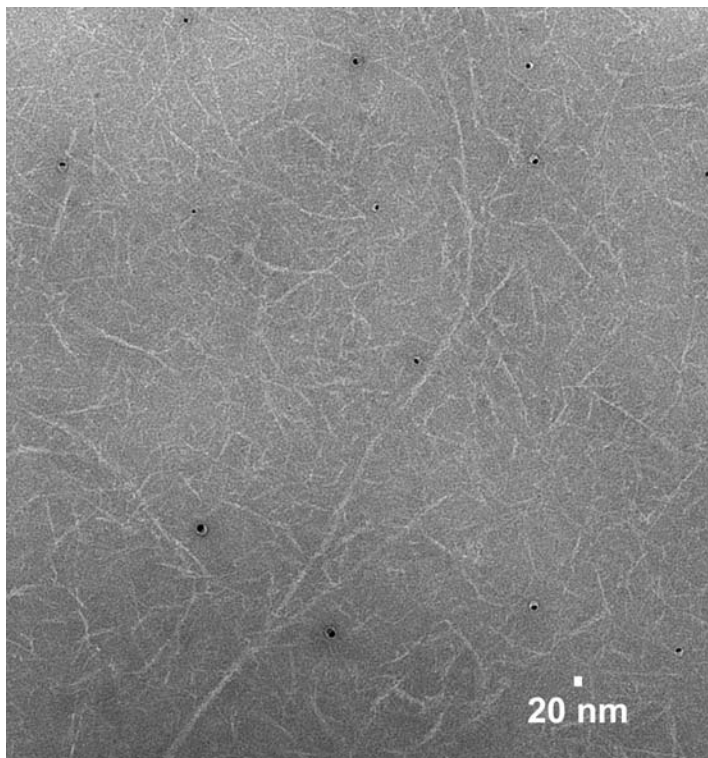
Figure 3.13.   High magnification TEM image of individual short fibrils of TZ1H that self-associate to form the larger diameter fibers.

The morphological features of the silver (I) ion-switched fibers are reminiscent of those observed in the pH-triggered fibers. The smallest discernable fibers observed by TEM imaging in the silver ion-triggered samples possess a significant number of fibrils with a diameter of 6.5 ± 0.2 nm. These species are similar in morphology to those observed in the pH-induced fiber samples, which we postulate as arising from either single three-stranded helical ropes or from small bundles of tightly associated ropes.

However, a distinct morphological difference between pH-induced and silver ion-induced fibers can be discerned in the extent of lateral association observed between fibrils. The unintended lateral interactions between pH-induced fibrils results in the formation of large diameter bundles, on the order of 100 nm or greater, which are prone to precipitation at much lower concentrations (ca. 100 μM **TZ1H**). Precipitation in solutions is known to complicate biophysical characterization techniques which are sensitive to light scattering, like circular dichroism spectrometry, and severely limits direct observation of small diameter fibers by TEM.

In silver ion-induced specimen, however, the dominant fiber species is < 100 nm (72.72 ± 2.85 nm), which shows no sign of precipitation even at peptide concentrations in excess of 500 μM. We postulate that the differences that are observed between the pH-triggered versus silver-induced fiber specimens arise from the different mechanisms that drive self-assembly. Individual peptides within the pH-induced fibrils have negligible net charge at near-neutral pH values, while peptides within the silver ion-induced fibers should have a net positive charge due the presence of one silver (I) ion per **TZ1H** peptide. The large positive charge on the latter is only partially compensated by co-localization of counterions such that Coulombic repulsion limits the extent of lateral association in comparison to the pH-induced fibers.

3.2.7 Energy-dispersive X-ray (EDX) analysis provides evidence for silver within the fiber

Direct evidence for the presence of silver ion within the fibers was sought by employing electron microscopy methodologies. EDX is a technique utilized in the

identification of elemental species using X-rays emitted by the observed sample. When an electron beam interacts with atoms of a sample, individual incident electrons experience one of two possible scattering events; elastic or inelastic (**Figure 3.14**). The former results from a direct change in trajectory, with little change in kinetic energy and velocity. However, inelastic scattering occurs when an incident electron collides with orbital shell electrons associated with the sample nuclei, resulting in the displacement of
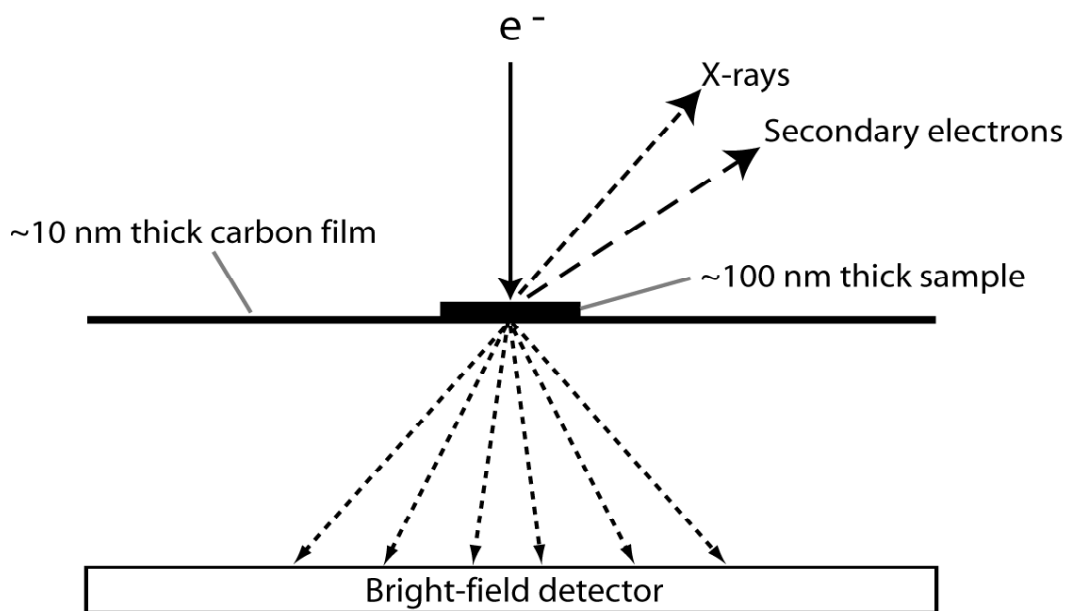
Figure 3.14. Diagram of a general bright-field STEM / BSE detector system in a scanning electron microscope. Above lens detectors collect secondary electrons which generate BSE and darkfield STEM images and a similarly situated detector collects x-rays to form the EDX spectrum. A below lens bright-field detector collects the portion of the electron beam which passes through the sample, forming the bright-field image in a manner similar to conventional TEM.

95

an electron from the sample. This places the molecule in an unstable, excited state which can only be returned to ground state by transferring a higher energy electron from the outer shell to the lower vacant inner shell. This event results in energy loss and the coupled emission of a single x-ray. Several peaks can be seen in an EDX spectrum due to multiple electron shell interactions.

Energy-dispersive X-ray (EDX) analysis of a concentrated fiber specimen indicated the presence of elemental silver (**Figure 3.15**). The strong signature for silver can be compared to the signal for phosphorus that originates from residual phosphate from the buffer. The latter is typically present at much higher concentration (10 mM sodium phosphate versus 100-200 µM silver (I) triflate) in the initial specimen prior to
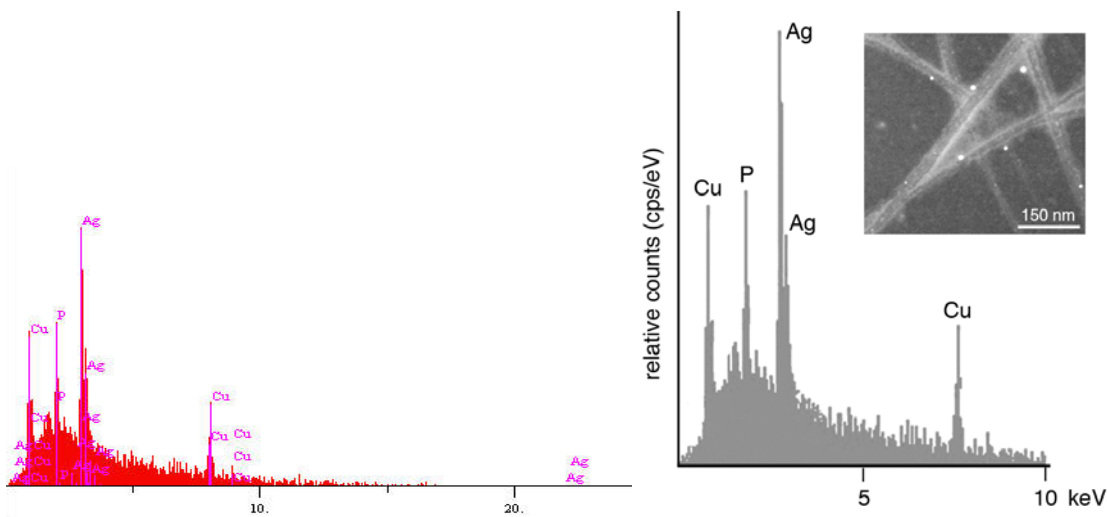
Figure 3.15. **(Left) EDX analysis of a concentrated preparation of silver ion-induced fibers of TZ1H at equimolar silver:peptide concentration. The presence of copper arises from the EM grid. (Right) Same EDX spectrum but focused on the 0 - 10 keV range in which Ag, Cu and P are most visible.**

isolation of the fibrils. The copper peaks observed in the EDX spectrum arise from the copper TEM grid on which is sample was deposited.

Further confirmation for the presence of silver was obtained from elemental analysis of isolated peptide specimens, in which the silver to peptide ratio was experimentally determined to 0.90 ± 0.02, fully supporting the binding model for the silver ion depicted.

3.2.8   High Angle Annular Dark Field (HAADF) scanning transmission electron microscopy (STEM) in Z-contrast imaging mode

Scanning transmission electron microscopy (STEM) was utilized to investigate the presence of metal ion within the internal structure of the silver ion-induced **TZ1H** peptide fibers. This microscopy technique offers a unique mode termed High Angle Annular Dark Field imaging, where the final image originates from elastically scattered electrons which have passed very close to the atomic nuclei in the sample. Therefore, the HAADF signal is proportional to the mass density of the region and to $Z^{3/2}$, where Z is the atomic number. Thus, in Z-contrast HAADF STEM mode, the contrast in the image is roughly proportional to the atomic number of the sample. This technique is very powerful because it can be utilized for inorganic or organic samples and exhibits 0.17 nm resolution at 200 keV accelerating voltage.

Dark-field STEM of dispersed preparations of the silver ion-induced **TZ1H** fibers indicated the existence of electron-dense regions against the electron-lucent background of the carbon film (**Figure 3.16** and **Figure 3.17**). The high contrast areas appeared in

two distinct forms, either co-localized with a fibrous material of expected dimensions for the **TZ1H** fibers, or as small isolated nanoparticles. We reasoned that the small spherical areas of high contrast were the result of silver aggregation of uncoordinated metal ion, while the high atomic number (Z) contrast co-localized with the bundles of fibrils provided evidence of silver ion coordination within the self-assembled peptide.
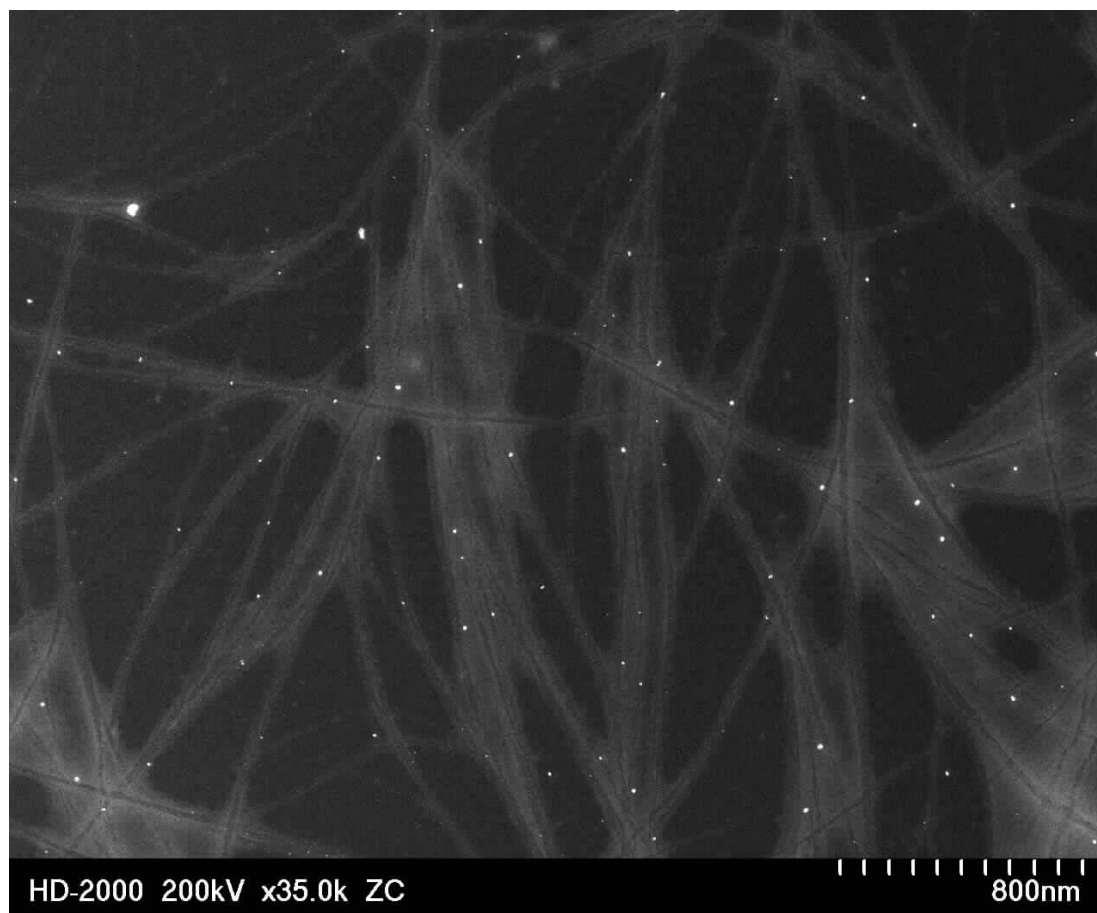
Figure 3.16. Medium-level magnification HAADF STEM image of a dispersed fibril specimen on a carbon-coated TEM grid.
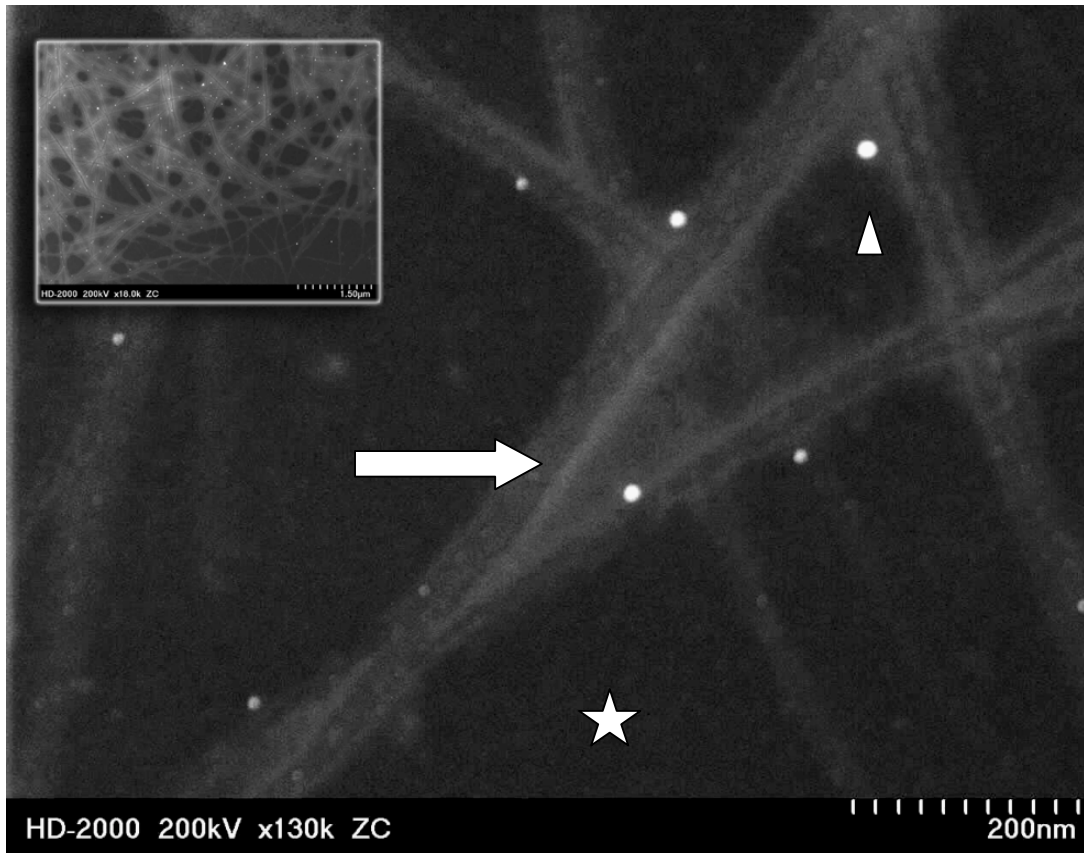
Figure 3.17. **High resolution HAADF STEM images of a dispersed fibril specimen. The star marks carbon substrate with no evidence of fiber, the arrow identifies an approximately 60 nm fiber, and the triangle identifies isolate silver clusters not incorporated into the fiber.**

3.2.9 Bright field low voltage STEM and backscatter secondary electron microscopy

Bright-field low-voltage scanning transmission electron microscopy (LV-STEM) and backscattered electron (BSE) imaging were similarly used to identify silver ions

co-localized with peptide fibers (**Figure 3.18**). In LV-STEM imaging mode, the image is formed by mass-thickness contrast which results in micrographs comparable to those acquired by conventional transmission electron microscopy. Concentrated **TZ1H** peptide prepared in the presence of equimolar silver ion displayed a continuous line of significant contrast, with respect to the background carbon film, along the fiber axis. Additionally, isolated clusters of unincorporated silver were observed on the grid as black spheres of variable diameters.

Complimentary back-scattered electron (BSE) images were collected by switching the image-forming detector to BSE mode, while holding the sample on the viewing stage in the identical position utilized in LV-STEM mode (**Figure 3.18**). In BSE imaging, the yield of the collected backscattered electrons increases monotonically with the specimen's atomic number, allowing distinction of one material from another. In this case, silver ions colocalized with fibers are visible in contrast to the carbon support film. The strong signal observed along the longitudinal axis of the fiber, represented as a bright white line, perfectly overlays the dark black LV-STEM trace. Furthermore, the small clusters of suspected silver ion observed in isolation as black spheres by bright-field LV-STEM mode, appear in BSE mode as bright white spheres.
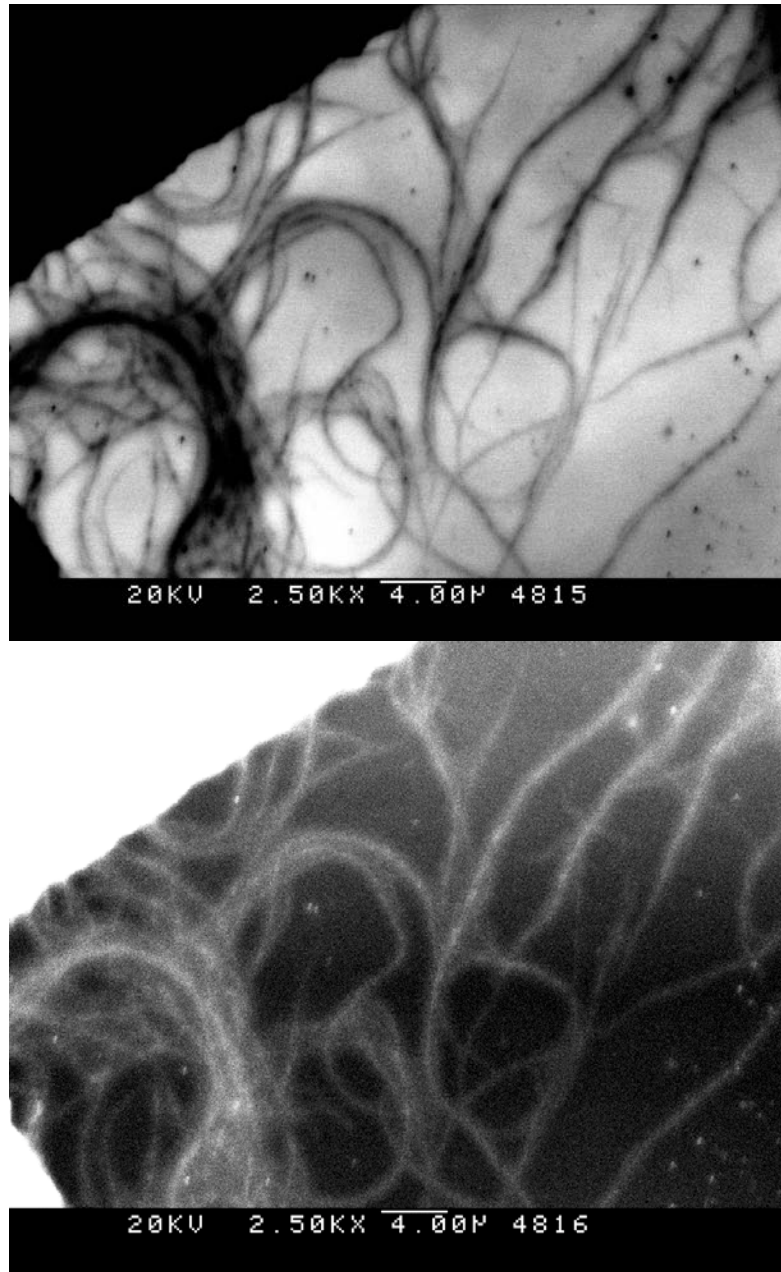
Figure 3.18. **Bright-field low-voltage scanning transmission electron microscopy (Top)
and backscatter electron microscopy (Bottom) images reveal high atomic number (Z)
element colocalized along the fiber axis.**

3.2.10 Circular dichroism for TZ1H in the presence of zinc or copper

In the preceding experiments, we show peptide **TZ1H** the silver (I) ion induces the required conformational transition for self-assembly of monomer to helical fibers. We predicted the conformational transition in **TZ1H** could be achieved by other metal ions. However, CD experiments showed titration of neither the (d^{10}) zinc (II) ion nor the (d^9) copper (II) ion were able to induce an equivalent conformational transition within **TZ1H** (**Figure 3.19** and **Figure 3.20**). We found that final metal concentrations in molar excess up to four- and three-fold, zinc (II) and copper (II) respectively, were unable to produce a helical CD spectra. Upon consideration of the available coordination geometries of silver(I), copper(II) and zinc (II), summarized in **Table 3.2**, it is apparent that silver(I) is the sole metal of the group which is capable of participating in the trigonal planar coordination geometry hypothesized by our model.

Oxidation state	Coordination number	Geometry
Ag(I), d^{10}	2, 3, 4	Linear, Trigonal, Tetrahedral
Cu(II), d^9	5, 5, 4, 6	Trigonal bipyramidal, Square pyramidal, Square, Distorted octahedral
Zn(II), d^{10}	2, 4, 5, 5	Linear, Tetrahedral, Distorted trigonal bipyramidal, Square pyramidal

Table 3.2. Coordination geometry of metals copper(II), silver(I) and zinc(II).[22]
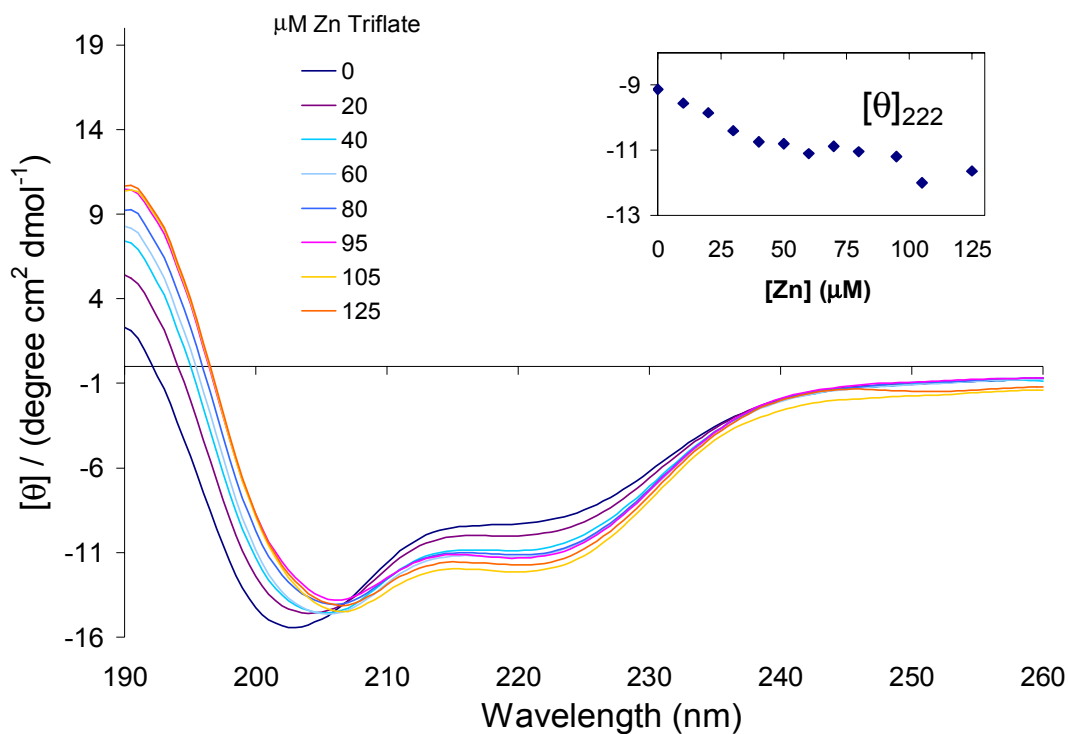
Figure 3.19. Circular dichroism spectra of peptide TZ1H (35 μM, 10 mM phosphate buffer, pH 5.6) titrated with zinc (II) triflate to nearly 4-fold above the initial peptide concentrations. Circular dichroism spectra indicate little metal-induced conformational change, with the minima at 202 nm shifted to 206 nm with a minor increase in negative ellipticity observed at 222 nm. Inset: Dependence of $[\theta]_{222}$ on metal ion concentration of zinc (II).
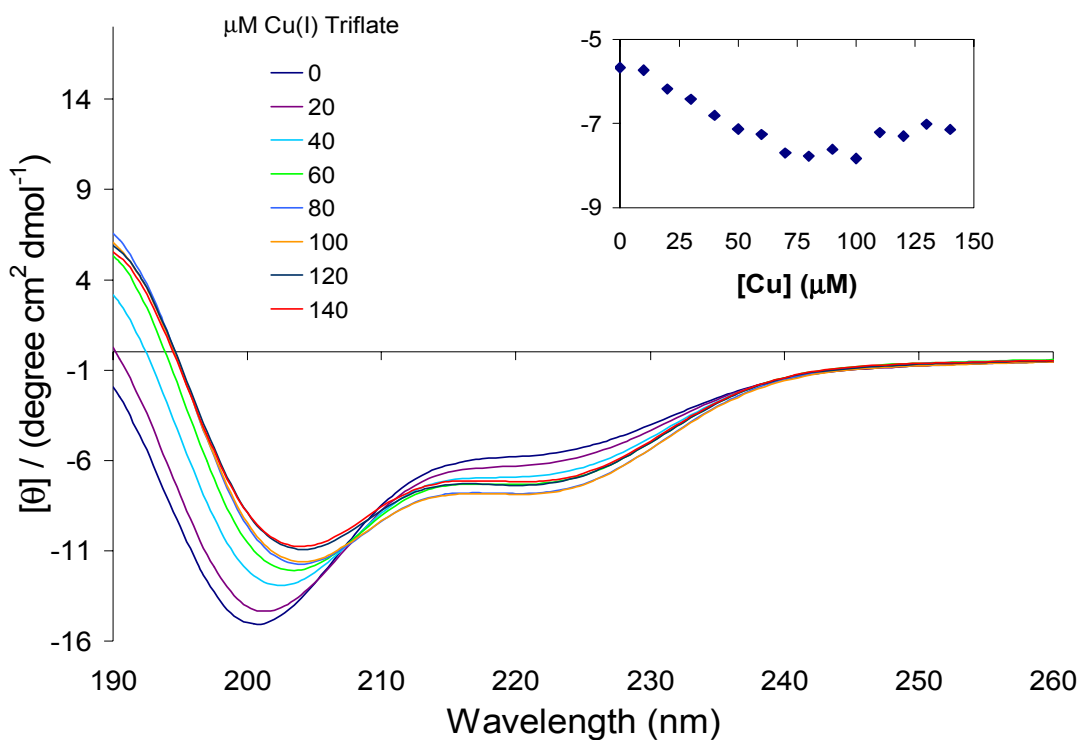
Figure 3.20. Circular dichroism spectra of peptide TZ1H titrated with copper (II) triflate to 3-fold molar excess above the initial peptide concentrations (50 μM, 10 mM phosphate buffer, pH 5.6). Circular dichroism spectra indicate little metal-induced conformational change, with the minima at 202 nm shifted to 206 nm with a minor increase in negative ellipticity observed at 222 nm. Inset: Dependence of $[\theta]_{222}$ on metal ion concentration of copper (II).

3.3 Summary

From the experiments described in this chapter, we conclude that an appropriately chosen metal ion can induce the self-assembly of a de novo-designed peptide to form a structurally defined nano-scale material. Silver (I) , a non-native metal ion, was shown to trigger a coil to helix transition in peptide **TZ1H** which leads to the formation of long aspect-ratio helical fibers. The **TZ1H** peptide sequence, inspired by a trimeric coiled-coil mutant GCN4-pII, is presumed to self-assemble in a staggered, triple-stranded helical bundle (**Figure 3.21**). Our model asserts a single metal binding site is composed of three histidine residues, where each of the three participating helices contributes a single sidechain imidazole. Based on crystallographic data from similar trimeric coiled-coil assemblies and other experimental evidence, we assert that the histidine residues are proximally-arranged into a single layer within the core. Previously, we have shown that protonation of these ionizable imidazole side chains results in electrostatic repulsion within the core of the peptide assembly which prevents coiled-coil formation.

In the silver (I) ion-binding experiments described in this chapter, the initial folded state of **TZ1H** is random coil since the peptide is prepared in buffer pH-adjusted below the pK_a of histidine. As a consequence, the binding of silver ion is linked to the deprotonation of the participating histidine sidechains. Specifically, the association of a single metal ion to the imidazole τ (tele) nitrogen involves the release of a proton. Evidence for this equilibrium is provided through the establishment of pH-dependence on the metal-binding event by both CD (**Figure 3.7**) and ITC (**Figure 3.10-13**).
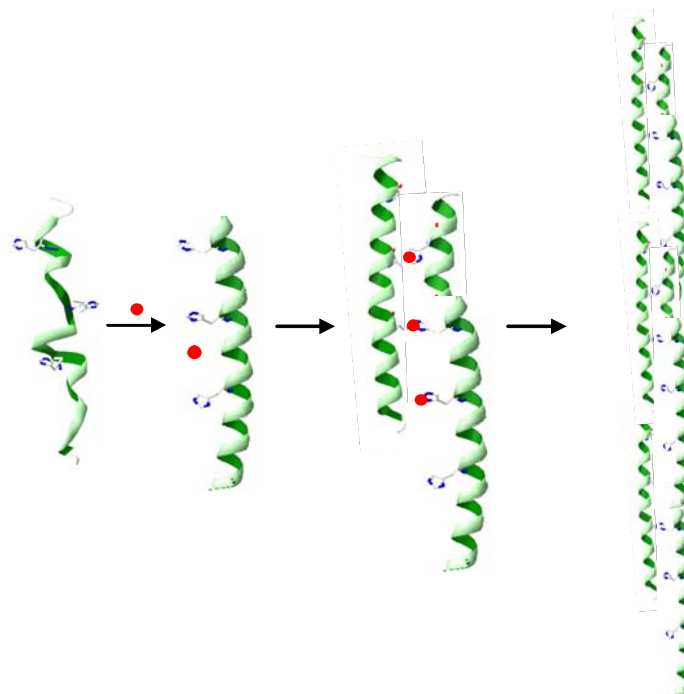
Figure 3.21. Proposed self-assembly scheme for peptide TZ1H prepared in the presence of silver (I) ion. The initial random coil state transitions to helical character upon the binding of silver (I) ion. This binding event is presumably coupled to the deprotonation of the histidine sidechain imidazole. Metal binding is coupled to the deprotonation of histidine side chains.

ITC determination for metal-to-peptide molar ratio in **TZ1H** peptide prepared at pH 5.3 (below the pK_a of a buried histidine sidechain) was reported as 3 silver ions per peptide, which is significantly higher than the 1:1 ratio observed at pH 5.6 by both ITC and CD spectrometry. Direct measurement of protons released upon metal binding can be accomplished by ITC. However, this requires the comparison of *Kb* values in three different buffers. Unfortunately, the pH range we must work in is outside the buffering capacity of most buffers.

3.3.1 Metal ion-binding sites residing in internal cavities provide selectivity

Our model asserts a single metal binding site is created by three histidine side chains, one ligand contributed by each of three participating helices, resulting in a planar trigonal coordination geometry (**Figure 3.22**). As a consequence, metals which prefer alternative coordination geometries will not be easily accommodated within the site.
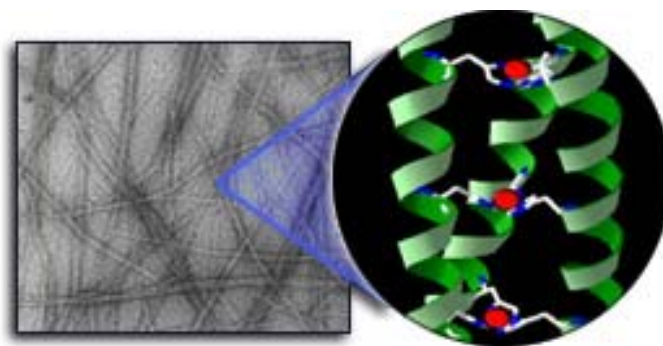
Figure 3.22.   TEM micrograph of silver ion-induced helical fibers set against a graphical representation of the proposed local structure including silver ion (red

This observation is critical to the rational design of selective metal ion-binding sites in *de novo*-designed peptides. It suggests that locating metal ion-binding sites within cavities of peptide-based assemblies might provide selective steric constraints to the binding geometries which are not available in more flexible, solvent-exposed sites. This design element is complementary to standard methodologies focusing on the identity and conformation of amino acid ligands to achieve selectivity in metal binding.

3.4 Experimental Section

3.4.1 Materials

N-α-Fmoc protected amino acids, HBTU, Rink amide resin, and solid phase peptide synthesis reagents were purchased from Anaspec, Inc. (San Jose, CA). Solvents and reagents used in peptide synthesis and cleavage were obtained through Aldrich Chemical Co. (Milwaukee, WI). Similarly, silver (I) trifluoromethanesulfonate (> 99%), zinc (II) trifluoromethanesulfonate (> 98%), and copper (II) trifluoromethanesulfonate (> 98%) were purchased as anhydrous salts from Aldrich. Sodium mono- and dibasic phosphate was obtained from Fisher Scientific, Inc. (Waltham, MA).

3.4.2 Peptide Synthesis and Purification

Peptide **TZ1H** was prepared via automated solid-phase peptide synthesis on a Rink amide resin (0.4-0.6 meq/g) on a Rainin Symphony Quartet peptide synthesizer (Peptide Technologies, Inc., Tucson, AZ) as described previously. Standard FMOC protection chemistry was employed with coupling cycles based on HBTU/NMM-mediated activation protocols and base-induced deprotection (20% piperidine in DMF) of the FMOC group. The N-terminus of the peptides was capped with acetic anhydride prior to cleavage from the resin. The peptide was isolated from the resin as the C-terminal amide derivative after acidic cleavage of the side chain protecting groups with a cocktail of trifluoroacetic acid (TFA), thioanisole, ethanedithiol and anisole (90:5:3:2). Crude peptides were precipitated in ice-cold ether and centrifuged at 6000 rcf at 4 $^{\circ}$C for

20 minutes. After pelleting, the supernatant was decanted and the process repeated until thiol odor is no longer present. The resulting pellet was then dried under nitrogen flow and stored at -20 $^{\circ}$C until purification.

Prior to purification, the precipitated peptide was thoroughly dissolved in 15 - 25 mL solution of 60% ddH$_2$0 / 40% acetonitrile in the presence of 0.1% trifluoroacetic acid (TFA). Reverse-phase HPLC purification was performed using a Waters 600 purification system (Waters Corp., Milford, MA) with a Waters 996 photodiode array and a reverse phase C-18 column (Atlantis dC18, 10 μm, 19 x 256 mm) with a linear gradient of acetonitrile and water (0.1% trifluoroacetic acid) at 10 mL / minute. The molar mass of **TZ1H** was confirmed by MALDI-TOF mass spectrometry on a Voyager-DE STR instrument (Perseptive Biosystems, Framingham, MA) using equal volumes of α-Cyano-4-hydroxycinnamic acid (saturated solution in 0.1% TFA ddH$_2$O) matrix and HPLC purified peptide. Fractions were combined and rotary evaporated to remove acetonitrile and TFA before lyophilization. Lyophilized peptides were stored at -20 $^{\circ}$C until used. The expected mass for **TZ1H** peptide is 4905.6 Da and the observed peak by MALDI was 4904.15.

3.4.3 Circular Dichroism

CD spectra were obtained using a JASCO J-810 CD spectropolarimeter (Jasco Inc., Easton, MD) equipped with a PFD-425S Peltier temperature control unit, using a 1 mm quartz cell. Peptide **TZ1H** was prepared in 10 mM phosphate buffer, which was pH-adjusted to the desired value using a mixture of 0.2 M mono- and dibasic sodium

phosphate solutions. Metal trifluoromethanesulfonate solutions were prepared in either doubly distilled water or 10 mM phosphate solutions (pH 5.6). Total sample volume used in CD measurements was typically 300 μL. Silver (I) titration spectra were recorded at 4 °C at 0.5 nm intervals, 1 nm bandwidth, 20 nm min^{-1}, and 8 sec response time. Spectra were baseline corrected before converting to mean residue ellipticities. Fractional helix content was calculated from MRE at 222 nm using equation F_{helix} = $[\theta]_{obs}$ - $[\theta]_{coil}$ / $[\theta]_{helix}$ - $[\theta]_{coil}$, where $[\theta]_{helix}$ and $[\theta]_{coil}$ in MRE are described as (-42,500 * (1 – (3 / (# residues)))) and + 645, respectively. Thermal melting curves were generated by monitoring the absorbance at 222 nm of **TZ1H,** typically 70 μM peptide in 10 mM sodium phosphate buffer (pH 5.6) including ~70 μM silver trifluoromethanesulfonic acid in a 1 mm quartz cuvette. Temperature ramping was performed from 4 - 98 °C at a rate of 1 °C/minute. The value of the T_m was determined from the first derivative of the CD melting curve.

3.4.4 Isothermal Titration Calorimetry

Silver-binding was assayed by measuring enthalpy changes associated with the titration of silver trifluoromethanesulfonate into **TZ1H** peptide solution (70 μM, 10 mM phosphate buffer, pH 5.6) using a VP-ITC microcalorimeter (Microcal, Northampton, MA) at 5 °C. The sample cell (1.4 mL volume) was loaded with 10 mM phosphate buffer pH 5.6, in either the presence or absence of peptide **TZ1H**. The reference cell contained the identical 10 mM phosphate buffer solution, at the same volume. All samples were

thoroughly degassed at 25 °C (ThermoVac, MicroCal) for a minimum of five minutes before loading into the cell.

In a typical silver titration experiment, 34 injections of silver (I) trifluoromethane solution (0.9 mM, 10 mM phosphate, pH 5.6) in 9 μL aliquots were performed through an automated titration syringe at 3.5 minute intervals into a cell containing **TZ1H** peptide solution. An initial injection of 0.5 μL was performed prior to the standard 9 μL injection to account for low enthalpy of binding in the initial ligand injection compared to that of subsequent injections. This is a standard technique used to compensate for leaking of ligand solution from the injection syringe or improper positioning of the syringe plunger with respect to the driving piston. During the experiment, the liquid in the sample cell was stirred by the syringe unit at 270 rpm, which allows appropriate mixing without frothing of the peptide solution. Blank injections of silver triflate solution into 10 mM sodium phosphate buffer (pH 5.6) were used to account for the heats of mixing and dilution.

Data analysis was performed on ORIGIN software (version 8) provided by the manufacturer. For curve fitting, a single-binding site was assumed and all fitting function parameters were free floating. Prior to and following each experiment, the ITC injection syringe, sample and reference cells were cleaned by flushing with 100 mL of 2% Contrad detergent solution (Decon Laboratories, Bryn Mawr, PA) and 100 mL doubly deionized water.

3.4.5 Transmission electron microscopy

Transmission electron microscopy was performed on either a JEOL 1210 (Tokyo, Japan) equipped with a lanthanum hexaboride (LaB_6) thermionic electron source or Philips LS-410 (Amsterdam, Netherlands) equipped with a tungsten filament. Imaging was performed at 90 kV (JEOL 1210) or 80 kV (Philips LS 410) accelerating voltage. Typical peptide concentrations used in electron microscopy studies were between 70 and 156 μM. An aliquot of **TZ1H** peptide solutions (10 μL) was pipetted onto a 200-mesh carbon-coated copper grid (Electron Microscopy Sciences, Hatfield, PA) and let stand for 1 min before excess solution was wicked away with a triangle of filter paper, leaving a thin layer on the grid surface. An additional wash with 10 μL doubly deionized water was performed, similar to sample deposition.   Negatively-stained samples for transmission electron microscopy were prepared with a 1:1 mixture of near-neutral stains Nano methylamine vanadate (pH 8.0) and Nano methylamine tungstate (pH 6.8), were used (NanoProbes, Yaphank, NY). Stain (3 μL) was applied to the grid and incubated for less than 1 minute before being wicked away with a triangle of filter paper.   The incubation times were significantly shorter than suggested by the manufacturer's instructions, to lessen the possibility of pH and / or metal influence on fiber formation of the sample on the grid during preparation. After repeating staining procedure once more, the grid was transferred to a grid box and stored under vacuum a minimum of 24 hours.

Electron micrographs were recorded on Kodax Electron Microscopy 4489 film and scanned on an AGFA Duoscan T2500 scanner to 2000 pixels per inch (ppi) resolution. Image measurements were performed using the software ImageJ, version 1.36b, freely available from U. S. National Institutes of Health, Bethesda, Maryland,

USA (http://rsb.info.nih.gov/ij/). The spatial scale was set to a known distance in the image and the distance in pixels. The segmented line tool was used to trace the diameter of fibrils or fiber segments that displaced well defined edges. Thirty independent diameter measurements were made from fibers spanning every quadrant of the image. Errors in the distance measurements are reported as standard error of the mean.

3.4.6   Scanning transmission electron microscopy

Low voltage scanning transmission electron microscopy (LV-STEM) and backscatter electron microscopy (BSE) was performed on a Topcon (Pleasanton, CA) DS-150 scanning electron microscope equipped with a Schottky field-emission electron source, STEM and backscatter detector. Accelerating voltages employed in BSE and LV-STEM imaging were between 15-20 kV.

Scanning transmission electron microscopy (STEM) imaging was performed on a Hitachi SD 2000 at 200 kV accelerating voltage. For scanning transmission electron microscopy, samples were prepared similar to unstained samples for TEM imaging described above. Peptide samples deposited on TEM grids were loaded onto a STEM sample mount and inserted into the first stage of the microscope.

3.4.7   Energy dispersive X-ray analysis

Energy dispersive X-ray analysis (EDX) was performed on a Hitachi S-800 field emission scanning electron microscope (Hitachi, Tokyo, Japan) at 15 kV accelerating

voltage. Aliquots of peptide fibers were deposited on a carbon-coated copper grid, without metal coating, and prescreened by TEM for the presence of fibers prior to EDX analysis. Before collecting spectra, the TEM grid was attached to an aluminum specimen mount with double-sided carbon tape.

3.4.8 Amino Acid Analysis (AAA) and Inductively Coupled Plasma Mass Spectrometry (ICP-MS)

ICP-MS analysis was employed to determine silver (I) ion concentration in samples of assembled fibers. ICP-MS was performed at the Chemical Analysis Laboratory (CAL) at the University of Georgia (http://www.cal.uga.edu). A solution of 10 mM silver (I) trifluoromethanesulfonate was utilized as a calibrant. Solutions of peptide **TZ1H** fibrils initially containing a minimum of equimolar silver ion was split into two equal aliquots and the fibrils were isolated via centrifugation at 16,100g for 1 hour at 4 ºC. The resulting pellets were washed with an equal volume of 10 mM phosphate buffer (pH 5.6) to remove unbound silver ion. This process was repeated once. The fibrils were re-suspended in 10 mM phosphate buffer (pH 5.6) to the initial sample volume. For ICP-MS analysis, the sample was diluted to 2 mL in the same 10 mM phosphate buffer (pH 5.6) to provide sufficient sample volume for analysis.

Quantitative amino acid analysis AAA analysis was performed at the Keck Biotechnology Resource Laboratory at Yale University (http://keck.med.yale.edu) on the same samples prepped for ICP-MS. The peptide solution was lyophilized via speed vacuum and sent as a dried pellet. For analysis, each sample was dissolved with 500 µl

of 70% formic acid and a 10 µl (2%) aliquot was used for hydrolysis. After hydrolysis, 20% of each aliquot was run on a Hitachi L-8900 amino acid analyzer.

Concentrations were calculated using the following equations:

Ag$^+$ / Peptide Ratio $\qquad = \qquad \dfrac{[Ag+]mM}{[Peptide]mM}$

Concentration of Ag$^+$ (mM) $\quad = \quad \dfrac{[Ag^+]_{ICP-MS}(ppb)\times 10^{-3}\times 2000(\mu L)}{107(amu)\times 200\ (\mu L)}$

Concentration of Peptide (mM) $\ = \ \dfrac{nmole\ \ average\ by\ AAA\ (nmole)\times 10^{-6}}{Injection\ Volume\ (\mu L)\times 10^{-6}}$

Peptide concentration was also quantitated from the UV absorption of the single, solvent-accessible tyrosine residue under denaturing conditions.   Peptide **TZ1H** concentration (c), reported in mg / mL, was determined in 6 M guanidinium chloride solution using UV absorbance at 280 nm of the single tyrosine residue, where c = Molecular weight x A$_{280}$ / 1280.

3.5 References

1.   Shi, W.; Zhan, C.; Ignatov, A.; Manjasetty, B. A.; Marinkovic, N.; Sullivan, M.; Huang, R.; Chance, M. R., Metalloproteomics: high-throughput structural and functional annotation of proteins in structural genomics. *Structure* **2005,** 13, (10), 1473-86.

2.   Ghosh, D.; Pecoraro, V. L., Probing metal-protein interactions using a de novo design approach. *Curr Opin Chem Biol* **2005,** 9, (2), 97-103.

3.   Berg, J. M.; Godwin, H. A., Lessons from zinc-binding peptides. *Annu Rev Biophys Biomol Struct* **1997,** 26, 357-71.

4.   Hong, J.; Kharenko, O. A.; Ogawa, M. Y., Incorporating electron-transfer functionality into synthetic metalloproteins from the bottom-up. *Inorg Chem* **2006,** 45, (25), 9974-84.

5.   Baltzer, L.; Nilsson, J., Emerging principles of de novo catalyst design. *Curr Opin Biotechnol* **2001,** 12, (4), 355-60.

6.   Benson, D. E.; Wisz, M. S.; Hellinga, H. W., Rational design of nascent metalloenzymes. *Proc Natl Acad Sci U S A* **2000,** 97, (12), 6292-7.

7.   DeGrado, W. F.; Summa, C. M.; Pavone, V.; Nastri, F.; Lombardi, A., De novo design and structural characterization of proteins and metalloproteins. *Annu Rev Biochem* **1999,** 68, 779-819.

8.   Tanaka, T.; Mizuno, T.; Fukui, S.; Hiroaki, H.; Oku, J.; Kanaori, K.; Tajima, K.; Shirakawa, M., Two-metal ion, Ni(II) and Cu(II), binding alpha-helical coiled coil peptide. *J Am Chem Soc* **2004,** 126, (43), 14023-8.

9.   Kiyokawa, T.; Kanaori, K.; Tajima, K.; Koike, M.; Mizuno, T.; Oku, J. I.; Tanaka, T., Binding of Cu(II) or Zn(II) in a de novo designed triple-stranded alpha-helical coiled-coil toward a prototype for a metalloenzyme. *J Pept Res* **2004,** 63, (4), 347-53.

10.   Li, X.; Suzuki, K.; Kanaori, K.; Tajima, K.; Kashiwada, A.; Hiroaki, H.; Kohda, D.; Tanaka, T., Soft metal ions, Cd(II) and Hg(II), induce triple-stranded alpha-helical assembly and folding of a de novo designed peptide in their trigonal geometries. *Protein Sci* **2000,** 9, (7), 1327-33.

11.   Matzapetakis, M.; Farrer, B. T.; Weng, T. C.; Hemmingsen, L.; Penner-Hahn, J. E.; Pecoraro, V. L., Comparison of the binding of cadmium(II), mercury(II), and arsenic(III) to the de novo designed peptides TRI L12C and TRI L16C. *J Am Chem Soc* **2002,** 124, (27), 8042-54.

12.   Farrer, B. T.; Pecoraro, V. L., Hg(II) binding to a weakly associated coiled coil nucleates an encoded metalloprotein fold: a kinetic analysis. *Proc Natl Acad Sci U S A* **2003,** 100, (7), 3760-5.

13.   Cerasoli, E.; Sharpe, B. K.; Woolfson, D. N., ZiCo: a peptide designed to switch folded state upon binding zinc. *J Am Chem Soc* **2005,** 127, (43), 15008-9.

14.   Pagel, K.; Vagt, T.; Kohajda, T.; Koksch, B., From alpha-helix to beta-sheet--a reversible metal ion induced peptide secondary structure switch. *Org Biomol Chem* **2005,** 3, (14), 2500-2.

15.   Ghadiri, M. R.; Choi, C., Secondary structure nucleation in peptides. Transition metal ion stabilized .alpha.-helices. *J. Am. Chem. Soc.* **1990,** 112, (4), 1630-1632.

16.   Kohn, W. D.; Kay, C. M.; Sykes, B. D.; Hodges, R. S., Metal Ion Induced Folding of a de Novo Designed Coiled-Coil Peptide. *J. Am. Chem. Soc.* **1998,** 120, (6), 1124-1132.

17.   Dieckmann, G. R.; McRorie, D. K.; Tierney, D. L.; Utschig, L. M.; Singer, C. P.; O'Halloran, T. V.; Penner-Hahn, J. E.; DeGrado, W. F.; Pecoraro, V. L., De Novo Design of Mercury-Binding Two- and Three-Helical Bundles. *J. Am. Chem. Soc.* **1997,** 119, (26), 6195-6196.

18.   Allen, F. H., The Cambridge Structural Database: a quarter of a million crystal structures and rising. *Acta Crystallogr B* **2002,** 58, (Pt 3 Pt 1), 380-8.

19.   Eckert, D. M.; Malashkevich, V. N.; Kim, P. S., Crystal structure of GCN4-pIQI, a trimeric coiled coil with buried polar residues. *J Mol Biol* **1998,** 284, (4), 859-65.

20.   Hodges, R. S., De novo design of α-helical proteins: Basic research to medical applications. *Biochemistry and Cell Biology* **1996,** 74, (2), 133-154.

21.   Saran, L.; Cavalheiro, E.; Neves, E. A., New aspects of the reaction of silver(I) cations with the ethylenediaminetetraacetate ion. *Talanta* **1995,** 42, (12), 2027-2032.

22.   Cotton, F.; Wilkinson, F., *Advanced Inorganic Chemistry*. 2nd ed.; Interscience Publishers: New York, 1967; p 1136.

Chapter IV: Structural plasticity - Merging α-helix and β-sheet elements into a single peptide sequence

4.1 Introduction

A variety of neurological diseases, including Alzheimer's, Parkinson's and other prion diseases, are thought to arise from a common molecular origin.[1] The defining event of these disease states is a spontaneous conformational change in the secondary or tertiary structure of a native protein, which occurs without alteration of the primary sequence. Unlike productive structural transitions which facilitate native protein functionality, as in the viral-coat proteins which direct virus-host membrane interactions, this phenomenon instead results in the transformation of a functional protein into a toxic element within the living system through a refolding event.[2] This results in a number of detrimental consequences to the organism, including significant tissue damage, inhibition of native biological function of the protein, and / or directing improper trafficking behavior.

In the case of the aforementioned diseases, the pathological aggregate is thought to arise from a gross conformational transition from α-helix to β-sheet content in the affected protein through a mechanism which is not completely understood. Particular interest has been expressed in the role amino acid sequence may play in facilitating conformational switching in amyloid-associated proteins. To this end, synthetic model peptides have been designed to exhibit α-β structural duality in hopes of advancing our

understanding of the molecular basis for the switching of conformational states in native proteins. Designed peptide systems have been described which exhibit control over conformational transitions through the stabilization of a preferred secondary structure, frequently with the assistance of changes in pH, metal ion concentration, ionic strength or targeted mutations in native sequences. [3,4,5]

A particularly elegant switching system was reported by Woolfson and coworkers, which achieved structural duality through the merging of positive design elements for both a dimeric, α-helical coiled-coil and β-hairpin into a single primary sequence.[6] The introduction of β-sheet character into a canonical leucine zipper system was accomplished through the incorporation of threonine, a high β-sheet propensity amino acid, into the *f*-positions of the heptad repeat units. Usually, this position is occupied by the helix-promoting amino acid alanine in native and designed coiled-coils. The resulting peptide, Template α-T, exhibits a heat-induced helix to β-sheet transformation which results in the formation of amyloid-like fibrils. This work is significant because it suggests that specific, structure-defining elements within a primary sequence can promote β-sheet structure, even within a canonical coiled-coil sequence. This hypothesis challenges conventional paradigms which impose more restrictive rules for generating β-sheet forming sequences, such as hydrophobic-polar residue alternating patterns (H-P-H-P-H-P-H) and the utilization of structural conflict regions.[7,8]

In this chapter, a peptide sequence composed of a canonical coiled-coil heptad motif and characterized as a helical coiled-coil, is shown to also self-assemble into long-aspect ratio β-sheet fibrils. This quality was achieved through a conservative substitution in the primary sequence of a helical peptide, in which an amino acid known

for high β-sheet propensity is introduced in a position which comprises the inter-helical interface. Consequently, this peptide provides a simplistic model for understanding how a single amino acid mutation in the core-forming region of a canonical coiled-coil assembly can facilitate a gross conformational change in the complex.

4.2 Results

4.2.1 Design of TZ1T peptide sequence

The amino acid sequence of peptide **TZ1T** was derived from peptide **TZ1H,** the later of which was shown to form long aspect-ratio, α-helical fibers under basic buffering conditions.[9] The 41-residue peptide sequence is organized into six tandem heptad repeats ([*a-b-c-d-e-f-g*]$_6$), in a fashion reminiscent of the native coiled-coil structural motif (**Figure 4.1**). The parental sequence for both **TZ1H** and **TZ1T** is the isoleucine zipper peptide GCN4-pII, a synthetic coiled-coil which was shown by crystallographic data to favor the formation of a trimeric assembly.[10] Structural studies of native and mutant coiled-coil complexes have established that the identity of residues occupying the core-forming *a-* and *d*-positions in the heptad strongly influences the oligomerization state of coiled-coil assemblies. The incorporation of isoleucine residues into the majority of the core-forming positions of peptide GCN-pII was shown to be the driving force for the formation of the trimeric oligomerization state. Additionally, control of lateral
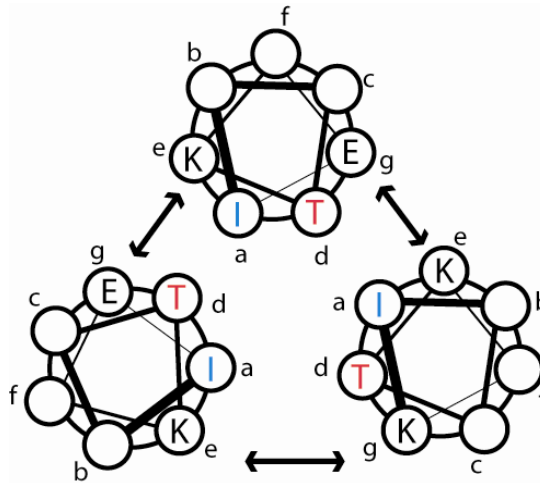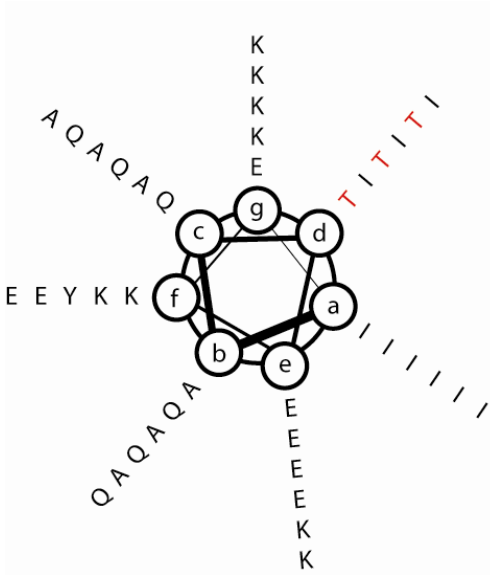
Figure 4.1. (Top). Helical wheel diagram of a single TZ1T helical peptide and (below) the associated primary sequence. (Bottom). Cross-sectional view of a triple-stranded helical bundle formed through the self-assembly showing core-forming *a*- and *d*-position occupied by isoleucine (blue) or threonine (red). Note, the majority of the hydrophobic core consists of isoleucine residues expect for threonine in the *d*-position of alternate heptads.

registration of adjacent helical protomers was engineered into the peptide sequence through the exploitation electrostatic interactions between charged residues in the *e*- and *g*-heptad positions. In this scheme, cooperative Columbic interactions between e- and g-position residues on adjacent helical protomers are charge-complementary only if alignment occurs in a two-heptad staggered formation, in which self-assembly favors the formation of an α-helical fiber composed of three helical strands.

Introduction of a β-strand element in the canonical coil-coiled system was accomplished by the introduction of three threonine residues into the *d*-positions of alternate heptads (**Figure 4.1, Bottom**). Threonine is an amino acid known to have a particularly high propensity for β-sheet formation.[11] However, this polar residue has also been shown to be tolerated within the hydrophobic core of a three-stranded, in-register coiled-coil assembly.[12] The reported structure was shown by crystallographic data to accommodate a single layer of *d*-position threonine residues at the interhelical interface by positioning the side chain hydroxyl group toward the solvent-accessible face to participate in an *i* to (*i*-4) hydrogen bond with the carbonyl of the previous *g*-position lysine (**Figure 4.2**). This preferred arrangement has the additional stabilizing effect of positioning the side chain methyl group into the hydrophobic core. A nearly identical packing geometry was reported in a synthetic four-helix coiled-coil possessing a single *d*-layer of threonine residues.[13]
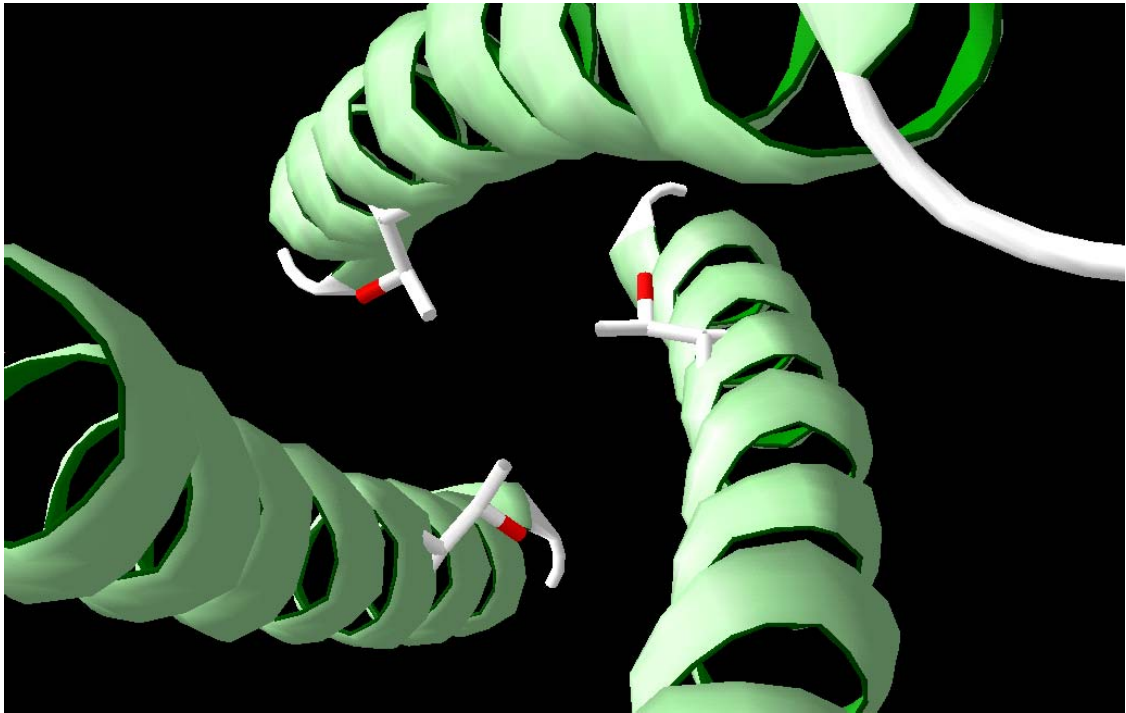
Figure 4.2. Crystal structure of a homotrimeric coiled-coil mutant composed of peptides containing a threonine residue in a single *d*-position (PDB 1IJ1). The hydroxyl group of the Thr 12 side chain makes an *i* to (*i* − 4) backbone hydrogen bond to the peptide carbonyl of Lys8, which directs the threonine methyl groups into the core.

4.2.2   Circular Dichroism of TZ1T

Investigation of the conformation of peptide **TZ1T** in solution (10 mM phosphate, buffer pH 7.0) was performed via circular dichroism spectroscopy. Surprisingly, at pH 7.0 the CD spectrum displayed a prominent minimum at 201 nm, indicating significant random coil content due to the dominance of unassembled peptide in solution (**Figure 4.3**). Previously in our group, Dr. Yuri Zimenkov has shown brief heating to

100 ºC was critical to the self-assembly of an all isoleucine-core peptide **S6K** into α-helical fibers under neutral pH buffering conditions. Therefore, an aliquot of peptide **TZ1T** prepared in pH 7.0 buffer was heated to approximately 100 ºC in a 500 mL beaker of boiling water and allowed to cool slowly overnight in a manner identical to the assembly conditions for the triple-stranded **S6K** fibers. Strikingly, the CD spectra for the peptide solution before and after heating were distinctly different. After heating and cooling overnight, the minima at 201 nm associated with high random coil content was replaced by a new minimum at 218 nm, strongly suggestive of β-sheet conformation (**Figure 4.3**).
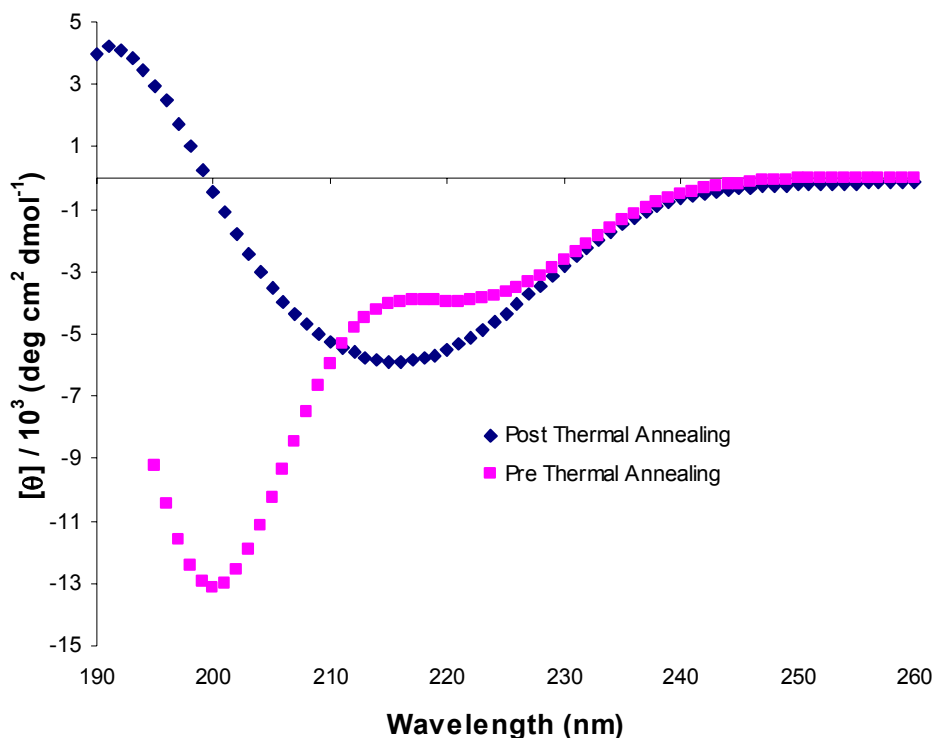
Figure 4.3 **CD spectrum of 100 μM TZ1T peptide assembled in 10 mM phosphate buffer (pH 7.0) after briefly thermal heating to 100 ºC and then cooled slowly overnight.**

Furthermore, it was possible to follow the transformation from random coil to β-sheet conformation by circular dichroism, through the overlay of full wavelength spectra scans collected from 4 to 100 ℃ in 1 ℃ intervals (**Figure 4.4**). A sharp decrease in signal at 201 nm followed by the arrival of a new minimum at 218 nm is observed to occur between the temperature range of 50 to 60 ℃, suggesting the transition to β-sheet occurs within this temperature regime.
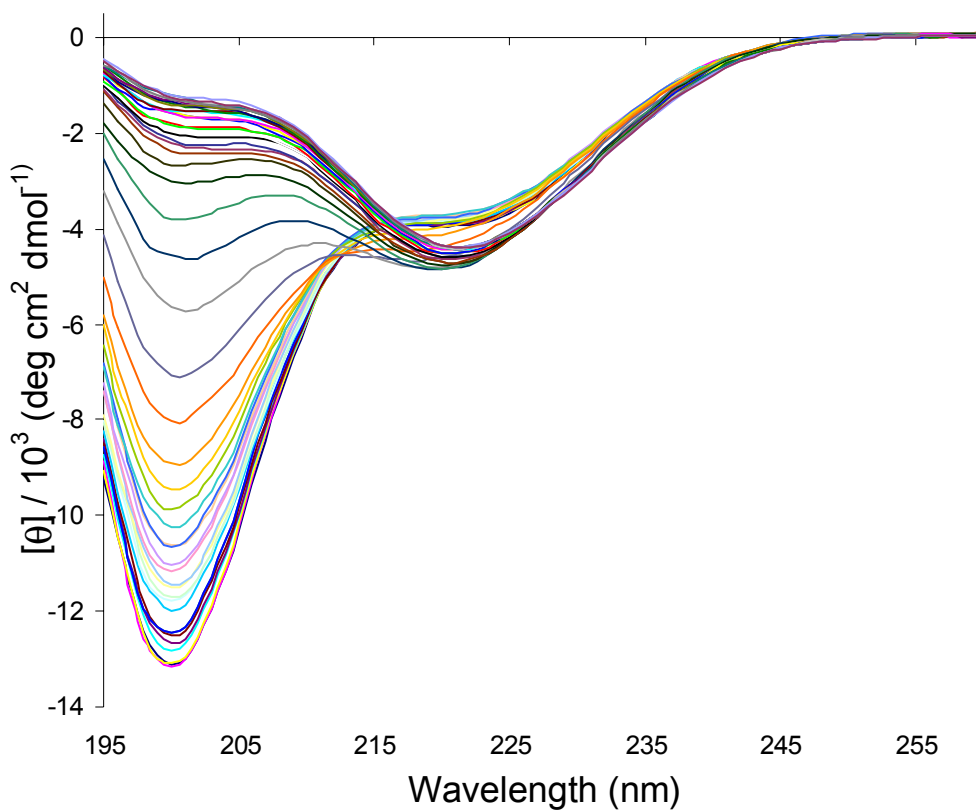
Figure 4.4. Overlay of CD spectra collected from 4 to 100 °C in 1 °C intervals shows a conformational transition from random-coil (4 °C, minimum at 201 nm) to β-sheet (100 °C, minimum at 218 nm)

This transition can also be followed by monitoring the thermal unfolding of the random coil conformation of peptide **TZ1T** by CD spectroscopy. In the resulting spectrum, $[\theta]_{201\ nm}$ attributed to random coil conformation is plotted versus temperature. The disappearance of absorption at 201 nm was observed to occur as a sigmoidal curve indicating a cooperative unfolding transition with a calculated T_m of 55 ºC (**Figure 4.5**).
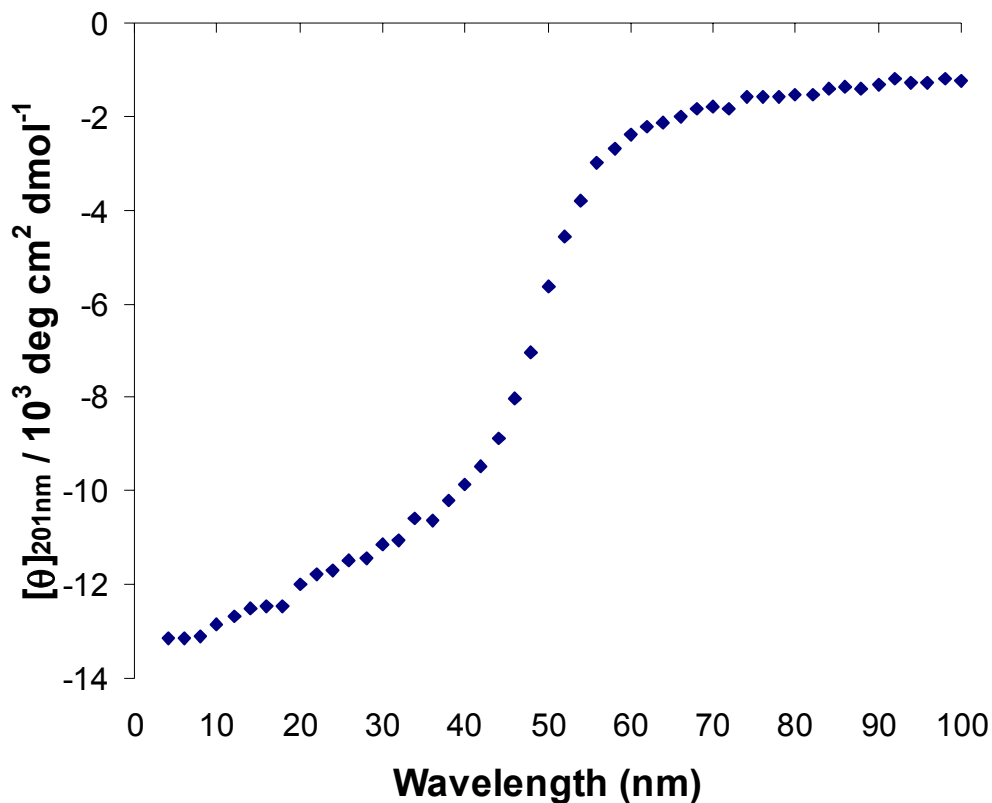
Figure 4.5. Thermal denaturation of 70 μM TZ1T (10 mM phosphate, pH 7.0), monitoring the wavelength associated with random coil content (201 nm). The T_m is determined to be 55 °C.

Furthermore, the coil-sheet transition was shown to occur spontaneously over time in **TZ1T** peptide solutions prepared at pH 7 which was allowed to age at 20 °C for a minimum of 64 hours. The time-dependant CD spectra closely resembled the heat-induced CD spectra, in which the replacement of the minima at 201 nm is replaced by new minima at 218 nm (**Figure 4.6**). A distinct isodichroic point at 212 nm in the time-dependant CD manifold consistent with a two-state coil-to-sheet transition.[14]
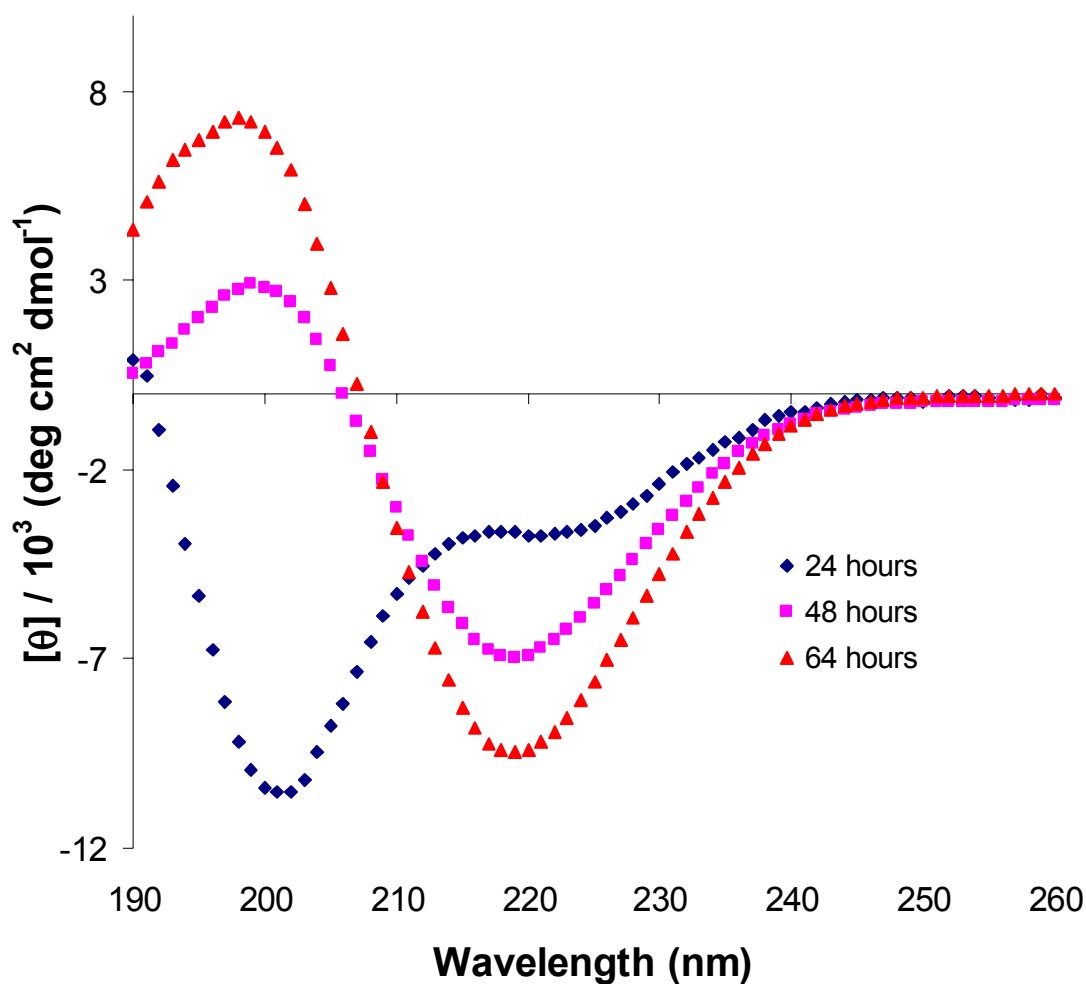
Figure 4.6. CD spectral change in 70 μM peptide TZ1T (10 mM phosphate, pH 7.0, 22 °C) over the course of 62 hours.

The absence of α-helical content in peptide **TZ1T** solution at pH 7.0 inspired a further investigation of the influence of pH on the self-assembly of the system. To assay the pH-dependant assembly of **TZ1T**, aliquots of the peptide were assembled in 10 mM phosphate buffer across a pH gradient ranging from 4.0 to 7.0 in approximately 0.5 unit intervals. Circular dichroism spectroscopy revealed a strong dependence of peptide conformation on environmental pH (**Figure 4.7**). Peptides assembled between pH values 7.0 and 5.5 displayed a characteristic random coil signature, with a minimum between wavelengths 201 and 203 nm. However, at pH values between 5.0 and 4.0, two new minima occur at 208 and 222 nm, indicating the appearance of α-helical secondary structure. The major helix-to-coil transition occurred between the 4.0-5.5 pH range, with the sharpest decrease in α-helicity seen in the 0.5 pH unit interval between 4.0 and 4.5, which define the range flanking the accepted pK_a value (4.07) for the glutamic acid side chain (**Figure 4.7, inset**). This suggests the helix-coil conformational transition is dependent on the protonation state of the *e*-position glutamic acid.

For the α-helical species, the limiting value for fractional helicity was observed as 63% at pH 4.0 which is an acceptable value for a non-traditional α helical assembly. The value of the $[\theta]_{222}$ / $[\theta]_{208\ nm}$ ratio was determined to be 0.945, close to the theoretical value of 1.0 for a coiled-coil assembly. A near-isodichroic point was documented at 204 nm, which is consistent with a coil-to-helix conversion. The coil-to-helix conversion was fully reversible in the 4.0 -7.0 pH range.
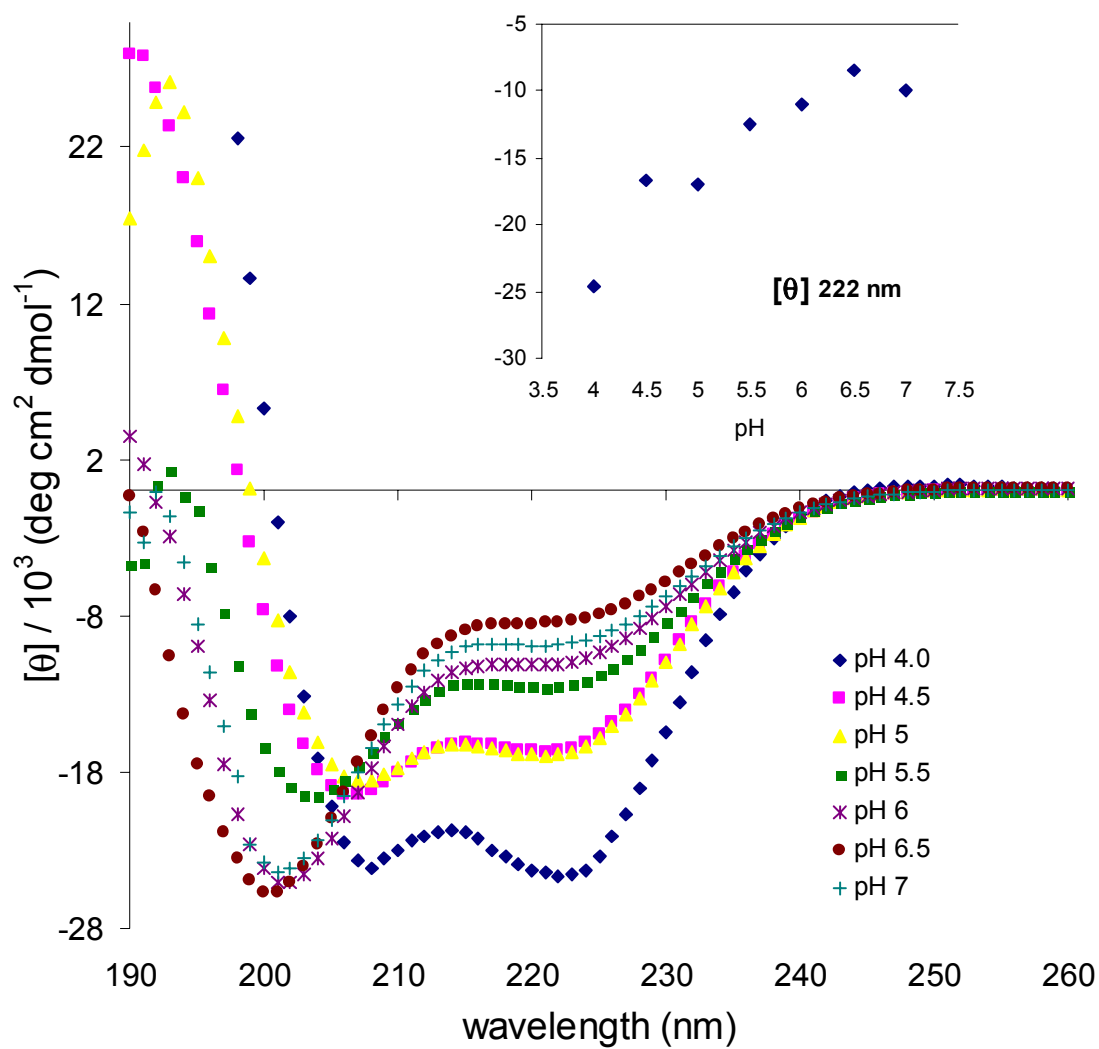
Figure 4.7. pH dependence of peptide conformation of 70 μM TZ1T assayed by CD spectroscopy. (Inset) A plot of pH versus MRE 222 nm shows direct correlation between intensity of α-helical content and pH.

The inclusion of threonine at the hydrophobic core-forming positions in the **TZ1T** peptide sequence greatly affects the stability of the helical assembly, which exhibits a melting transition under acidic conditions at 40 °C (**Figure 4.8**)   This suggests the helical assembly is significantly destabilized with respect to the all-isoleucine parental peptide **S6K** and the histidine containing peptide **TZ1H**.
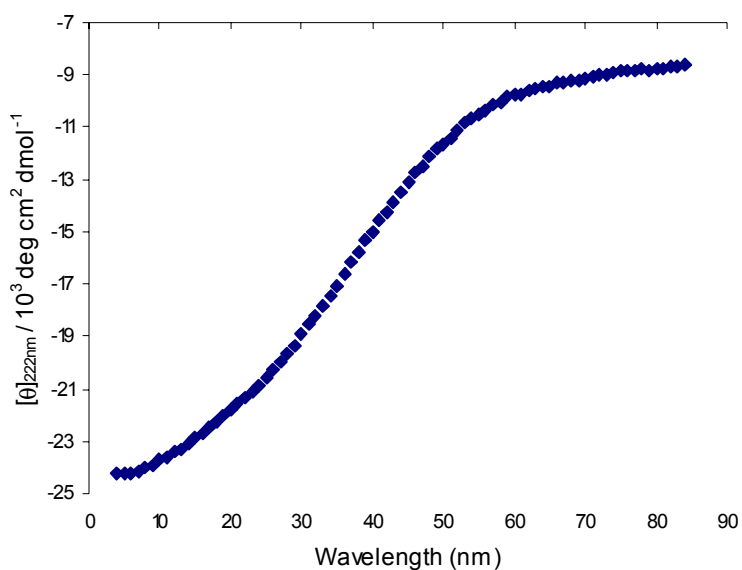
Figure 4.8.   Thermal denaturation of the α-helical species of TZ1T peptide prepared at 60 μM peptide concentration in 10 mM phosphate buffer (pH 4.0).

4.2.3   Differential Scanning Calorimetry (DSC)

Further investigation of the thermal rearrangement was performed by differential scanning calorimetry (DSC). A solution of peptide **TZ1T** at pH 7.0 heated from 20 to 100 ºC displayed a sharp, irreversible peak at 55 °C, indicating a single step denaturation.

The transition temperature (T_m 55 °C) observed closely correlates with the transition temperature determined by CD spectrometry (**Figure 4.9**).
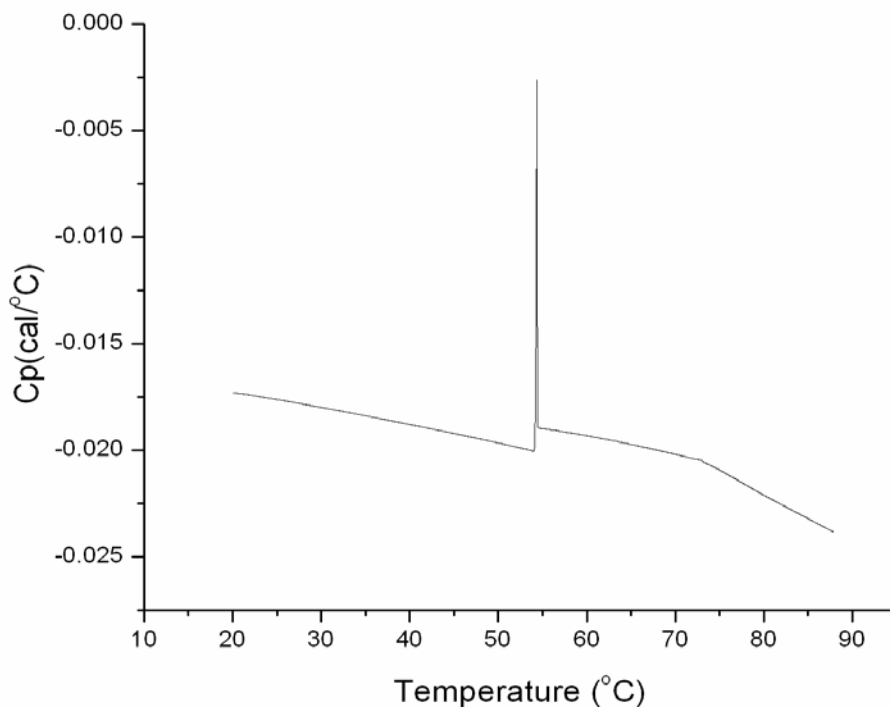
Figure 4.9. Differential scanning calorimetry of 175 μM TZ1T peptide (10 mM phosphate, pH 7.0) shows sharp, irreversible transition at 55 °C.

4.2.4 Transmission electron microscopy

The presence of higher-order assembly in the β-sheet conformation of **TZ1T** was assayed by negative-stain TEM. Micrographs of peptide samples prepared at pH 7.0 and aged for three days displayed fibrous aggregates of several μm in length, among many smaller persistence length protomers (**Figure 4.10**). The long-aspect ratio fibers exhibit a loose helical twist reminiscent of β-sheet ribbons, with average diameter of 10.5 ± 0.44

nm for the region parallel to the TEM-grid carbon substrate (**Figure 4.11**). This experimentally determined diameter is within reason for an extended conformation of a 41 residue sequence, which is estimated to be approximately 14.3 nm. As a comparison, typical amyloid is characterized by an unbranched fiber of 7-12 nm diameters.[15] Also routinely visualized were dense patches of entangled, short length fibrils, which were mainly isolated geographically on the grid apart from the μm length fibers (**Figure 4.12**).

Similarly, peptide **TZ1T** prepared under helix-forming conditions (10 mM phosphate, pH 4.0) showed evidence of fiber formation (**Figure 4.13**). However, the morphology resembled more closely previously described helical fibers, with a smooth, barrel-like topography devoid of any ribbon structure. The fibers were on average < 1 μM in length, which is considerably shorter than the previously described β-sheet morphology and even other helical fibers developed in our lab. Presumably, the stunted fibril growth results from improper lateral registration of adjacent helical protomers since the charged glutamic acid residues in the *e*- and *g*-heptad positions are neutralized in acidic buffering conditions. Abolishing the cooperative electrostatic interactions programmed into the **TZ1T** peptide sequence will remove the element which enforces the proper fiber-inducing heptad stagger. Additionally, the observed diameter of 21.6 ± 1.0 nm is exactly twice the size of the β-sheet conformation.
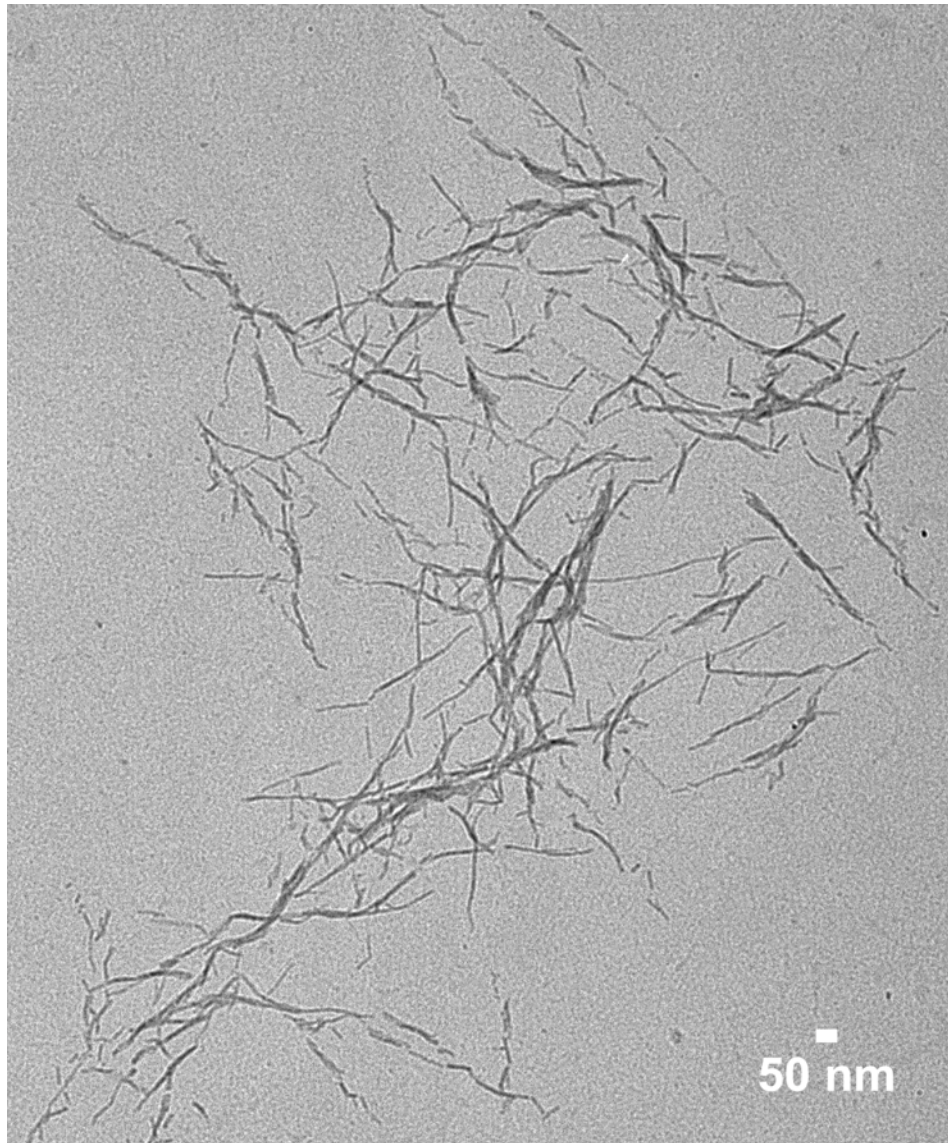
Figure 4.10. **TEM micrograph of 100 μM peptide TZ1T fibers (10 mM phosphate, pH 7.0, heat-induced transformation) of β-sheet conformation. Average fiber diameter was determined to be 10.5 ± 0.44 nm.**
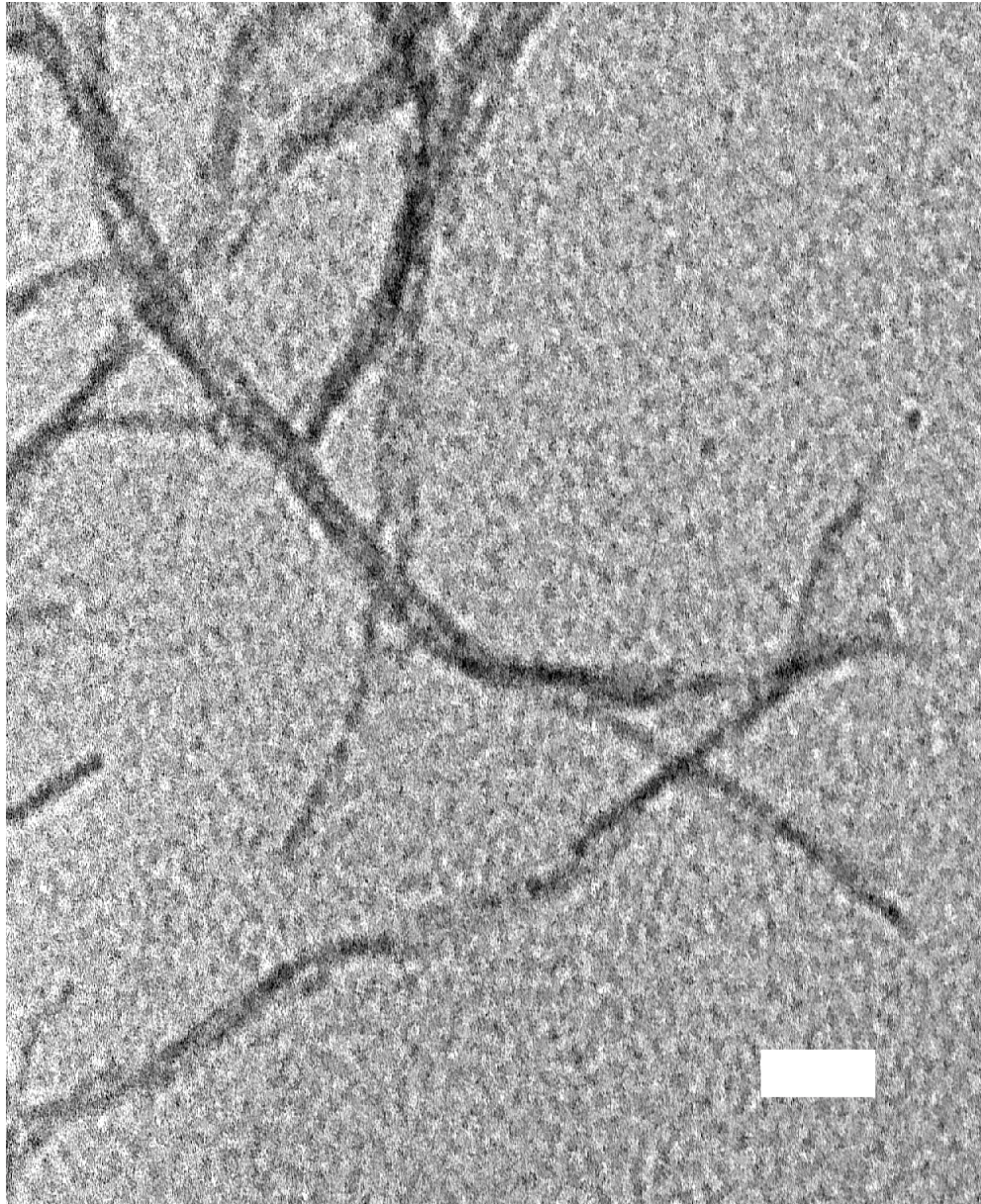
Figure 4.11. High magnification image of TZ1T fibers in Figure 4.9 shows loose helical twist reminiscent of β-sheet ribbons. Scale bar = 40 nm.
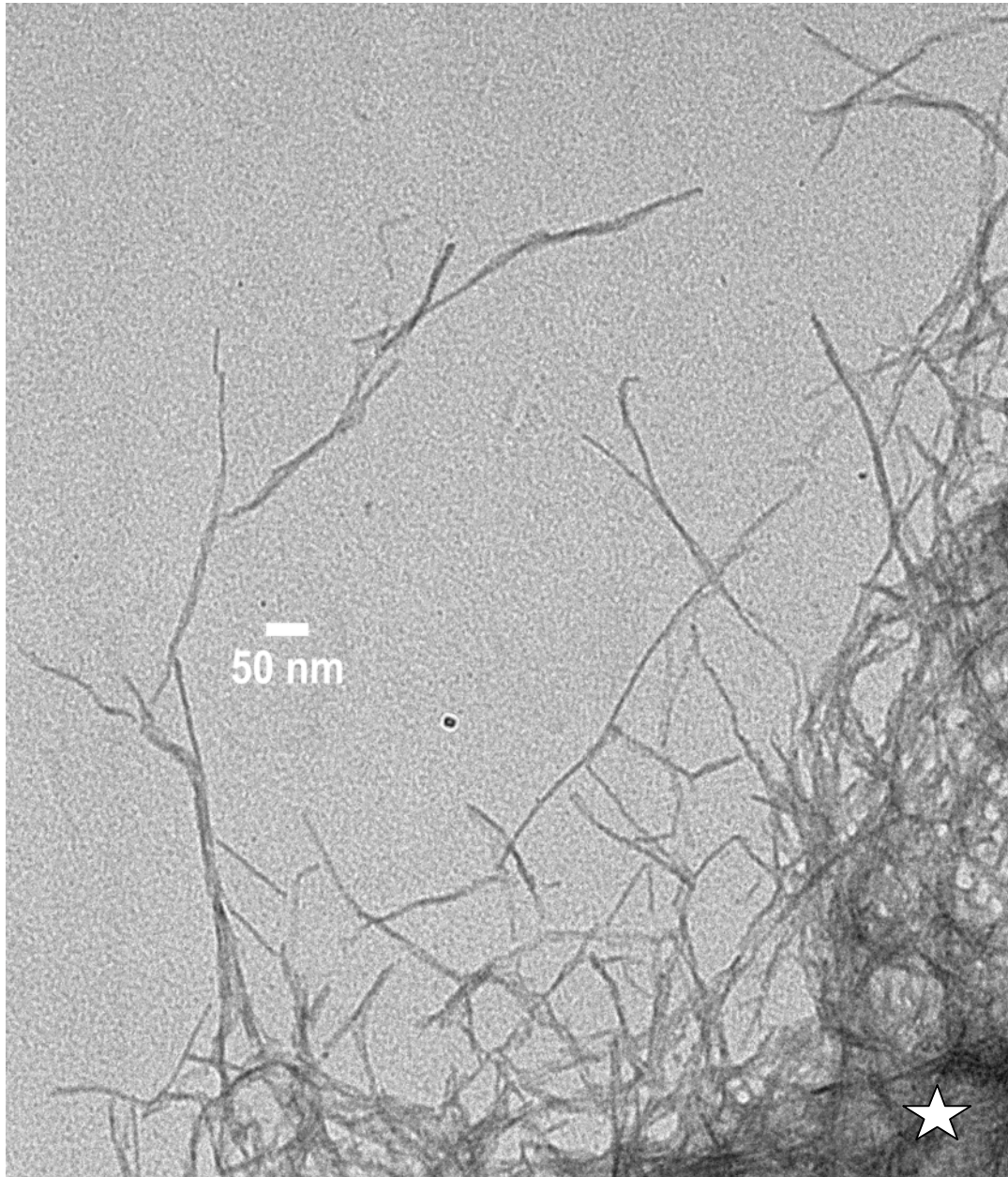
Figure 4.12. **Transmission electron microscopy of 100 μM TZ1T peptide (10 mM phosphate, pH 7.0, heat-induced β-sheet conformation). The white star marks area of dense, entangled fibers.**

Figure 4.13. TEM micrograph of 100 μM TZ1T peptide solution assembled under α-helical fiber-forming conditions (10 mM phosphate buffer, pH 4.0).

4.2.5 Fourier Transform Infrared (FTIR) Spectroscopy of TZ1T

FTIR spectroscopy was employed to confirm the coil-helix and coil-sheet transitions first identified by CD spectrometry. While several amide mode vibrations occur within peptide structures, the amide I provides the most useful information for conformational analysis.[16] The amide I mode arises primarily from the C = O stretching vibration of the amide group and is observed in the region 1600-1700 cm^{-1}. In most proteins and peptides, the α-helical band frequency is located in the range of 1650-1655, while the β-sheet band frequencies are in the 1620-1640 range.

The IR spectrum of an air-dried **TZ1T** peptide sample assembled at pH 7.0 and aged for three days shows strong absorption in the amide I region at 1627 cm^{-1} and a relatively weak absorbance at 1693 and 1693 cm^{-1} (**Figure 4.14, Top**). The peak at 1627 cm^{-1} is indicative of β-sheet conformation in the **TZ1T** peptide assembly, which confirms the similar observation by CD spectroscopy performed on peptide assembled under similar conditions. Additionally, the peak at weak absorption at 1693 cm^{-1} suggests significant anti-parallel β-sheet component. Also present in the same region are absorption peaks at 1654 and 1648 cm^{-1} which suggest an α-helical component is also present.

In contrast, the IR spectrum for **TZ1T** peptide sample assembled under acidic conditions (10 mM phosphate, pH 4.0) displayed a single, major peak at 1654 cm^{-1} (**Figure 4.14, Bottom**). This indicated significant α-helical content in the sample, confirming identical secondary structure determination by CD spectroscopy. Notably, no significant absorbance was observed in the 1620-1640 cm^{-1} region, suggesting the
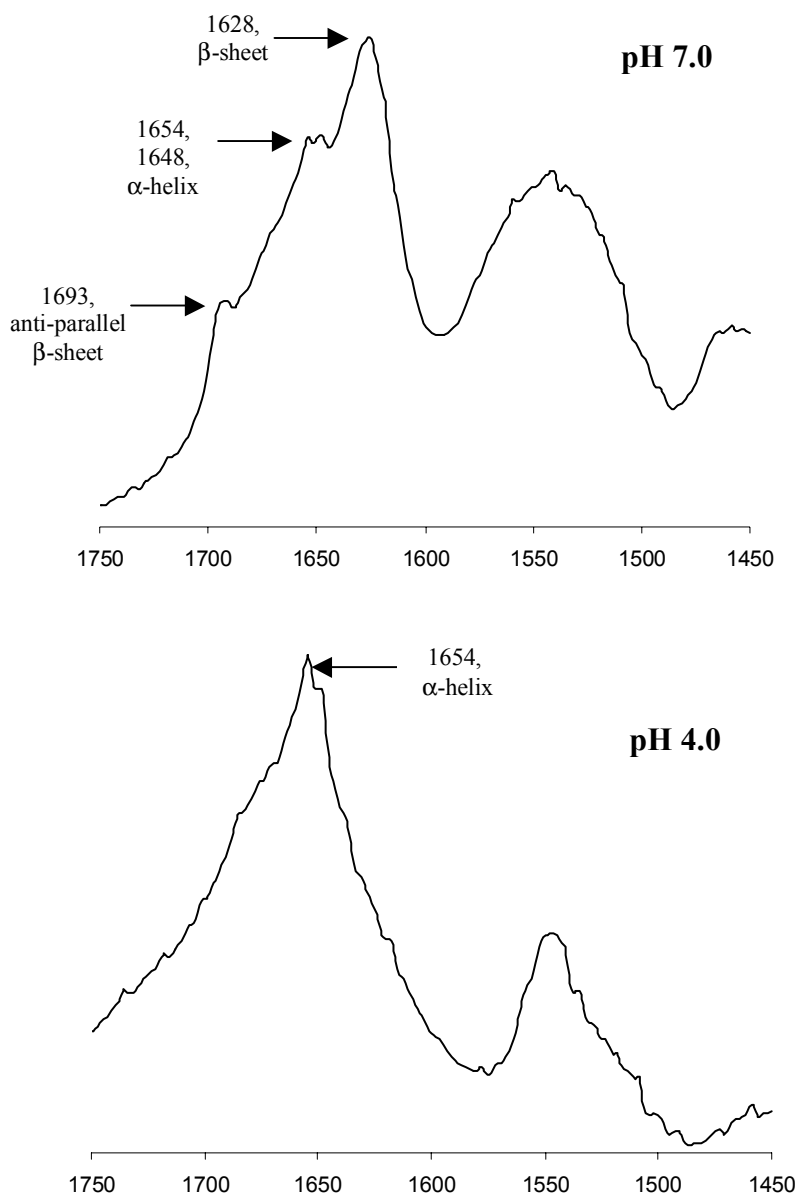
Figure 4.14. **IR spectra of assembled TZ1T peptide in 10 mM phosphate buffer.** (Top) Sample prepared at pH 7.0 and heat-induced for β-sheet transition. Peaks at 1628 and 1693 cm^{-1} in the amide I region indicate anti-parallel, β-sheet conformation. Additionally, the peak at 1654 cm^{-1} indicates the presence of α-helical species in the sample. (Bottom) TZ1T prepared at pH 4.0 shows peak at 1654 cm^{-1} indicating α-helical content.

a

139

bsence of β-sheet content in peptide samples assembled under acidic conditions.

4.2.6 Low-Temperature Scanning Electron Microscopy (LT-HRSEM)

Conventional negative-stain TEM sample preparation can induce artifacts associated with increased local concentrations of sample due to air drying on the carbon substrate of the TEM grid. In the case of **TZ1T** specimens, the concern is that the ribbon-like morphology captured by TEM could be a result of induced flattening of the fiber morphology during drying. However, cryoHRSEM images of vitrified **TZ1T** peptide solutions prepared under β-sheet forming conditions, confirm the ribbon-like morphology of the assembled fibers viewed previously by TEM (**Figure 4.15**).
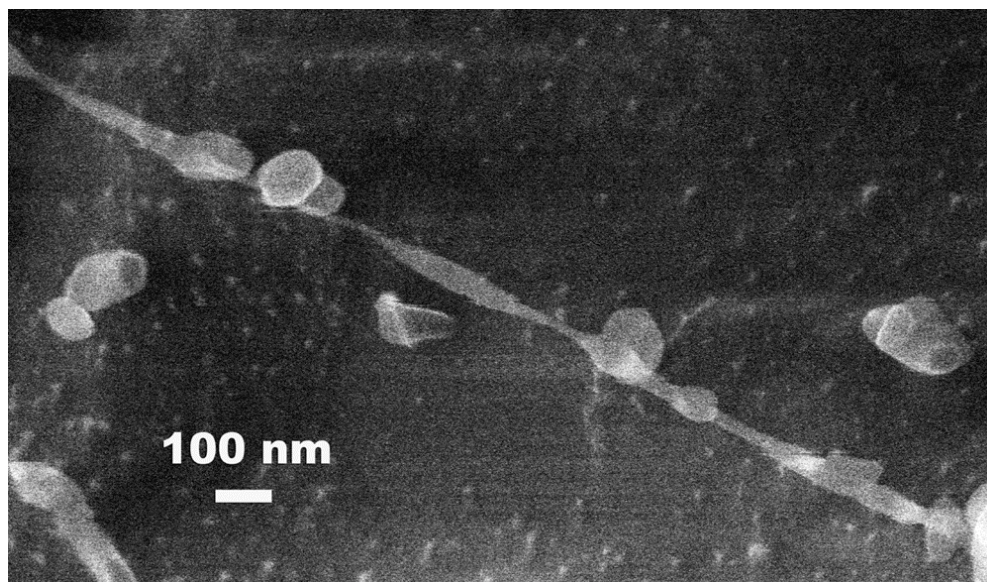
Figure 4.15. The morphology of TZ1T fibers examined by low-temperature, high-resolution scanning electron microscopy. Vitrified TZ1T samples prepared at pH 7 in 10 mM phosphate buffer and heat-annealed to induce β-sheet character show a loose helical twist common to β-sheet ribbons.

4.3 Summary

The primary sequence of peptide **TZ1T** is based on a canonical α-helical coiled coil sequence, the later being known as a parental motif for synthetic peptides which can respond to environmental changes by altering their conformation. Frequently, the secondary structure of the switching peptides will display a prominent transition from either coil to helix or β-sheet. Rational design strategies for developing switching mechanisms in coiled-coil assemblies frequently preserve the majority of key α-helical, coiled-coil forming positions which provide favorable hydrophobic and electrostatic interactions and insert the β-sheet element with minimal disruption to the native structure. This allows the resulting peptide to display two unique secondary structure elements which are ultimately in direct competition with each other.

The incorporation of β-sheet character into peptide **TZ1T** is achieved through an isoleucine to threonine substitution into the core-forming *d*-positions of an α-helical peptide fiber. The environmental pH was shown to be a strong determinant of the preferred secondary structure and indirectly controls the time-dependent aggregation behavior of the peptide (**Figure 4.16, A**). Thus, the formation of **TZ1T** fibrils can be discernibly inhibited or triggered by a change of pH.

There are several possible factors which may be driving the formation of β-sheet versus α-helical structure, foremost being environmental pH. Peptide solutions prepared below pH 4.5 preferably assemble into α-helical fibers of attenuated lengths. Glutamic acid residues responsible for proper registration of adjacent peptides are protonated to their neutral form under acidic pH conditions, thereby abolishing the

141
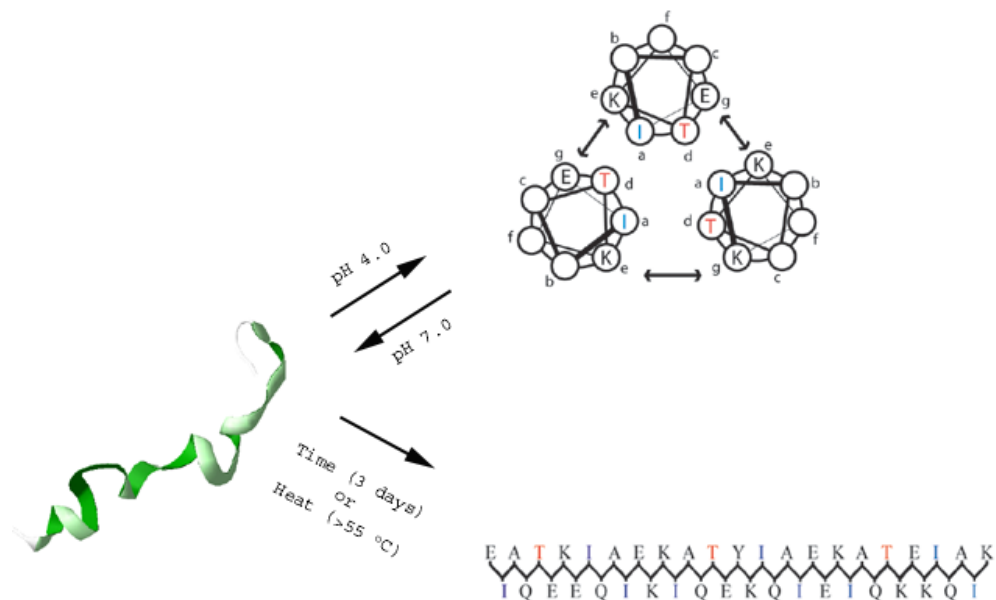
Hypothetical anti-parallel, β-sheet arrangement
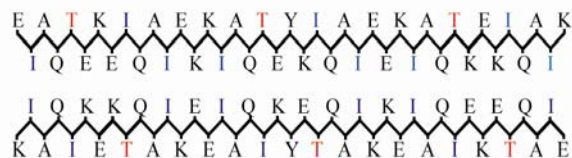
Figure 4.16. **Proposed self-assembly diagram of TZ1T peptide system. The random coil structure at pH 7.0 can undergo a reversible conversion to α-helical content. The β-sheet structure can only be accessed through the random coil conformation upon brief heating or after three days at room temperature. Below, the proposed arrangement of two extended TZ1T primary sequences into a conventional anti-parallel β-sheet conformation.**

cooperative electrostatic interactions in these positions. Since the forces dominating the folding of coiled-coil assemblies are primarily hydrophobic and electrostatic in nature, the α-helical conformation observed in peptide **TZ1T** prepared at pH 4.0 must be driven by hydrophobic interactions. The generation of α-helical fiber in the absence of a defined strand-staggering regime is possible, as shown in a reported pH-induced, α-β switch peptide by Koksch and coworkers.[17] However, the **TZ1T** requires approximately 6 times less peptide concentration than Koksch's system for fiber formation.

Conversely, the β-sheet conformation of **TZ1T** is seen only in peptide solutions prepared above the pK_a of the glutamic acid, where the amino acid side chain exhibits a negative charge. This suggests the β-sheet conformation may be selectively stabilized through cooperative electrostatic interactions. A proposed scheme for the self-assembly of β-sheet fibers from **TZ1T** peptides is offered in **Figure 4.16,** in which adjacent strands arranged in an anti-parallel fashion are shown to form eight cooperative electrostatic interactions between adjacent protomers.

Furthermore, the observation that heat can be used to accelerate the coil-to-sheet transition is consistent with the formation of other β–structured systems.[6,18,19] These studies show β-sheet formation proceeds in these systems through a partially unfolded intermediate as a necessary precursor. Threonine residues in multiple *d*-positions of the heptad sequence may interact disfavorably with *e*- and *g*-positions to facilitate the unfolding of **TZ1T** peptide at pH 7.0, affording the precursor protomer for the generation of the fibrous aggregation state. This is surprising, however, since there are multiple reports of incorporation of threonine residues in the *d*-position of synthetic, in-register coiled-coils. Future rational design schemes of long-aspect ratio fibers based on

in-register coiled-coils will need to consider that key elements of primary sequences for discrete bundles may not translate directly to the generation of higher-order fibers.

4.4   Materials and Methods

4.4.1   Peptide Synthesis and Purification

Peptide **TZ1T** was prepared via automated solid-phase peptide synthesis on a Rink amide resin (0.4-0.6 meq/g) on a Rainin Symphony Quartet peptide synthesizer (Peptide Technologies, Inc., Tucson, AZ) as described previously.   Standard FMOC protection chemistry was employed with coupling cycles based on HBTU/NMM-mediated activation protocols and base-induced deprotection (20% piperidine in DMF) of the FMOC group.   The N-terminus of the peptides was capped with acetic anhydride prior to cleavage from the resin.   The peptide was isolated from the resin as the C-terminal amide derivative after acidic cleavage of the side chain protecting groups with a cocktail of trifluoroacetic acid (TFA), thioanisole, ethanedithiol and anisole (90:5:3:2). Crude peptides were precipitated in ice-cold ether and centrifuged at 6000 rcf at 4 $^{\circ}$C for 20 minutes. After pelleting, the supernatant was decanted and the process repeated until thiol odor is no longer present. The resulting pellet was then dried under nitrogen flow and stored at -20 $^{\circ}$C until purification.

Prior to purification, the precipitated peptide was thoroughly dissolved in 15-25 mL solution of 60% ddH$_2$0 / 40% acetonitrile in the presence of 0.1% trifluoroacetic acid (TFA). Reverse-phase HPLC purification was performed using a Waters 600 purification

system (Waters Corp., Milford, MA) with a Waters 996 photodiode array and a reverse phase C-18 column (Atlantis dC$_{18}$, 10 μm, 19 x 256 mm) with a linear gradient of acetonitrile and water (0.1% trifluoroacetic acid) at 10 mL / minute. The molar mass of **TZ1T** was confirmed by MALDI-TOF mass spectrometry on a Voyager-DE STR instrument (Perseptive Biosystems, Framingham, MA) using equal volumes of α-Cyano-4-hydroxycinnamic acid (saturated solution in 0.1% TFA in ddH$_2$O) matrix and HPLC purified peptide. Fractions were combined and rotary evaporated to remove acetonitrile and TFA before lyophilization. Lyophilized peptides were stored at -20 $^{\circ}$C until used. The expected mass of **TZ1T** peptide is 4797.6 and the observed peak by MALDI mass spectrometry was 4797.6.

4.4.2   Circular Dichroism

CD spectra were obtained using a JASCO J-810 CD spectropolarimeter (Jasco Inc., Easton, MD) equipped with a PFD-425S Peltier temperature control unit, using a 1 mm quartz cell. Peptide **TZ1T** was prepared in 10 mM phosphate buffer, which was pH-adjusted to the desired value using a mixture of 0.2 M mono- and dibasic sodium phosphate solutions. Total sample volume used in CD measurements was typically 300 μL. Spectra were recorded at 4 ºC at 0.5 nm intervals, 1 nm bandwidth, 20 nm min^{-1}, and 8 sec response time. Spectra were baseline corrected before converting to mean residue ellipticities. Fractional helix content was calculated from MRE at 222 nm using equation $F_{helix} = [\theta]_{obs} - [\theta]_{coil} / [\theta]_{helix} - [\theta]_{coil}$, where $[\theta]_{helix}$ and $[\theta]_{coil}$ in MRE are described as (-42,500 * (1 – (3 / (# residues)))) and + 645, respectively. Thermal melting curves

were generated by monitoring the absorbance at 201 or 222 nm of **TZ1T,** typically 70 µM peptide in 10 mM sodium phosphate in a 1 mm quartz cuvette. Temperature ramping was performed from 4 - 98 $^{\circ}$C at a rate of 1 $^{\circ}$C/minute. The value of the T_m was determined from the first derivative of the CD melting curve.

4.4.3 FTIR Spectroscopy

FTIR spectra were obtained on a Nicolet MAGNA-IR 560 Spectrometer ESP (Thermo Scientific, Waltham, MA) instrument. Spectra were collected at 2 cm^{-1} resolution and averaged 128 scans. Background spectra were collected every five minutes. Solubilized peptides were prepared for analysis by either lyophilization on a Flexi-Dry MP benchtop lyophilizer (FTS Systems, Stone Ridge, NY) or concentration on a RC 10.10 vacuum concentrator (Thermo Scientific) to $\leq$ 10 mL and allowed to dry at room temperature. All samples were prepared as KBr pellets.

4.4.4 Differential Scanning Calorimetry

Calorimetric measurements were performed on a Microcal MC-2 differential scanning calorimeter at a scan rate of 1 $^{\circ}$C per minute in 10 mM phosphate buffer, pH 7.0. Protein concentrations were determined by duplicate measurements of the protein absorbance at 280 nm. The calorimetric measurements were performed using protein samples of approximately 1 mg/mL.

4.4.5 Transmission electron microscopy

Transmission electron microscopy was performed on either a JEOL 1210 (Tokyo, Japan) equipped with a lanthanum hexaboride (LaB$_6$) thermionic electron source or Philips LS-410 (Amsterdam, Netherlands) equipped with a tungsten filament. Imaging was performed at 90 kV (JEOL 1210) or 80 kV (Philips LS 410) accelerating voltage. Typical peptide concentrations used in electron microscopy studies were between 70 and 156 μM. An aliquot of **TZ1T** peptide solutions (10 μL) was pipetted onto a 200-mesh carbon-coated copper grid (Electron Microscopy Sciences, Hatfield, PA) and let stand for 1 min before excess solution was wicked away with a triangle of filter paper, leaving a thin layer on the grid surface. An additional wash with 10 μL doubly deionized water was performed in a manner similar to sample deposition. Negatively-stained samples for transmission electron microscopy were prepared with a 1:1 mixture of near-neutral stains Nano methylamine vanadate (pH 8.0) and Nano methylamine tungstate (pH 6.8), were used (NanoProbes, Yaphank, NY). Stain (3 μL) was applied to the grid and incubated for less than 1 minute before being wicked away with a triangle of filter paper. After repeating staining procedure once more, the grid was transferred to a grid box and stored under vacuum a minimum of 24 hours.

Electron micrographs were recorded on Kodax Electron Microscopy 4489 film and scanned on an AGFA Duoscan T2500 scanner to 2000 pixels per inch (ppi) resolution. Image measurements were performed using the software ImageJ, version 1.36b, freely available from U. S. National Institutes of Health, Bethesda, Maryland, USA (http://rsb.info.nih.gov/ij/). The spatial scale was set to a known distance in the image and the distance in pixels. The segmented line tool was used to trace the diameter

of fibrils or fiber segments that displaced well defined edges. Thirty independent diameter measurements were made from fibers spanning every quadrant of the image. Errors in the distance measurements are reported as standard error of the mean.

4.4.6 Low temperature high resolution scanning electron microscopy

For low-temperature scanning electron microscopy, a 10 μL aliquot of **TZ1T** peptide solution (1 mg / mL, 10 mM phosphate buffer, pH 7.0) was applied to a 200 mesh, carbon-coated copper grid (Electron Microscopy Sciences, Hatfield, PA). Excess solution was wicked away with a triangle of filter paper, leaving a thin aqueous film of approximately 100 nm on the grid. Cryo-immobilization was achieved by plunging the sample in liquid ethane (-183.3 ^{o}C). The grid was then rapidly loaded into a Gatan CT 3500 cryostage which was pre-chilled to -170 ^{o}C and subsequently transferred into the Denton DV-602 chromium coater. After achieving a vacuum of 4×10^{-7} torr, the sample temperature was raised to -85 ^{o}C in a controlled fashion and held for 5 minutes to sublime bulk, low temperature water past the hydration shell. Finally, a thin (2 nm) continuous coating of chromium metal was sputter-coated onto the sample and the stage was rapidly transferred from the coater to the upper stage of a TOPCON / ISI (Tokyo, Japan) DS-130 field-emission SEM for imaging.

4.5 References

1.   Takahashi, Y.; Ueno, A.; Mihara, H., Optimization of hydrophobic domains in peptides that undergo transformation from alpha-helix to beta-fibril. *Bioorg Med Chem* **1999,** 7, (1), 177-85.

2.   Skehel, J. J.; Wiley, D. C., Receptor binding and membrane fusion in virus entry: the influenza hemagglutinin. *Annu Rev Biochem* **2000,** 69, 531-69.

3.   Taubes, G., Misfolding the way to disease. *Science* **1996,** 271, (5255), 1493-5.

4.   Wetzel, R., For protein misassembly, it's the "I" decade. *Cell* **1996,** 86, (5), 699-702.

5.   Kelly, J. W., Alternative conformations of amyloidogenic proteins govern their behavior. *Curr Opin Struct Biol* **1996,** 6, (1), 11-7.

6.   Ciani, B.; Hutchinson, E. G.; Sessions, R. B.; Woolfson, D. N., A designed system for assessing how sequence affects alpha to beta conformational transitions in proteins. *J Biol Chem* **2002,** 277, (12), 10150-5.

7.   West, M. W.; Wang, W.; Patterson, J.; Mancias, J. D.; Beasley, J. R.; Hecht, M. H., De novo amyloid proteins from designed combinatorial libraries. *Proc Natl Acad Sci U S A* **1999,** 96, (20), 11211-6.

8.   Kallberg, Y.; Gustafsson, M.; Persson, B.; Thyberg, J.; Johansson, J., Prediction of amyloid fibril-forming proteins. *J Biol Chem* **2001,** 276, (16), 12945-50.

9.   Zimenkov, Y.; Dublin, S. N.; Ni, R.; Tu, R. S.; Breedveld, V.; Apkarian, R. P.; Conticello, V. P., Rational design of a reversible pH-responsive switch for peptide self-assembly. *J Am Chem Soc* **2006,** 128, (21), 6770-1.

10.   Harbury, P. B.; Kim, P. S.; Alber, T., Crystal structure of an isoleucine-zipper trimer. *Nature* **1994,** 371, (6492), 80-83.

11.   Minor, D. L., Jr.; Kim, P. S., Measurement of the beta-sheet-forming propensities of amino acids. *Nature* **1994,** 367, (6464), 660-3.

12.   Akey, D. L.; Malashkevich, V. N.; Kim, P. S., Buried polar residues in coiled-coil interfaces. *Biochemistry* **2001,** 40, (21), 6352-60.

13.   Yadav, M. K.; Redman, J. E.; Leman, L. J.; Alvarez-Gutierrez, J. M.; Zhang, Y.; Stout, C. D.; Ghadiri, M. R., Structure-based engineering of internal cavities in coiled-coil peptides. *Biochemistry* **2005,** 44, (28), 9723-32.

14.   Doig, A. J., A three stranded b-sheet peptide in aqueous solution containing N-methyl amino acids to prevent aggregation. *Chem. Commun.,* **1997**, (22), 2153-2154.

15.   Wolfgang H. Binder, O. W. S., Self-Assembly of Fibers and Fibrils. *ChemInform* **2007,** 38, (6).

16.   Parvez I. Haris, D. C., The conformational analysis of peptides using fourier transform IR spectroscopy. *Biopolymers* **1995,** 37, (4), 251-263.

17.   Pagel, K.; Wagner, S. C.; Samedov, K.; von Berlepsch, H.; Bottcher, C.; Koksch, B., Random coils, beta-sheet ribbons, and alpha-helical fibers: one peptide adopting three different secondary structures at will. *J Am Chem Soc* **2006,** 128, (7), 2196-7.

18.   Chiti, F.; Webster, P.; Taddei, N.; Clark, A.; Stefani, M.; Ramponi, G.; Dobson, C. M., Designing conditions for in vitro formation of amyloid protofilaments and fibrils. *Proc Natl Acad Sci U S A* **1999,** 96, (7), 3590-4.

19.   Ramirez-Alvarado, M.; Merkel, J. S.; Regan, L., A systematic exploration of the influence of the protein stability on amyloid fibril formation in vitro. *Proc Natl Acad Sci U S A* **2000,** 97, (16), 8979-84.

Chapter V: Efforts toward engineering an allosteric switch into a helical fiber

5.1 Introduction

The previous chapters describe synthetic coiled-coil peptides designed to self-assemble into well-defined fibrous aggregates in response to environmental cues. A related challenge remains in the rational design of selective ligand binding sites in self-assembling peptide systems. Ultimately, these model systems could be useful in engineering proteins with novel ligand-binding sites which undergo allosteric structural changes in the presence of a small molecule. Potential applications of such systems include but are not limited to chemical sensors or conditional oligomerization sequences.[1] In building an allosteric switch, two distinct structural conformations must be available for the free or bound state. The α-helical coiled-coil motif has been shown to be a useful scaffold for designing peptides which undergo conformational changes in the presence of such environmental cues as temperature, pH and metal ions.[2,3,4]

As discussed previously, primary sequence elements greatly influence the morphology of the coiled-coil structure. In particular, the oligomerization state of the complex is determined by side chain packing at the helical interface of the coiled-coil. The native GCN4-pI coiled-coil is known to form a dimeric coiled-coil in which all the core-residues possess hydrophobic character except a single, conserved asparagine in position 16 of the 33 amino acid peptide.[5] The polar Asn16 is thought to serve as a

152

determinant of the two-stranded oligomerization state, supported by crystallographic data which shows the two asparagines side chains hydrogen bonded together in the hydrophobic core.[5] Mutation of this position in the peptide to valine was shown to result in a mixture of dimeric and trimeric coiled-coils.[6]

Alber and coworkers used this oligomerization equilibrium to design an allosteric switch in a synthetic, in-register leucine zipper.[7] Their design was based on the observation that allosteric transitions can be induced by preferential binding of a ligand to a minor conformer. In the coiled-coil paradigm, this translates into the stabilization of one oligomerization state over another based on a specific ligand-binding event. To this end, they mutated the dimer-determinant asparagine residue to an alanine in the central core positions of the GCN4 leucine zipper. This mutation was hypothesized to generate a cavity which would destabilize the trimeric oligomerization state and provide a ligand-binding site in the empty space (**Figure 5.1**). Benzene was utilized as the guest ligand molecule since it is a small hydrophobic molecule which would prefer the internal cavity over surrounding aqueous solvent. Furthermore, experimental evidence exists for benzene binding in an alanine-generated cavity of mutant T4 lysozyme and computational modeling of synthetic GCN4 assemblies suggested a single benzene molecule could fit into the cavity generated in an Asn16Ala trimer.[8]

The engineered Asn16Ala mutant indeed switches from dimeric to trimeric oligomerization state upon binding of hydrophobic benzene and cyclohexane molecules, as determined by sedimentation equilibrium and x-ray crystallography. Additionally, the system exhibited a >90% helical signal by CD, indicating a near absence of unfolded
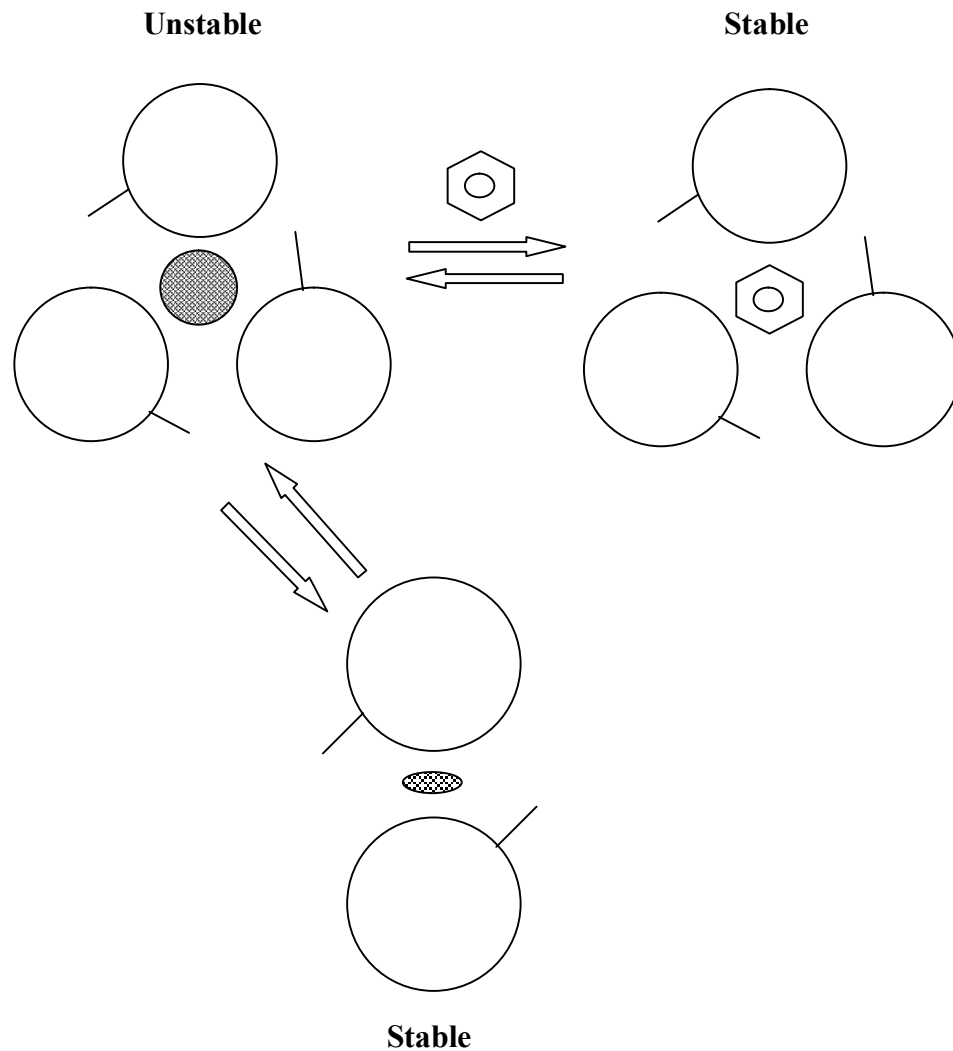
Figure 5.1. **Schematic representation of Alber's ligand-induced oligomerization switch in which white circles represent helical peptides and dark circles are cavities. In this diagram, the Asn16Ala mutation is shown to create a cavity at the helical interface. Since the largest cavity is in the trimeric state, the dimer is favored in the absence of ligand. However, binding of benzene, which is only possible in the trimer due to steric constraints, favors the trimer.**

monomer in solution. Finally, the apparent T_m of the system was increased by 9.0 °C over the non-benzene bound sample, implying an increased thermal stability in the ligand-bound state. The results of this study suggest the coiled-coil is a powerful model for developing more advanced molecular switches based on the binding of small molecules.

Subsequent reports of GCN4 alanine-core mutants have been described in the literature in which stabilization of the complex is achieved through ligand binding within the induced cavity. Kennan and coworkers designed a three-stranded coiled-coil assembly composed of heterotrimers which specifically associated due to steric matching of hydrophobic core side chains (**Figure 5.2**).[9] In this study, a 2:1 heterotrimeric
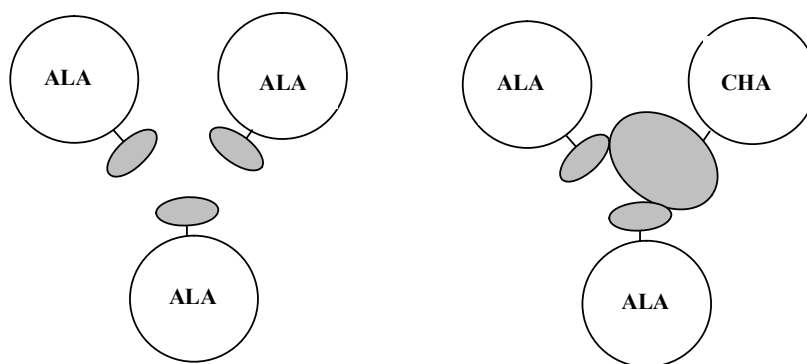
Figure 5.2. Graphical representation of Kennan's alanine and cyclohexylalanine peptides assemblies. (Left) A three-stranded homotrimeric coiled-coil containing alanine residues in the central core position is destabilized by the generation of a cavity in the hydrophobic core due to the short alanine side chain. (Right) Compensation through shape complementarity by of the larger cyclohexylalanine side chain in the heterotrimer partially fills the void, resulting in higher thermodynamic stability of the complex.

architecture is formed by peptides containing alanine or cyclohexylalanine at a central core residue. The all-alanine homotrimer was shown to be significantly less stable than a specific 2:1 heterotrimer formed from three independent peptide strands, where one peptide possesses a large side chain (cyclohexylalanine) and the other two possess the small (alanine) side chain at the same position. The observed complementation of the alanine-containing peptides by cyclohexylalanine peptides is considered to be analogous to the binding of cyclohexane within an alanine-induced cavity.

Similarly, McLendon and coworkers designed and characterized a three-stranded coiled-coil GCN4-pI mutant which binds small hydrophobic molecules in a hydrophobic cavity created by an N16A substitution.[10] This work was significant because the group used ^{19}F NMR to obtain ligand-binding affinity values for a series of small molecules. Their results show all hydrophobic molecules bound with greater affinity then polar molecules, which was attributed to the preference for the polar ligand to be preferentially solvated in the buffer. Furthermore, they observed a higher affinity binding of cyclohexane ($K_I = 3 \times 10^{-6}$ M) over benzene ($K_I = 4 \times 10^{-5}$ M), where K_I is the apparent binding constant of hexafluorobenzene in the presence of a competing ligand. This in turn can be used to calculate the inhibition constant KI of the competing ligand..

In this chapter, an allosteric switch is described which seeks to control fiber formation through the binding of a small, hydrophobic molecule in an engineered cavity of a synthetic coiled-coil. The proposed mechanism is designed to switch between a ligand-free state comprised of a thermally unstable peptide fiber and a ligand-bound state which exists as a discrete, in-register coiled-coil bundle, upon binding a small hydrophobic molecule.

Additionally, in the process of designing peptide **SKA**, we modified the parental the canonical **S6K** peptide sequence to address the problem of fiber thickening of the three-stranded helical aggregate. Solvent-accessible *f*-position residues in the heptad were all mutated to a charged glutamic acid, resulting in a decrease in the observed fiber diameter and the disappearance of solution clouding. We hypothesize this change in morphology is a consequence of eliminating complementary electrostatic interactions along the solvent-accessible helical surface and decreasing the overall net charge of the peptide.

5.2   Results

5.2.1   Design of first generation SKA peptide sequence

The amino acid sequence of peptide **SKA** was derived from peptide **S6K,** the later of which was shown to form long aspect-ratio, helical fibers at neutral pH conditions. The 41-residue peptide **SKA** is organized into six tandem heptad repeats ($[a$-b-c-d-e-f-$g]_6$), in a fashion reminiscent of a native coiled-coil structural motif (**Figure 5.3**). The incorporation of isoleucine residues into the majority of the core-forming positions of the **SKA** primary sequence is presumed to bias the oligomerization state of the peptide formation to a triple-stranded coiled-coil.[11] Additionally, control of lateral registration between adjacent helical protomers was engineered into the peptide sequence through the introduction of cooperative electrostatic interactions between charged residues in the *e*- and *g*-heptad positions. In this scheme, cooperative Coulombic interactions between *e*-
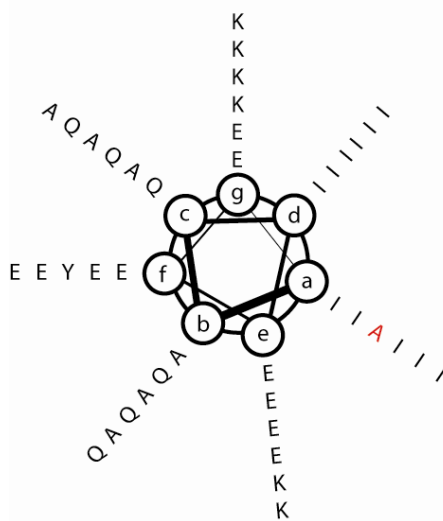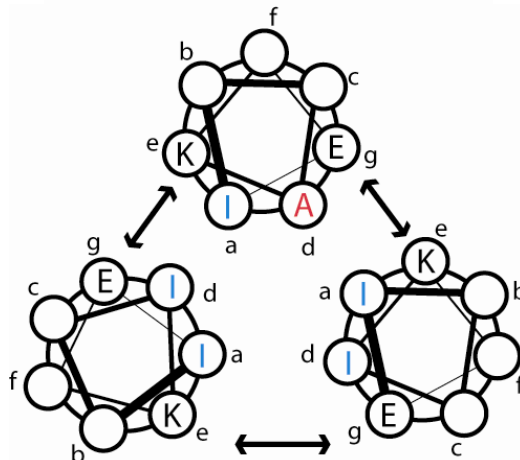
Figure 5.3. **(A.) Helical wheel diagram of a single SKA helical peptide and (below) the associated primary sequence. (B.) Cross-sectional view of a triple-stranded helical bundle formed through the self-assembly showing core-forming *a*- and *d*-positions occupied by isoleucine (blue) or alanine (red). Note, the majority of the hydrophobic core consists of isoleucine residues except for alanine in a single *a*-position of the central heptad.**

and *g*-position residues on adjacent helical protomers are charge-complementary only if alignment occurs in a two-heptad staggered formation, in which self-assembly favors the formation of a helical fiber composed of three helical strands.

An allosteric switching mechanism was engineered into the primary sequence of the **SKA** peptide through the introduction of a single alanine residue into a central, core-forming *d*-position (**Figure 5.3.B**). The Ile23Ala mutation is hypothesized to generate a disruption in side chain packing at the helical interface of a three-stranded coiled-coil fiber. Crystal structures of an all-isoleucine core coiled-coil show a tight hydrophobic packing between isoleucine side chains in the three-stranded assembly.[11] The mutation of a single isoleucine residue to the smaller and less hydrophobic alanine side chain provides a poor packing partner across adjacent helical protomers.

We hypothesized the conformation equilibrium between the fiber and discrete bundle could be shifted to favor the discrete bundle over fiber with the addition of benzene (**Figure 5.4**). When **SKA** peptides are arranged in the charge-complimentary staggered alignment coinciding with fiber formation, a single *d*-layer will be composed of one alanine and two isoleucine residues. In this arrangement, a cavity is formed resulting in a disruptive side chain pairing which is propagated along the fiber axis. This presumably results in the formation of an energetically unfavorable structure, with respect to an all-isoleucine core fiber.

An alternative structure available to the **SKA** peptide is an in-register assembly, which would place three alanine residues on the same *d*-layer plane, resulting in the creation of a significantly larger cavity localized in center of a discrete coil-coiled bundle. This hypothetical structure resembles Alber's mutant GCN4-pI coiled-coil, which was

Destabilized α-helical fiber

In-register coiled-coil

Unstable   Stable
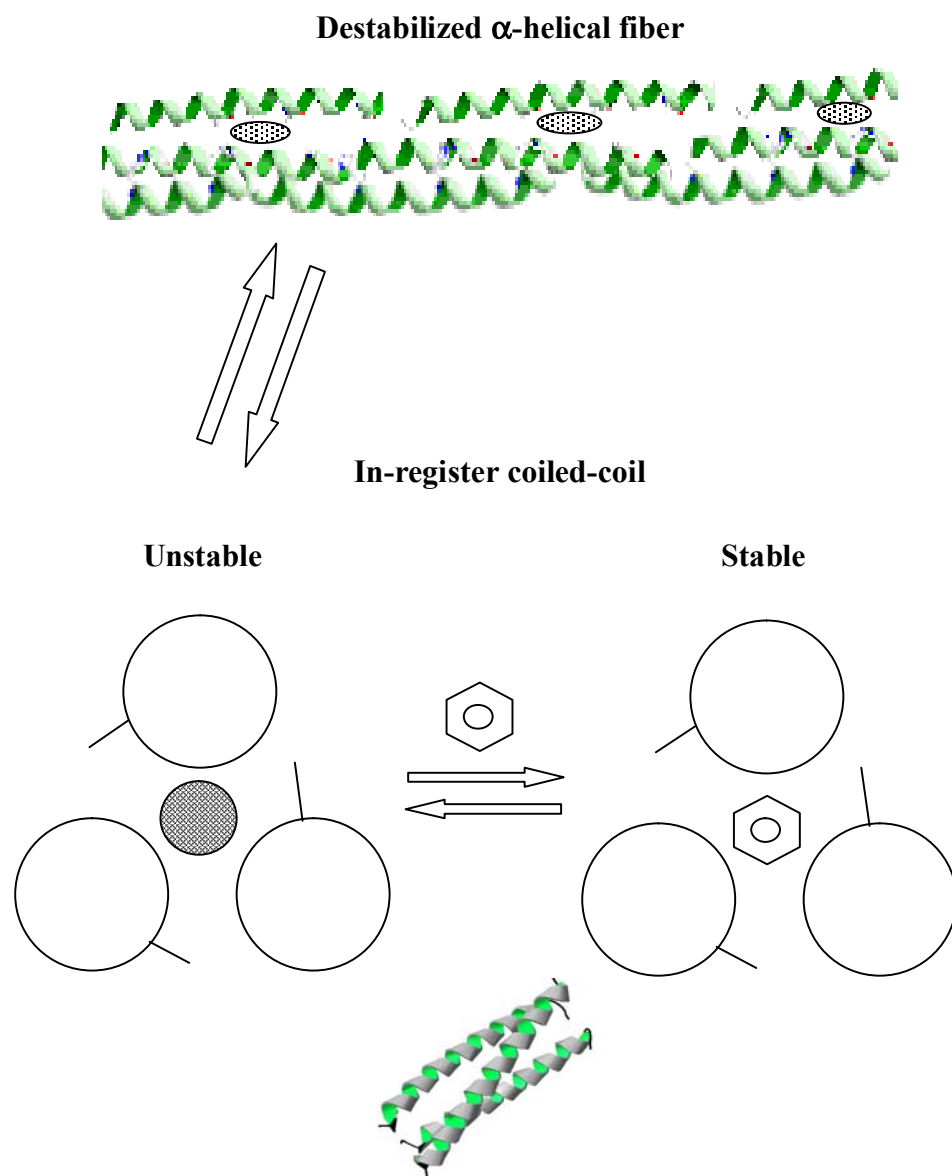
Figure 5.4 General scheme for a hypothetical ligand-induced assembly switch for self-assembly. This diagram illustrates the structural equilibrium in the absence (Left) and presence (Right) of a small, hydrophobic molecule like benzene. The Ile23Ala mutation creates a disruption on side chain packing at the helical interface, resulting in a relatively unstable fibrous assembly. Binding of benzene in the hydrophobic pocket stabilizes the alternative in-register coiled-coil state.

sufficiently stabilized through the binding of benzene in the cavity. In a similar manner, we hypothesized the in-register **SKA** coiled-coil could be stabilized through the addition of a small, hydrophobic molecule such as benzene or cyclohexane.

5.2.2 Circular dichroism of peptide SKA

Circular dichroism spectrometry was employed to investigate the effect of the Ile23Ala substitution on the conformation of peptide **SKA** in solution. In 10 mM phosphate buffer (pH 7.), the CD spectrum showed a characteristic α-helical trace with two minima at 208 and 222 nm wavelength (**Figure 5.5**). However, the exaggerated value of 1.27 for the ratio of $[\theta]_{222\ nm} / [\theta]_{208\ nm}$, an indicator of helix-helix interactions, is a result of severe attenuation and red-shifting of the 208 nm wavelength in the CD spectrum. This attenuation indicates significant light scattering in the solution as a result of sample clouding due to precipitation. Indeed, visual inspection of the solution showed a cloudy precipitate formed in the bottom portion of the cuvette. This phenomenon occurred across a wide range of peptide concentrations from 50 to >100 μM. Multiple attempts at obtaining a thermal unfolding temperature (T_m) for peptide **SKA** were unsuccessful due to irreproducibility of unfolding curves, most likely also a consequence of the significant precipitation of the sample.
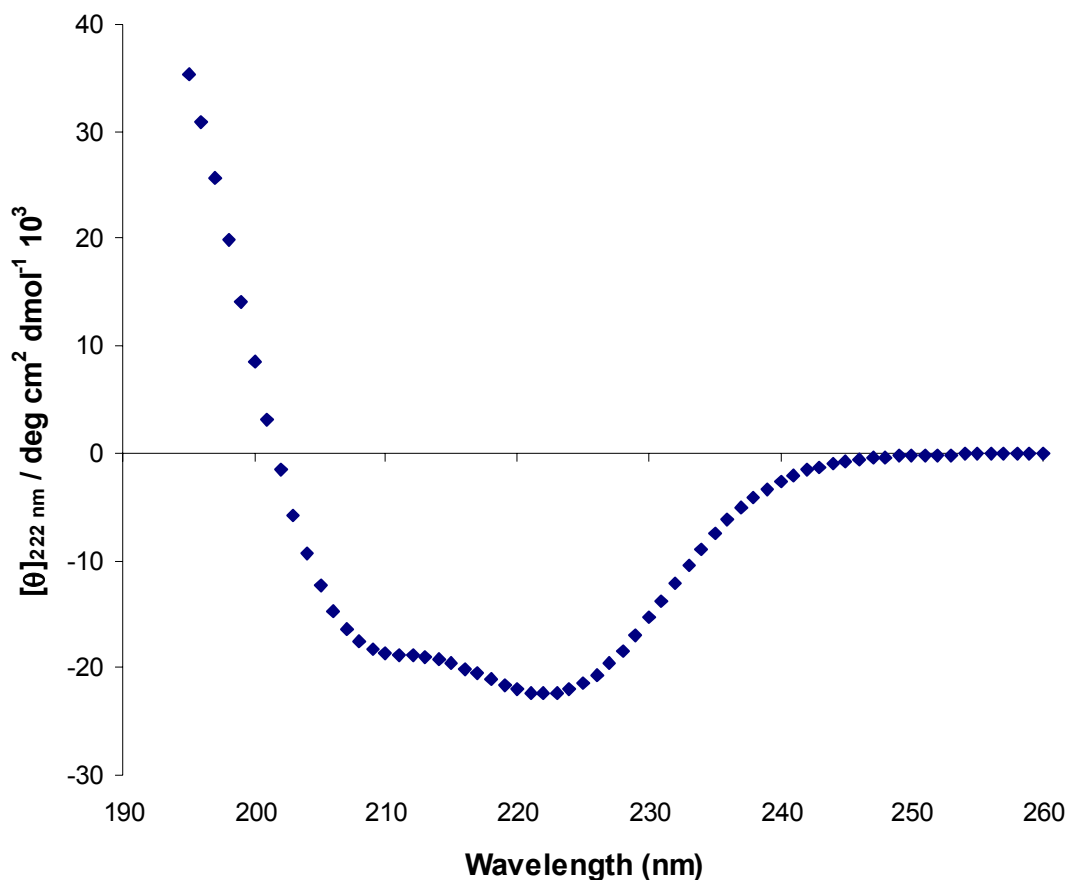
Figure 5.5. CD spectrum for 70 μM peptide SKA prepared in 10 mM phosphate, pH 7.0 at 4 °C. Significant light scattering in the solution is suggested by the extreme attenuation and red-shifting of the 208 nm wavelength.

Consequently, the **SKA** peptide sequence was redesigned with the intent of minimizing precipitation under the desired assembly conditions (**Figure 5.6**). Our approach was to make changes in the primary sequence to introduce a net charge to the currently net zero charge peptide. The net charge on a protein at a given pH is determined by the pKa values of the ionizable groups. The solubility of a protein is proportional to the square of the net charge on the protein and, as a consequence, proteins

are expected to be least soluble near their isoelectric points (pI).[12] The first generation **SKA** peptide possesses a calculated pI of 7.3 and therefore a zero net charge at pH 7.0, which certainly plays a role in the observed insolubility.

Therefore, a second generation of peptide **SKA** was designed in which polar glutamic acid residues were chosen to occupy all of the solvent-accessible *f*-positions in the heptad repeat sequence. This resulted in a decrease of the calculated pI to 4.4 and a corresponding downward transition of the net charge from 0.0 to (-4.0) at pH 7.0. Additionally, since the *f*-position residues form the helical surface exposed to the solvent and other formed fibers, this mutation results in a uniform charge along the axial length of the assembled coiled-coil fiber. This replaces an E-E-Y-K-K pattern which may provide a source of cooperative electrostatic interactions between adjacent fibers, resulting in the fiber thickening seen by TEM in peptide **S6K** assembly.

```
         abcdefg abcdefg abcdefg abcdefg abcdefg abcde
S6K  AcNH- E IAQIEKE IQAIEKK IAQIEYK IQAIEEK IAQIKEK IQAIK -CONH2
S6KE AcNH- E IAQIEEE IQAIEEK IAQIEYK IQAIEEK IAQIKEK IQAIK -CONH2
SKA  AcNH- E IAQIEKE IQAIEKK IAQIEYK AQAIEEK IAQIKEK IQAIK -CONH2
SKAE AcNH- E IAQIEEE IQAIEEK IAQIEYK AQAIEEK IAQIKEK IQAIK -CONH2
```

Figure 5.6 Amino acid sequences including the parental peptide S6K, the 1st generation allosteric switch peptide SKA, the redesigned peptide S6KE, and 2nd generation SKAE which includes the glutamic acid residues (green) in the solvent-accessible *f*-positions. Positions containing alanine are red.

5.2.3 Circular dichroism spectroscopy and TEM of peptide S6KE solution

First, it was important to assay the effect of the proposed glutamic acid mutation on the self-assembly of the general, three-stranded peptide fiber scheme. Therefore, the parental peptide sequence **S6K**, lacking the alanine mutation, was mutated to include glutamic acid residues in all *f*-positions. CD spectropolarimetry was employed to assay the conformation of the newly designed **S6KE** peptide assembled in 100 μM peptide concentration in 10 mM phosphate at pH 7.0 (**Figure 5.7**). The resulting spectrum showed minima at 222 and 208 nm, indicating significant helical content in the sample with a limiting value for fractional helicity at 71%. Furthermore, no evidence of precipitation in the solution was seen either by attenuation and red-shifting of the 208 nm wavelength ($[\theta]_{222\,nm}/[\theta]_{208\,nm} = 1.06$) or by simple visual inspection. In fact, no evidence of precipitation was observed by either method across a wide range of peptide concentrations from 10 μM – 1 mM. This observation established that inclusion of glutamic acid residues in all *f*-positions of the heptads does not disrupt coiled-coil formation and significant solubility of the peptide assembly.
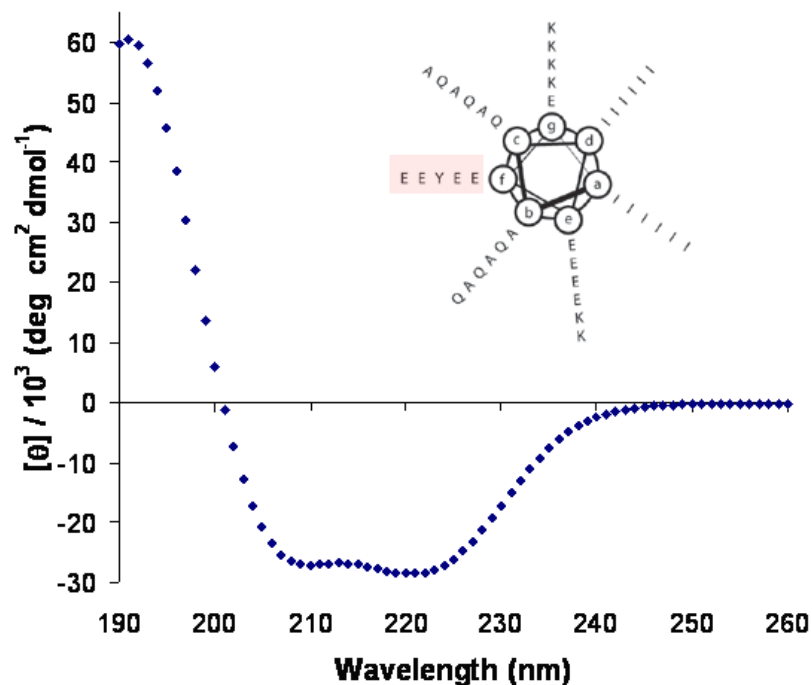
Figure 5.7. CD spectrum of 50 μM S6KE assembled in 10 mM phosphate buffer pH 7.0 shows α-helical coiled-coil assembly of the redesigned peptide system. Introduction of glutamic acid residues into all heptad *f*-positions marked in pink.

Furthermore, TEM showed the redesigned peptide **S6KE** is capable of self-assembling into helical fibers (**Figure 5.8**). The fiber diameters were observed as 6.21 ± 0.21 nm, which is significantly smaller than reported fibers originating from the parental **S6K** system. This suggests our glutamic acid mutations interrupt undesirable fiber thickening due to lateral association, possibly through the introduction of key sequence elements which promote charge-charge repulsion between formed fibers.

Multiple attempts at obtaining a thermal unfolding spectrum by CD of **S6KE** helical fibers suggest the system does not denature, even when the solution temperature exceeded 100 °C. Furthermore, the observation that the peptide system thickens to a

gel-like material at elevated temperatures hampers the utilization of differential scanning

calorimetry to obtain transition temperatures.
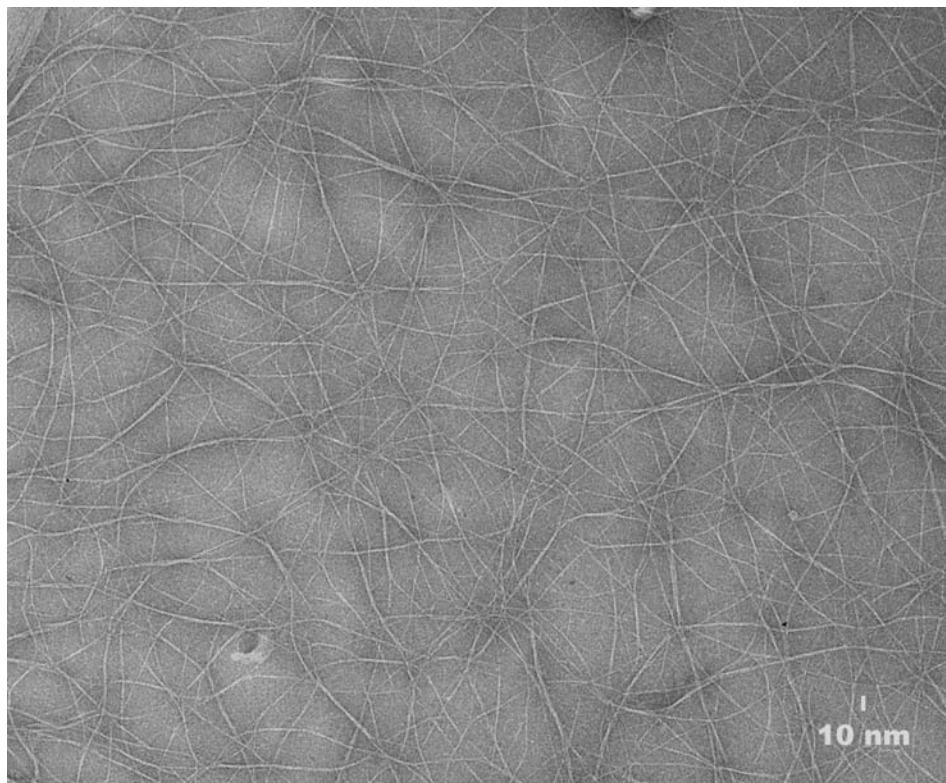
Figure 5.8.   Negative stain TEM of 100 μM S6KE in which all *f* position residues

are occupied by glutamic acid shows fiber diameters of 6.21 ± 0.21 nm.

5.2.4   Circular dichroism of SKAE peptide

Having established the utility of the **S6KE** peptide system, we performed the Ile23Ala mutation on this peptide scaffold to afford peptide **SKAE**. Our design predicted peptide **SKAE** assembled in the absence of benzene should generate an α-helical fiber. Indeed, circular dichroism spectrum of 100 μM **SKAE** in 10 mM phosphate buffer at pH 7.0 shows a characteristic α-helical trace with an attenuated 208 nm signal, which frequently corresponds to helical fiber formation in the **S6K** systems (**Figure 5.9, blue**). The limiting value for fractional helicity in this system is observed as 58 %, suggesting a lowered helical content.

Our hypothesis also predicts peptide **SKAE** assembled in the presence of benzene will adopt a discrete in-register coiled-coil structure. Reported in-register coiled-coils are known to display high helical content (> 90%), even for those containing engineered cavities. Therefore, we expected to see an increase in helicity of the **SKAE** peptide assembled in the presence of benzene, with respect to helicity observed in the fibrous aggregate formed in the absence of a small molecule. In fact, a dramatic change was observed in the CD spectrum of peptide assembled in the presence of 6 mM benzene (**Figure 5.9, pink**). The minima at wavelengths 222 and 208 nm both displayed an increase in negative value indicating higher helicity. The limiting value for fractional helicity increased to nearly 70%. Additionally, the attenuation of the signal at 208 nm was decreased, resulting in a $[\theta]_{222\ nm}/[\theta]_{208\ nm}$ of 1.03 which is an ideal value for an in-register coiled-coil.
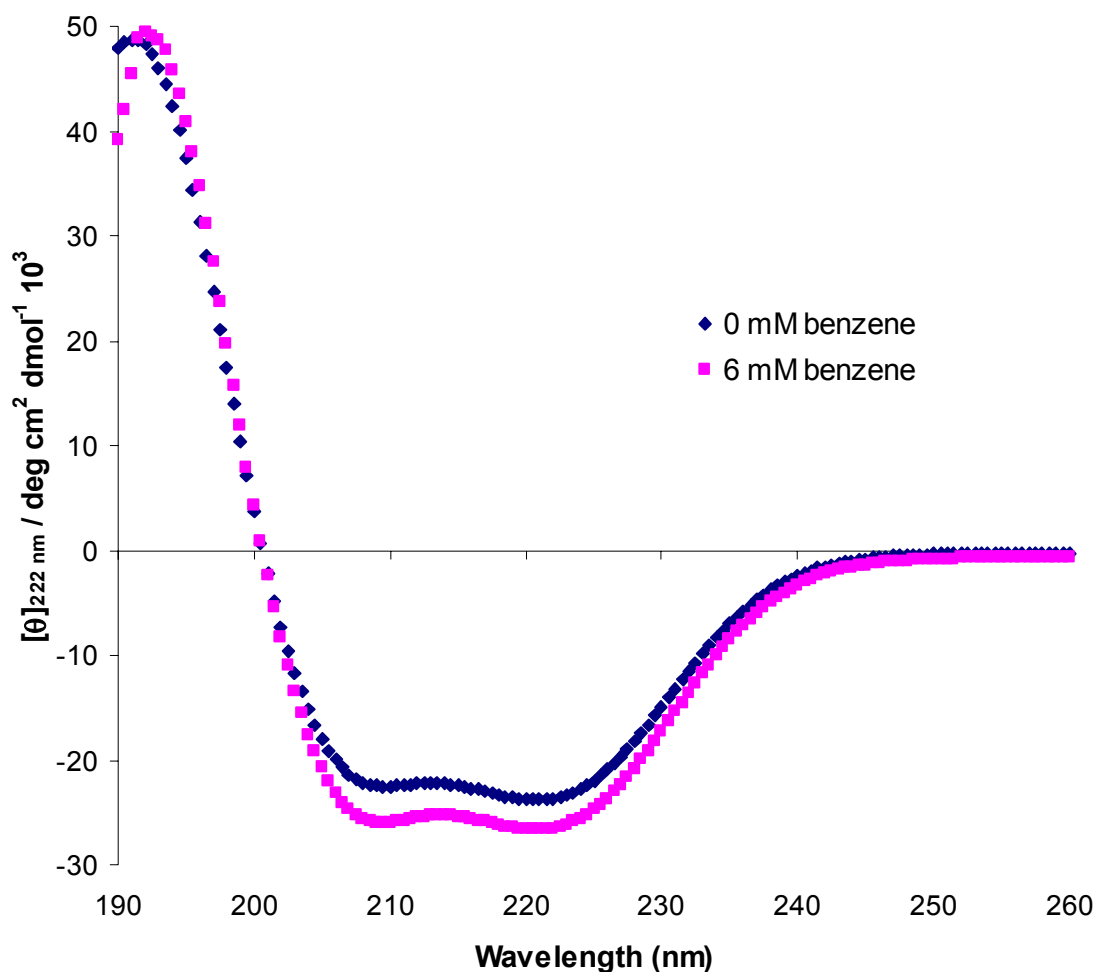
Figure 5.9 Circular dichroism spectra of 70 µM SKAE peptide solution assembled in the absence (blue) and presence (pink) of 6 mM benzene.

It was predicted that the binding of benzene within the engineered cavity would provide stability to the in-register coiled-coil species, which would result in an increased T_m value. Indeed, the presence of benzene increased the observed T_m of **SKAE** by 6 ºC (**Figure 5.10**). This value is in the range of a reported small molecule stabilized coiled-coil with an engineered cavity, where a 6.6 ºC increase in T_m was seen in a system utilizing 10 µM peptide and 5.3 mM benzene.
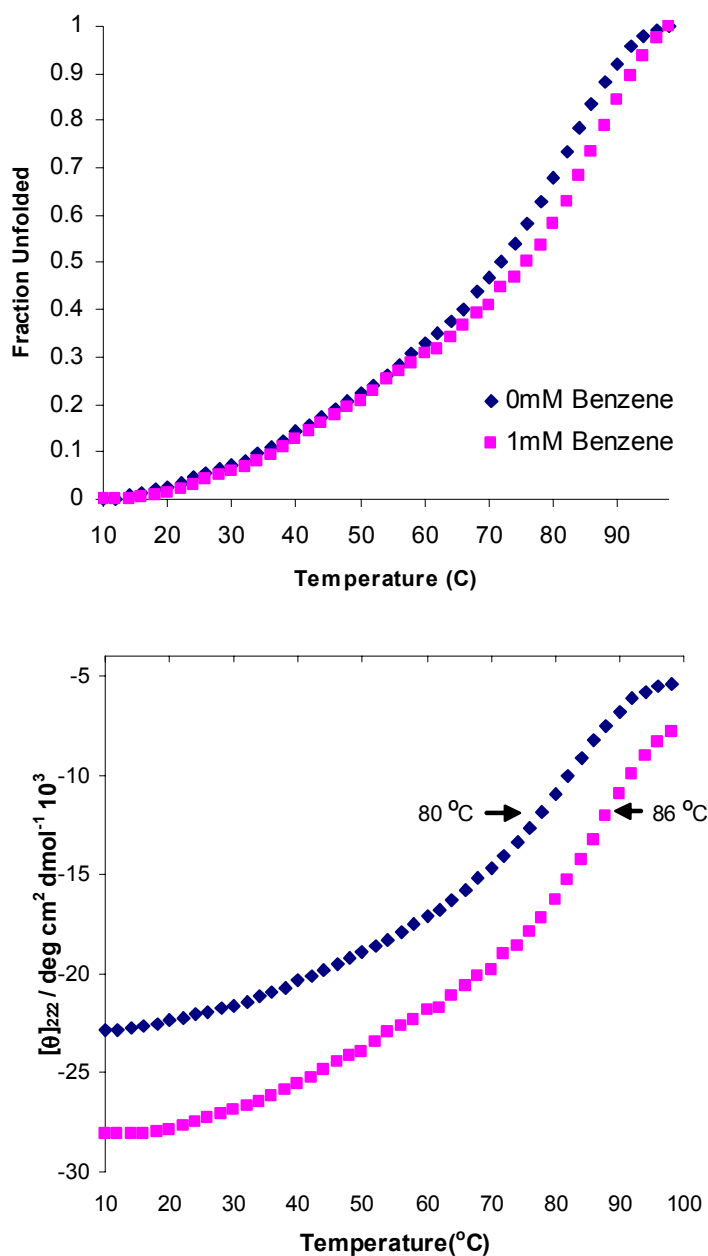
Figure 5.10. Thermal unfolding of 100 μM SKAE in 10 mM phosphate, pH 7.0 between the temperature range 10–100 ºC in the presence and absence of benzene. An increase of 6 ºC is seen in SKAE assembled in the presence of benzene.

5.2.5 TEM of SKAE in the presence and absence of benzene

Circular dichroism suggested **SKAE** peptide assembled in the absence of benzene possessed an α-helical structure which was predicted to exist as a fibrous aggregate. We utilized TEM imaging to assay for the existence of fibers in the sample. In fact, TEM micrographs showed evidence of the long aspect-ratio fibers similar in dimension and morphology to the parental **S6KE** peptide (**Figure 5.11**). The measured diameter of the fibrous species was 4.83 ± 0.17 nm, approximately 1 nm smaller than the **S6KE** fiber.
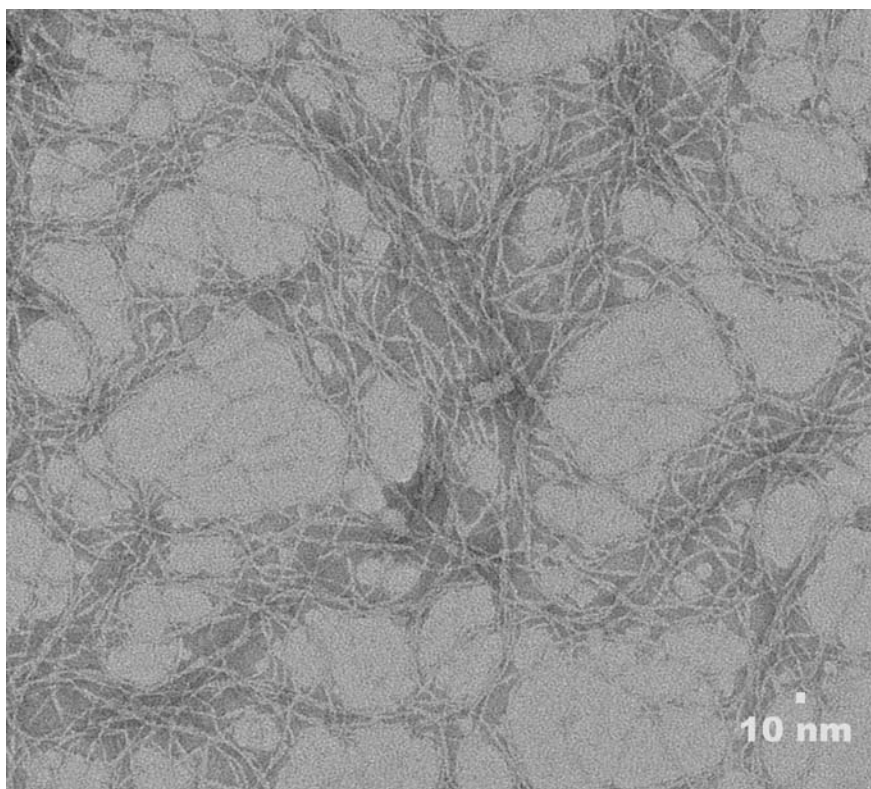
Figure 5.11. Negative stain TEM of 100 μM SKAE peptide prepared in 10 mM phosphate, pH 7.0.

that of the all-isoleucine core **S6KE** fiber to afford a slightly smaller fiber diameter. Furthermore, this suggests the glutamic acid mutation of the *f*-position residues can insure well-defined small diameter fibers even when the self-assembly process is challenged by a disruption in the hydrophobic character of the coiled-coil core.

Multiple attempts at imaging **SKAE** specimens prepared in the presence of benzene resulted in negligible evidence of fiber formation. This is in agreement with our hypothesis that the presence of benzene pushed the structure equilibrium toward the discrete in-register bundles and away from the helical fiber. Crystallographic data for an in-register, three-stranded coiled-coil shows the structure as a cylinder of ~24 Å in diameter and ~48 Å in length, which is a scale that is difficult to capture by negative stain TEM.

5.2.6 Small angle X-ray scattering measurements of SKAE and S6KE fibers

TEM micrographs suggested the lateral staggering regime engineered into the primary sequence of peptides **S6KE** and its mutant **SKAE** was successful, as evident by the observation of fibers in the sample. Further information concerning the dimensions of the structural subunits which compose the observed fiber was sought in the employment of small angle x-ray scattering (SAXS). This technique is known to provide low resolution information on the size, morphology and composition of macromolecular structures in solution under experimental concentrations and room temperature. The range of sensitivity for this technique is between 1 to 50 nm, which is within the predicted range of a three-stranded helical assembly.

The cross-sectional radius of gyration was calculated from experimental data and utilized in determining the average diameter of the fiber to provide qualitative insight into the packing arrangement of the assembly. A minimal diameter of 16.5 Å was estimated for a coiled coil trimer based on the sum of the average diameters of an α-helix (5.01 Å) and the super-helix of the coiled coil trimer (11.5 Å). In the analysis, the superhelical characteristics were determined by fitting Cα backbones to Crick's supercoil parameterization.[13] These diameters describe a lower limit for the diameter of the structure since they do not consider steric contributions from the amino acid side chains. The calculated diameters derived from the modified Guinier analyses of the small-angle X-ray scattering data for **S6KE** and **SKAE** peptide solutions were 59.67 ± 0.37 Å and 59.05 ± 0.17 Å, respectively (**Figure 5.12**). These values are in general agreement with the average diameter seen in TEM micrographs but approximately 3.5 times larger than expected for a trimeric coiled-coil assembly. This observation is consistent with a system exhibiting lateral association.

A significant observation of the SAXS analysis is that the fiber diameters obtained from both **S6KE** and **SKAE** peptide solutions were nearly identical. This suggests the loss of fiber formation in **SKAE** is not attributable merely to the presence of the alanine-induced cavity within the coiled-coil core. As observed also by TEM, the alanine-mutant (**SKAE**) peptide fibers formed in the absence of benzene exhibit diameters similar to the all-isoleucine core (**S6KE**) peptide and only in the presence of benzene does the fiber morphology radically change.
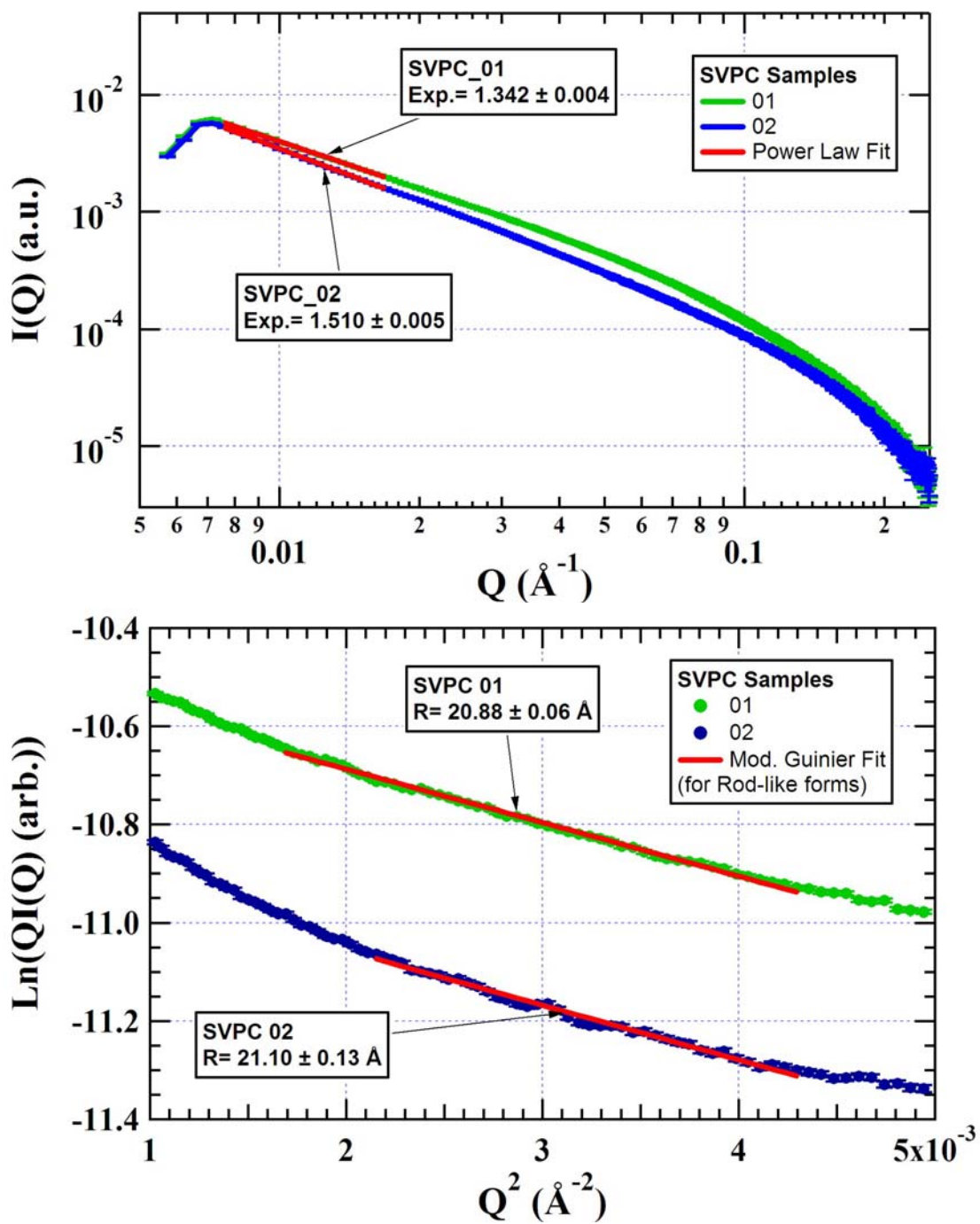
Figure 5.12. Modified Guinier plots of small angle x-ray scattering (SAXS) data with calculated analyses for a rod-shaped form for 100 µM SKAE (SVPC 01) and S6KE (SVPC 02).

5.2.7 Sedimentation equilibrium ultracentrifugation

Our hypothesis states that the addition of benzene to assembled **SKAE** peptide solutions initiates the disassembly of the fibrous aggregate. Circular dichroism spectroscopy data obtained from **SKAE** samples assembled in the presence of benzene showed an increase in both α-helicity and thermal denaturation temperature with respect to the peptide assembled in buffer without benzene. Furthermore, TEM analysis shows evidence that fiber formation occurs preferably in the presence of the benzene. Our model parses this data as evidence of a conformational transition from the fiber-forming staggered arrangement of helical peptides to an in-register coiled-coil assembly due to the stabilization of the discrete coiled-coil architecture through binding of the small molecule in the engineered hydrophobic pocket. Consequently, the presence of benzene we predicted analytical ultracentrifugation may be useful in providing evidence for the disappearance of the high molecular weight fibrous species and the appearance of smaller molecular weight, discrete coiled-coil architecture upon addition of benzene. To assay this behavior, we employed analytical sedimentation equilibrium ultracentrifugation to document the affect of small hydrophobic molecules on the observed molecular weight of the peptide assembly,.

Sedimentation equilibrium is a technique known to facilitate determination of molecular weights of stable oligomeric assemblies in native solvents.[14] Experiments can be performed in dissociating solvents, typically urea or guanidine hydrochloride, to quantify subunit molecular weight or weight-average molecular weight in a sample with more than one uniquely identifiable species. For **SKAE** peptide system, the disassociating solvent can be considered to be benzene-containing buffer. If multiple

species with different molecular weights are present in a solution, each will be dispersed

at sedimentation equilibrium according to the following equation:

$$M = \frac{2RT}{(1-\bar{v}\rho)\omega^2} \times \frac{d(\ln c)}{dr^2}$$
  (Equation 5.1)

where M is the solute molar weight in g/mol, $\bar{v}$ is the partial specific volume in mL/g,

ω is the angular velocity of the rotor, ρ is the solvent density in g/mL, and c is the

concentration of the solute in g/L at a radial distance r from the axis of rotation. As a

consequence of the above equation, a plot of log (concentration) versus (radius)^2 for a

single ideal solute at sedimentation equilibrium results in a slope which is proportional to

the molar weight. Tangents to the ln(c) versus r^2 at various points yield an average

molecular weight which is based on the proportion of weight of the various species

present. This weight is a statistical average of molecular weight, known as the weight-

average molecular weigh, M_w.

In order to test our disassembly hypothesis, I carried out a series of sedimentation

equilibrium experiments with the help of Daphne Salick (from Prof. Joel Schneider's

group, University of Delaware) on a 345 μM peptide **SKAE** solution in 10 mM

phosphate (pH 7.0) which was subsequently spiked with either 6 mM benzene or

cyclohexane (**Figure 5.13**). Data was collected at 22, 24 and 26 hours at 3,000, 25,000

and 35,000 rpm. Sedimentation occurred for the small molecule containing sample at

25,000 rpm, where an overlay of the data points at each radius interval showed little

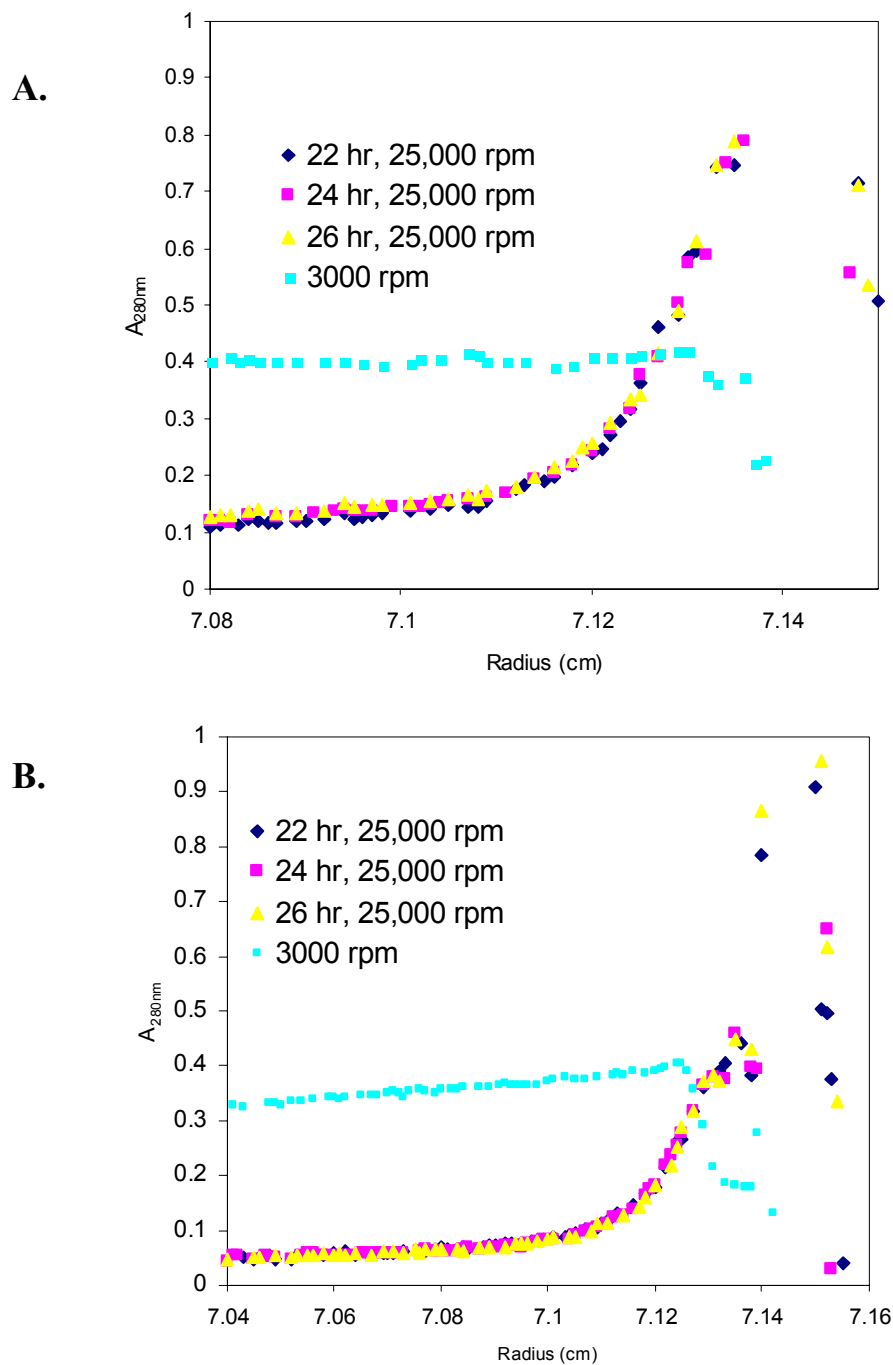variance over time. The partial specific volume, $\bar{v}$, at 25 °C was calculated to be 0.7608

Figure 5.13. **Sedimentation equilibrium data for 345 μM SKAE peptide in benzene (A.) and cyclohexane (B.) at 25 k rpm and 25 °C over the course of 22, 24 and 26 hours. Overlap of points shows the sample reached equilibrium at 25k rpm after 26 hours. Slower 3,000 rpm speed data shown in blue.**

ml g^{-1} using the known amino acid composition.[15] The solvent density, ρ, was taken as 1.006 g ml^{-1} based on the previous reports of coiled-coil assemblies in phosphate buffer containing 6 mM benzene.[7]

Using these parameters, a plot of ln(c) versus r^2 was generated and a least squares line was fit through the points (**Figure 5.14**). This analysis revealed a weight-average molecular weight (M_w) of 156,067 and 145,659 for **SKAE** spiked with 6 mM benzene and cyclohexane, respectively. The slight curve of the line indicates a heterogenous distribution of molecular masses, indicating the disassembly process does not proceed to a single species.[16] Consequently, the observed value for M_w in both samples containing small molecules has contributions form a wide range of potential species, from partially assembled aggregates to the theoretical in-register coiled-coil. However, any conclusive evidence of the discrete helical bundle would be masked by the significantly larger molecular weight contribution of the fibrous aggregate in solution.

The AUC experiment described above was performed on **SKAE** peptide first solubilized in phosphate buffer to allow fiber formation and then spiked with benzene or cyclohexane solution. We also collected data on samples prepared with an alternative protocol, in which **SKAE** peptide was solubilized in benzene- or cyclohexane-containing buffer solution (**Figure 5.15**). We theorized the presence of small molecule in the buffer during assembly could inhibit the process of fiber formation by preferentially stabilizing the in-register coiled-coil architecture over the staggered alignment which coincides with the fibrous species. The M_w value for **SKAE** peptide solution prepared in this manner was observed as 92,250, just slightly larger then ½ the M_w value of the sample spiked with small molecule. While this does not provide conclusive evidence a majority in-

A.

$y = 5.1438x - 262.11$
$R^2 = 0.9771$

M_w = Weight-Average Molecular Weight
  = 156067.69

B.

$y = 4.7987x - 244.95$
$R^2 = 0.9647$

M_w = Weight-Average Molecular Weight
  = 145659.13

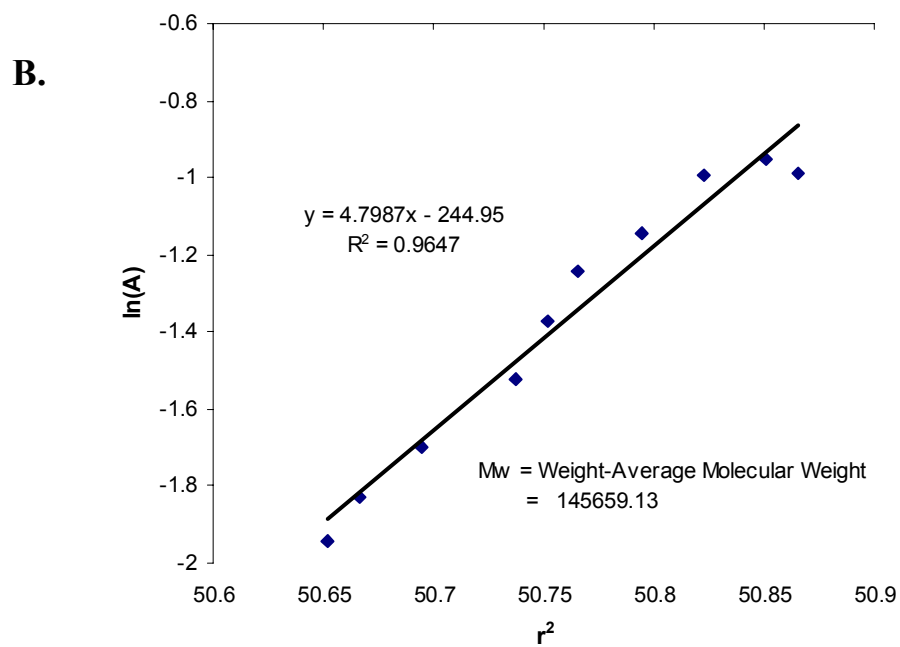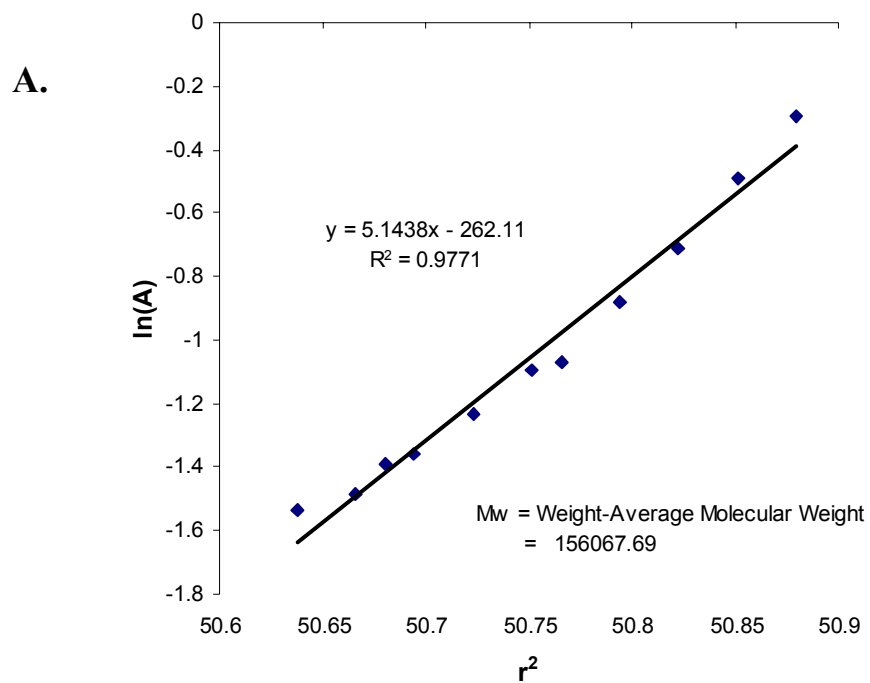**Figure 5.14. Least squares line fit to data collected at 25,000 rpm shows weight-average molecular weight of SKAE peptide system in the presence of benzene (A.) and cyclohexane (B.).**
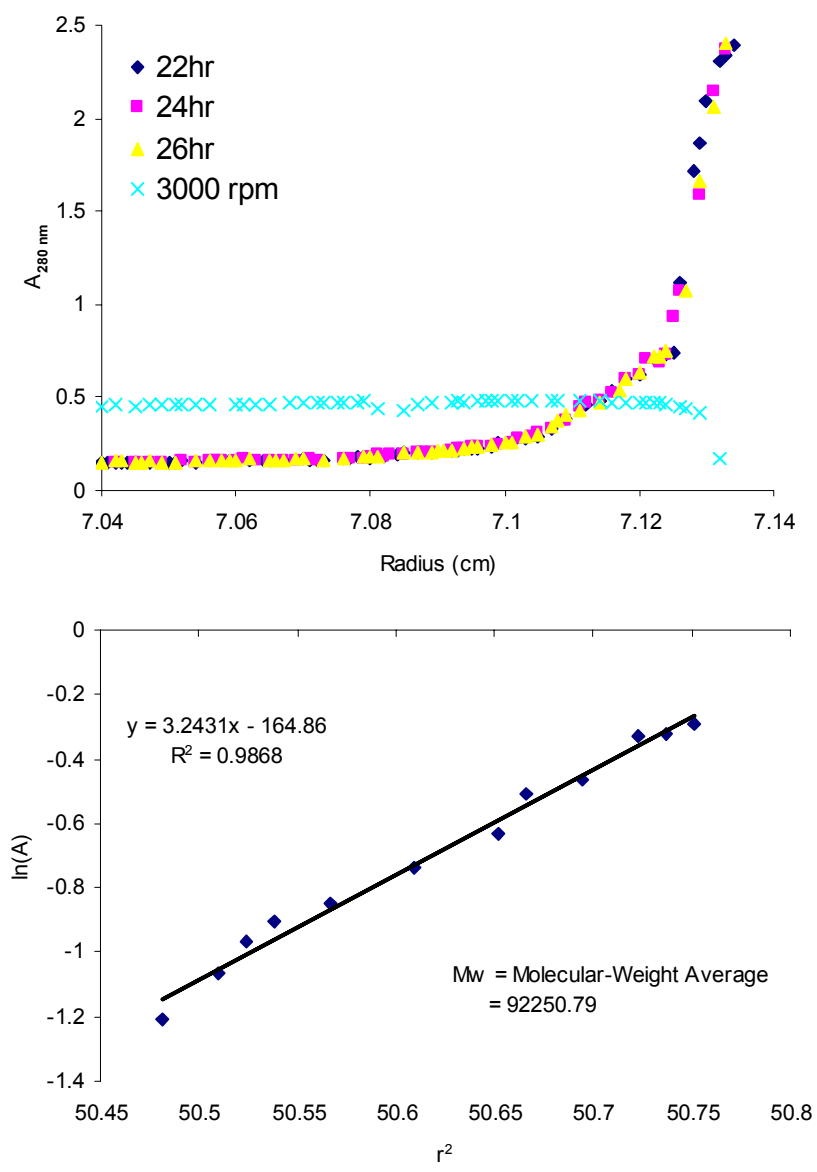
Figure 5.15. Sedimentation equilibrium data for SKAE peptide in which assembly is initiated in benzene at 25,000 rpm and 25 °C over the course of 22, 24 and 26 hours. Least squares line fit to data collected at 25,000 rpm.

register coiled-coil complex in solutions prepared in the presence of small molecule, the trend downwards is encouraging.

The negative control sample containing peptide formed under fiber-forming conditions in the absence of benzene, rapid sedimentation at the slower speed of 3,000 rpm for short time intervals in a benchtop microcentrifuge suggests the presence of mainly large molecular weight fibrous aggregate in solution. This confirms the observation by TEM that fibers are not present in solvent containing benzene molecules. Further examination of the negative control sample by sedimentation velocity ultracentrifugation is currently under consideration.

5.3   Summary

5.3.1   Redesign of peptide S6K decreases fiber diameters

Peptide **SKAE** was designed with inspiration from peptide **S6KE**, the later of which was shown to form axially-elongated helical fibers. Difficulties with sample clouding seen in the assembled parental **S6K** peptide hindered the ability to employ bioanalytical techniques such as analytical ultracentrifugation and small angle x-ray scattering in studies of this system. Therefore, the **S6K** peptide was redesigned to suppress sample precipitation by introducing of glutamic acid residues in all *f*-position heptads. This mutation resulted in the generation of homogenous fibers with significantly smaller diameters. The substitution of two glutamic acid residues into the **S6K** peptide sequence decrease the overall net charge of the peptide thereby increasing

solubility at pH 7.0. Furthermore, it is hypothesized that the polar glutamic acid residues project a uniform charge along the solvent-accessible helical face, which eliminates the possibility of lateral aggregation between adjacent, fully formed fibers.

The diameters of the fibers observed by TEM in the SKAE and S6KE peptide systems were similar those imaged in the metal-switched **TZ1H** peptide described in Chapter 4 of this work. In the later system, the coordination of the silver cation along the fiber axis could provide an equilvalent inhibitory effect on lateral association between adjacent fibers. This suggests fiber diameters can be controlled through the rational incorporation of charged species along the fiber axis and furthermore the design element can be of covalent or non-covalent binding character and cationic or anionic in nature. This may prove to be a valuable addition to future coiled-coil fiber sequence based on the **S6K** system.

5.3.2   Partial disassembly and increased thermostability imparted by ligand binding

Peptide **SKAE** was shown capable of self-assembling into helical fibers of approximately 6 nm diameter and several μm in length, despite the presence of an engineered cavity in the hydrophobic core of the aggregate. Both TEM images and SAXS measurements confirm the relatively homogeneous fiber dimension of the self-assembled **SKAE** peptide in the absence of small molecule. However, in the presence of hydrophobic benzene or cyclohexane molecule, the structural characteristics of the peptide solution change dramatically.

Circular dichroism spectrometry shows an increase in helicity and thermal unfolding transition with respect to the peptide solution in the absence of benzene or cyclohexane. Our hypothesis is that the peptide rearranges into discrete coiled-coil bundles based on the binding of a small hydrophobic molecule in the alanine-produced cavity. Sedimentation equilibrium analysis of the peptide solution in the presence of benzene or cyclohexane show a decreased weight-average molecular weight with respect to the larger fibrous aggregate dominant in the absence of small molecule. The calculated molecular weight determined corresponds to a value 10 times to expected value of an in-register three-stranded coiled-coil composed of peptide **SKAE**. This observation does not support our hypothesis that the binding of small molecule preferentially stabilizes the in-register coiled-coil assembly to afford a single triple-stranded complex in solution. However, the approximately 150,000 weight-average molecular weight is much smaller than that of the μm long fiber, and suggests disassembly of the fiber coincides with the presence of small molecule in solution.

5.3.3 Future improvements

The cooperative electrostatic interactions programmed into the **S6K** peptide sequence to afford the fibrous aggregate are a very strong driving force for the self-assembly of this peptide. To achieve total disassembly of the **SKAE** fiber these contributions must be overcome upon binding of the guest molecule. Several modifications to the system and protocol could be helpful in aiding this process. First,

the addition of charge-screening salts, such as KF, could bias the system towards the discrete coiled-coil bundle over the fiber. Next, more specific binding interactions could be designed into the binding pocket. Currently, the mode of binding is reliant only on the accommodation of a small hydrophobic molecule. Instead, the addition of alterative binding interactions like hydrogen bonding or other noncovalent interactions such as pi-stacking could be utilized. This could require the design of a new binding pocket with more sophisticated packing interactions.

5.4   Materials and Methods

5.4.1   Peptide Synthesis and Purification

Peptides were prepared via automated solid-phase peptide synthesis on a Rink amide resin (0.4-0.6 meq/g) on a Rainin Symphony Quartet peptide synthesizer (Peptide Technologies, Inc., Tucson, AZ) as described previously. Standard FMOC protection chemistry was employed with coupling cycles based on HBTU/NMM-mediated activation protocols and base-induced deprotection (20% piperidine in DMF) of the FMOC group. The N-terminus of the peptides was capped with acetic anhydride prior to cleavage from the resin. The peptide was isolated from the resin as the C-terminal amide derivative after acidic cleavage of the side chain protecting groups with a cocktail of trifluoroacetic acid (TFA), thioanisole, ethanedithiol and anisole (90:5:3:2). Crude peptides were precipitated in ice-cold ether and centrifuged at 6000 rcf at 4 $^{\circ}$C for 20 minutes. After pelleting, the supernatant was decanted and the process repeated until

thiol odor is no longer present. The resulting pellet was then dried under nitrogen flow and stored at -20 $^{\circ}$C until purification.

Prior to purification, the precipitated peptide was thoroughly dissolved in 15 - 25 mL solution of 60% ddH$_2$0 / 40% acetonitrile in the presence of 0.1% trifluoroacetic acid (TFA). Reverse-phase HPLC purification was performed using a Waters 600 purification system (Waters Corp., Milford, MA) with a Waters 996 photodiode array and a reverse phase C-18 column (Atlantis dC18, 10 μm, 19 x 256 mm) with a linear gradient of acetonitrile and water (0.1% trifluoroacetic acid) at 10 mL / minute. The molar mass of **TZ1H** was confirmed by MALDI-TOF mass spectrometry on a Voyager-DE STR instrument (Perseptive Biosystems, Framingham, MA) using equal volumes of α-Cyano-4-hydroxycinnamic acid (saturated solution in 0.1% TFA ddH$_2$O) matrix and HPLC purified peptide. Fractions were combined and rotary evaporated to remove acetonitrile and TFA before lyophilization. Lyophilized peptides were stored at -20 $^{\circ}$C until used. The expected mass for **S6K** peptide is 4833.7 Da and the observed peak by MALDI was 4832.5. For the glutamic acid mutant **S6KE** the expected mass is 4835.6 and the observed peak was at 4833.1. . The expected mass for **SKA** peptide is 4791.7 Da and the observed peak by MALDI was 4790.3. For the glutamic acid mutant **SKAE** the expected mass is 4793.5 and the observed peak was at 4792.1.

5.4.2 Small-angle X-ray scattering

Synchrotron SAXS experiments were performed at Argonne National Laboratory (Argonne, IL). Scattering data was collected at a sample concentration of 1 mg/mL of

S6KE peptide in 10 mM phosphate buffer (pH 7.0) at 25 $^{\circ}$C. The scattering data was corrected for background scattering arising from buffer prior to data analysis. In a dilute solution, small angle scattering intensity, I(Q), can be described by the following equation:

$$I(Q) = I_0 (\Delta\rho)^2 V^2 P(Q) + I_b$$

<div align="right">**Equation 5.2**</div>

where I_0 = instrument constant, $\Delta\rho$ = difference in scattering length density (contrast) between particles and solvent, V = volume of particles, I_b = flat background intensity and P(Q) = particle form factor.   The momentum transfer Q is described as $(4\pi / \lambda)\sin(\Theta / 2)$ where λ = x-ray wavelength and Θ = scattering angle.

Cross-sectional dimensions of the fibers can be extracted from the modified Guiner analysis for a rod-like form. Since I(Q) varies as Q-1 for an infinitely thin rod at low Q, the scattering equation $I(Q) = I_0 (\Delta\rho)^2 V^2 P(Q) + I_b$ Equation 5.2) can be modified to:

$$I(Q) = \pi Mw C (\rho_\rho - \rho_s)^2 / (1000\, N_A d^2 L) \exp(-Q^2 R^2 c / 2)$$

where L = length of the rod, Mw = mass per unit length, C = concentration of peptide in mg / mL, N_A = Avogadro's number and d = inverse of the partial specific volume of **S6KE**.

5.4.3 Sedimentation equilibrium ultracentrifugation

Sedimentation equilibrium data were collected on a Beckman XL-I Analytical Ultracentrifuge (Beckman Coulter, Fullerton, CA) with an AN-60 Ti rotor using 12-mm aluminum 2-sector center pieces at rotor speeds of 3, 25 and 35 k rpm. Proper rotor speeds were chosen by estimating the predicted molecular weight using charts from the manufacturer. Peptides were dissolved in 10 mM phosphate buffer, pH 7.0 to concentrations near 325 μM to afford an absorbance value at 280 nm greater than $A_{280\ nm}$ = 0.3. The wavelength 280 nm is contributed by a single tyrosine residue absorbance.

5.5 References

1. Spencer, D. M.; Wandless, T. J.; Schreiber, S. L.; Crabtree, G. R., Controlling signal transduction with synthetic ligands. *Science* **1993,** 262, (5136), 1019-24.

2. Dutta, K.; Alexandrov, A.; Huang, H.; Pascal, S. M., pH-induced folding of an apoptotic coiled coil. *Protein Sci* **2001,** 10, (12), 2531-40.

3. Zimenkov, Y.; Dublin, S. N.; Ni, R.; Tu, R. S.; Breedveld, V.; Apkarian, R. P.; Conticello, V. P., Rational design of a reversible pH-responsive switch for peptide self-assembly. *J Am Chem Soc* **2006,** 128, (21), 6770-1.

4. Pagel, K.; Vagt, T.; Kohajda, T.; Koksch, B., From alpha-helix to beta-sheet--a reversible metal ion induced peptide secondary structure switch. *Org Biomol Chem* **2005,** 3, (14), 2500-2.

5. O'Shea, E. K.; Klemm, J. D.; Kim, P. S.; Alber, T., X-ray structure of the GCN4 leucine zipper, a two-stranded, parallel coiled coil. *Science* **1991,** 254, (5031), 539-44.

6. Harbury, P. B.; Zhang, T., A switch between two-, three-, and four-stranded coiled coils in GCN4 leucine zipper mutants. *Science* **1993,** 262, (5138), 1401.

7. Gonzalez, L., Jr.; Plecs, J. J.; Alber, T., An engineered allosteric switch in leucine-zipper oligomerization. *Nat Struct Biol* **1996,** 3, (6), 510-5.

8. Eriksson, A. E.; Baase, W. A.; Zhang, X. J.; Heinz, D. W.; Blaber, M.; Baldwin, E. P.; Matthews, B. W., Response of a protein structure to cavity-creating mutations and its relation to the hydrophobic effect. *Science* **1992,** 255, (5041), 178-83.

9. Schnarr, N. A.; Kennan, A. J., Coiled-coil formation governed by unnatural hydrophobic core side chains. *J Am Chem Soc* **2001,** 123, (44), 11081-2.

10.   Doerr, A. J.; Case, M. A.; Pelczer, I.; McLendon, G. L., Design of a functional protein for molecular recognition: specificity of ligand binding in a metal-assembled protein cavity probed by 19f NMR. *J Am Chem Soc* **2004,** 126, (13), 4192-8.

11.   Harbury, P. B.; Kim, P. S.; Alber, T., Crystal structure of an isoleucine-zipper trimer. *Nature* **1994,** 371, (6492), 80-83.

12.   Schein, C. H., Solubility as a function of protein structure and solvent components. *Biotechnology (N Y)* **1990,** 8, (4), 308-17.

13.   Crick, F., The packing of [alpha]-helices: simple coiled-coils. *Acta Crystallographica* **1953,** 6, (8-9), 689-697.

14.   Laue, T. M.; Rhodes, D. G., Determination of size, molecular weight, and presence of subunits. *Methods Enzymol* **1990,** 182, 566-87.

15.   Perkins, S. J., Protein volumes and hydration effects. The calculations of partial specific volumes, neutron scattering matchpoints and 280-nm absorption coefficients for proteins and glycoproteins from amino acid sequences. *Eur J Biochem* **1986,** 157, (1), 169-80.

16.   Harding, S., *Protein: A Comprehensive Treatise*. Elsevier: London, 1999; Vol. 2, p 271-305.

Chapter VI: Conclusions and outlook

The studies described in this volume firmly establish a rational design scheme for the generation of functional nanoscale biomaterials based on the self-assembly of synthetic helical peptides. The purpose of these experiments was to define the primary sequence determinants which underlie the self-assembly process and to simultaneously establish guiding principles for the rational design of conformational switching mechanisms in the resulting peptide fibers. A series of synthetic peptides were synthesized in which artificial allosteric sites were generated through the mutation of residues in structurally-critical core positions in the peptide sequence. Through proper amino acid choice, self-assembly could be regulated through incremental changes in environmental stimuli such as pH, metal ion or small-molecule concentration.

6.1 Fiber thickening

The **S6K**-family peptide sequences, including all of the peptides described in this volume, possess isoleucine residues in all *a* and *d* heptad positions to encourage their self-assembly into a three-stranded helical rope. While the fiber diameter is estimated to be approximately 3 nm, initial observations by TEM for peptides **S6K** and **TZ1H** showed fiber diameters consistently an order of magnitude larger then the expected value. This behavior, termed fiber thickening, has been reported by other groups working in the area of self-assembling helical peptides.[1,2] In our system, fiber thickening hinders our ability to measure the true fiber diameter of a single helical fiber, which would provide qualitative affirmation that we have achieved the triple-stranded assembly.

Native coiled-coil proteins also show evidence of higher-order structures and lateral association of helical fibers.[3] In the majority of cases, this is due to Coulombic interactions on the solvent-accessible surface of the helices.[4,5] Alternating basic and acidic residues at the surface positions provide complementary charge patches along the fiber axis which encourage inter-helical interactions between formed fibers (**Figure 6.1**).

Staggered helical peptide   **Fibrillogenesis**

Fiber thickening

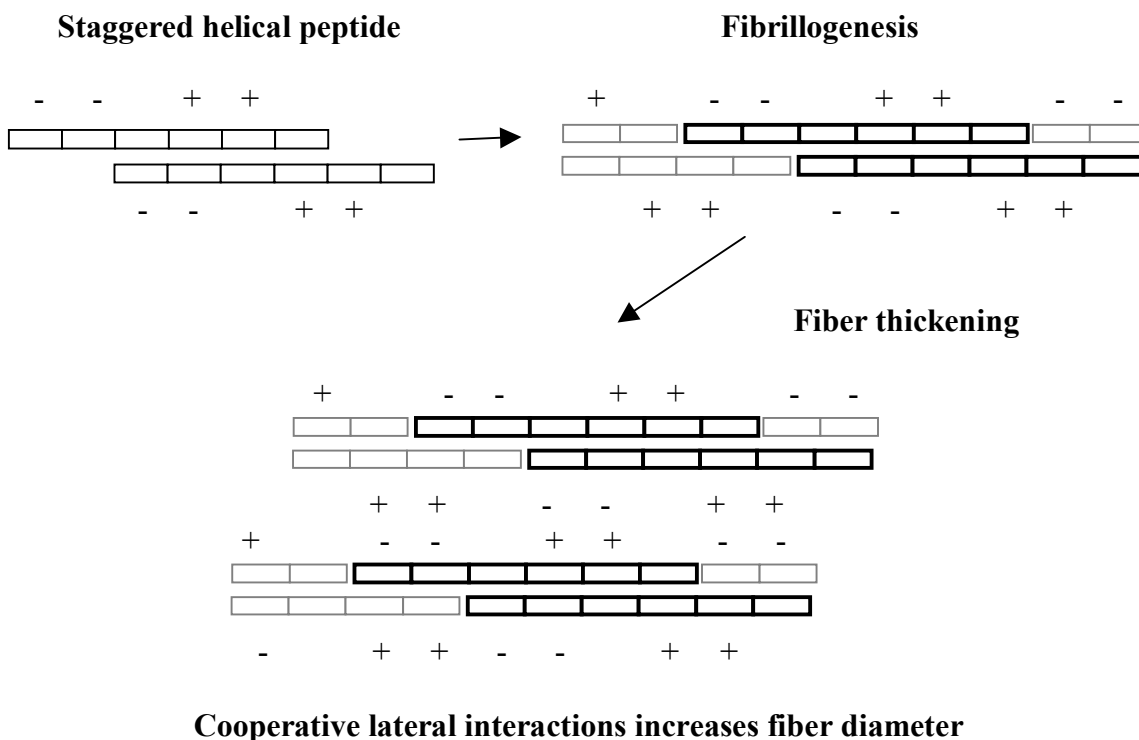**Cooperative lateral interactions increases fiber diameter**

Figure 6.1. Simplified representation of fiber thickening in a self-assembling helical peptide system based on the S6K peptide system. The scheme is illustrated as a dimeric assembly instead of trimeric assembly for simplicity sake. The (+) and (-) charges represent the identity of the residues in the solvent-accessible *f*-positions, lysine and glutamic acid, respectively.

Using this knowledge, we designed the second generation **S6K** peptide**,** named **S6KE** for the substitution of glutamic acid in the solvent-accessible *f*-position residue. This mutation placed a negative charge down the fibril axis, thereby eliminating the alternating basic / acidic patterning. The redesigned peptide showed a significantly decreased fiber diameter and was subsequently used as a template for an improved **SKA** peptide, aptly named **SKAE**. This was a significant achievement because the initial **SKA** peptide fibers showed a high propensity for aggregation which contributed to clouding of peptide solutions which, in turn, hindered most biophysical characterizations. The aforementioned CD, AUC and SAXS measurements were only possible due to this design improvement.

Interestingly, we were able to achieve similar results in the **TZ1H** peptide system without changing the primary sequence. The silver ion-induced helical fibers displayed thinner fiber diameters and increased solubility compared to the identical peptide sequence assembled under basic pH conditions in the absence of metal, where the resulting large helical bundles displayed diameters in excess of 100 nm. The major difference between the two suprastructures is the thin diameter fibers contain silver ion coordinated along the fiber axis, which suggests the binding of a cationic species, such as silver ion, similarly provides a deterrent to fiber thickening.

6.2 Future directions in discovering novel functionalities

The ability to rationally design reactive mechanisms into self-assembling peptide systems is highly dependant on the known properties of the individual amino acids

occupying the critical structural positions. This limits the choice of residues to those exhibiting properties such as the ability to coordinate metal, exhibit fluorescence or ionizability. Additionally, *a priori* knowledge of the final supramolecular structure is critical to achieving stimuli-specific functionality, particularly in engineered metal ion / small molecule binding sites. For example, the specificity of the engineered metal-binding site in peptide **TZ1H** for silver (I) ion was most certainly a consequence of the ligand-binding geometry exhibited by the histidine side chain imidazoles. Fortunately, we were able to predict the arrangement of the residues composing the engineered site using reported crystallographic data of analogous structures, including a well-defined coiled-coil assembly.

An alternative approach for generating coiled-coil assemblies which exhibit novel functionalities may lie in a combinatorial design strategy, in which a library of synthetic peptides is generated with randomized positions on the heptad known to be critical structural-determinants. Using an appropriate selection / screening scheme, such as the split GFP screen developed by the Regan group for identifying protein-protein interactions *in vivo*, peptides can be isolated from the pool which self-associate only in the presence of a small molecule. This approach requires no previous knowledge of the final supramolecular structure or binding site amino acid composition, could facilitate more specific binding interactions such as hydrogen bonding donor / acceptors, and would permit the process to be performed entirely *in vivo*, utilizing a common bacteria host like *E.coli*.

6.3 References

1. Wagner, D. E.; Phillips, C. L.; Ali, W. M.; Nybakken, G. E.; Crawford, E. D.; Schwab, A. D.; Smith, W. F.; Fairman, R., Toward the development of peptide nanofilaments and nanoropes as smart materials. *Proc Natl Acad Sci U S A* **2005,** 102, (36), 12656-61.

2. A. M. Smith, E. F. B. W. R. E. M. J. P. D. N. W., Engineering Increased Stability into Self-Assembled Protein Fibers. *Advanced Functional Materials* **2006,** 16, (8), 1022-1030.

3. Pollard, T. D.; Earnshaw, W. C., *Cell Biology*. Saunders: London, 2002.

4. Parry, D. A.; Crewther, W. G.; Fraser, R. D.; MacRae, T. P., Structure of alpha-keratin: structural implication of the amino acid sequences of the type I and type II chain segments. *J Mol Biol* **1977,** 113, (2), 449-54.

5. McLachlan, A. D.; Stewart, M., Periodic charge distribution in the intermediate filament proteins desmin and vimentin. *J Mol Biol* **1982,** 162, (3), 693-8.